AD-A070 531 DEBETTENCOURT (JOSEPH T) NEWTON MA* F/G 20/14
LITHOSPHERIC RADIO PROPAGATION MODELLING A FEASIBILITY STUDY.(U)
APR 79 J T DEBETTENCOURT, R W KING N00014-78-C-0668
UNCLASSIFIED DBK-2 NL

1 OF 2
AD
A070531

(14) Report No. DBK - 2

LEVEL

(11) April 1979

(2)

(6) LITHOSPHERIC RADIO PROPAGATION MODELLING
A FEASIBILITY STUDY.

by

(10) Joseph T./deBettencourt
and
Ronald W. P./King

(12) 138 pp.

(15) ONR CONTRACT N00014-78-C-0668

NR 081-319

(9) Final Report. 1 Sep 78 - 28 Feb 79,

CONTRACTOR:

Dr. Joseph T. deBettencourt
18 Sterling Street
West Newton, Massachusetts 02165
Phone: (617) 244-0724

S/C

394218

ABSTRACT

Radio wave propagation in the earth's crust is reviewed. This has been studied by many investigators who usually assume the crust to be a planar slab of low loss-tangent, bounded on top and bottom by regions of large loss-tangent. Available conceptual depth profiles of complex dielectric constant of the lithospheric waveguide are reviewed and theories extant summarized. Sources were usually VED's inserted through vertical bore-holes. For ocean emplaced antennas located near the ocean-lithosphere boundary, the sources are horizontally polarized and propagation is predominantly by means of lateral waves. Calculations are reported for a wide range of conditions. The useful characteristics of lateral wave transmission are discussed. The measured properties of scaled waveguide propagation that have been reported could not accurately scale the losses in the overburden since it was represented by a metal plate. The principles of electrodynamic similitude are delineated and two different experiments using similitude with different depth profiles are discussed.

To study the effects of boundaries on transmission (including wall losses) and simultaneously to make measurements of embedding and moving antennas in them, the laboratory models should have "walls" composed of a liquid with suitable excitation. For an orderly build-up of modelling measurements, a laboratory set-up is described. Included would be measurements with boundaries that are sloping, undulating or irregular. Though available materials may limit accurate modelling according to similitude scaling, meaningful and illuminating information could be obtained for better understanding of lithospheric transmission. The more complex depth profiles require a much more elaborate set-up, patterned possibly after that of Iizuka.

Unclassified

SECURITY CLASSIFICATION OF THIS PAGE (When Data Entered)

REPORT DOCUMENTATION PAGE		READ INSTRUCTIONS BEFORE COMPLETING FORM
1. REPORT NUMBER DBK-2	2. GOVT ACCESSION NO.	3. RECIPIENT'S CATALOG NUMBER
4. TITLE (and Subtitle) Lithospheric Radio Propagation Modelling - a Feasibility Study		5. TYPE OF REPORT & PERIOD COVERED FINAL - 9/1/78 to 2/28/79 6. PERFORMING ORG. REPORT NUMBER
7. AUTHOR(s) Joseph T. deBettencourt and Ronald W. P. King		8. CONTRACT OR GRANT NUMBER(s) N00014-78-C-0668
9. PERFORMING ORGANIZATION NAME AND ADDRESS Dr. Joseph T. deBettencourt 18 Sterling Street West Newton, MA 02165		10. PROGRAM ELEMENT, PROJECT, TASK AREA & WORK UNIT NUMBERS
11. CONTROLLING OFFICE NAME AND ADDRESS Office of Naval Research (Code 463) Department of the Navy, 800 N. Quincy St. Arlington, VA 22217		12. REPORT DATE April 1979 13. NUMBER OF PAGES 132
14. MONITORING AGENCY NAME & ADDRESS(if different from Controlling Office)		15. SECURITY CLASS. (of this report) Unclassified 15a. DECLASSIFICATION/ DOWNGRADING SCHEDULE

16. DISTRIBUTION STATEMENT (of this Report)

Approved for Public Release; Distribution Unlimited

17. DISTRIBUTION STATEMENT (of the abstract entered in Block 20, if different from Report)

18. SUPPLEMENTARY NOTES

19. KEY WORDS (Continue on reverse side if necessary and identify by block number)

Lithosphere
Lithospheric Radio Propagation
Radio Propagation
Conductivity Profiles
Electrodynamic Similitude
Lateral Waves in Lithosphere
Laboratory Propagation Modelling
Radio Propagation in Lossy Media

20. ABSTRACT (Continue on reverse side if necessary and identify by block number)

Radio wave propagation in the earth's crust is reviewed. This has been studied by many investigators who usually assume the crust to be a planar slab of low loss-tangent, bounded on top and bottom by regions of large loss-tangent. Available conceptual depth profiles of complex dielectric constant of the lithospheric waveguide are reviewed and theories extant summarized. Sources were usually VED's inserted through vertical bore-holes. For ocean emplaced antennas located near the ocean-lithosphere boundary, the sources are hori-

(Continued)

DD FORM 1 JAN 73 1473 EDITION OF 1 NOV 65 IS OBSOLETE
S/N 0102-014-6601

Unclassified

SECURITY CLASSIFICATION OF THIS PAGE (When Data Entered)

Block 20

zontally polarized and propagation is predominantly by means of lateral waves. Calculations are reported for a wide range of conditions. The useful characteristics of lateral wave transmission are discussed. The measured properties of scaled waveguide propagation that have been reported could not accurately scale the losses in the overburden since it was represented by a metal plate. The principles of electrodynamic similitude are delineated and two different experiments using similitude with different depth profiles are discussed.

To study the effects of boundaries on transmission (including wall losses) and simultaneously to make measurements of embedding and moving antennas in them, the laboratory models should have "walls" composed of a liquid with suitable excitation. For an orderly build-up of modelling measurements, a laboratory set-up is described. Included would be measurements with boundaries that are sloping, undulating or irregular. Though available materials may limit accurate modelling according to similitude scaling, meaningful and illuminating information could be obtained for better understanding of lithospheric transmission. The more complex depth profiles require a much more elaborate set-up, patterned possibly after that of Iizuka.

CONTENTS

LIST OF FIGURES AND CAPTIONS

LIST OF TABLES

1. Introduction

Interest in the electrical and geophysical properties of earth's crust has been recently encouraged by the possible existence of a lithospheric plane waveguide with conductivities lower than previously accepted. The region of the earth's crust forming this low conductivity waveguide was assumed to be a planar slab, 10 to 30 km thick, bounded on top by an overburden (or ocean) of high conductivity and on the bottom ("underburden") by a high conductivity mantle or Moho (as it is often referred to in the literature). A review of the crustal properties was given at an ONR Lithospheric Workshop in mid-March, 1978, chaired by J. Heacock with papers presented by G. Keller, G. Simmons, P. R. Bannister, and C. Cox amongst others.

There have been some excellent reviews of the field in recent years. For example, Wait (1971) in the AGU Monograph No. 14, covered principally the waveguide analytical approaches. And Bannister (1978) gave an excellent review of the idealized waveguide (homogeneous profile) of Wait and Spies plus the results of Field and Dore for non-homogeneous profiles of Levin, Keller, and Housley. We wish merely to supplement here some of their writings.

While most of the analytical work tended to treat waveguide modal solutions, there exists the possibility of lateral wave transmission between ocean emplaced HED transmitting and receiving antennas located near the ocean-lithosphere boundary.

It was desired to study the feasibility, in laboratory models, of measuring the properties of lithospheric transmission, including wall losses,

using the principles of electrodynamic similitude for scaling. Scaled models have been used for a homogeneous waveguide in one case, and in another for a non-homogeneous profile of conductivity increasing with depth. Both cases used metallic upper plate upper walls which do not accurately scale the properties of the overburden or ocean. There is a question of available materials for such modelling.

In Chapter 2, we present separately the various available conceptual depth profiles, starting from the 1961 work of Wheeler and that of Mott and Biggs in 1963, both works being expositions of concepts of communication from land via "A deep waveguide" in the crust to deeply submerged submarines. There follows a series of descriptions of several non-homogeneous depth profiles.

Chapter 3 contains a summary review of the various theoretical works on the profiles of Chapter 2. Most of these concern modal solutions for waveguides with plane boundaries; results are often illustrated with boundaries having infinite conductivities. In some cases, the lower boundary is sharp; in others the complex dielectric constant is tapered to increase with increasing depth. Finally, the work with antennas emplaced in the ocean near the ocean-lithosphere boundary is cited by way of introducing the next section.

In Chapter 4 is an expose with numerical calculations of lateral waves from an HED source emplaced in the water near the ocean-lithosphere boundary. A previous development of King and Sandler for an HED in water below air, which extended the work of Banos, is extended to the case where the lithosphere replaces the air. A wide range of parameters were used for calculating the fields.

Chapter 5 contains a brief development of expressions for electrodynamic similitude. Examples are given for laboratory frequency and distance scaling by Brown and Gangi for a homogeneous depth profile of dielectric constant and conductivity, plus some results of Iizuka with the non-homogeneous profiles achieved with an agar-agar gel diffused with sodium chloride.

In Chapter 6 is contained a discussion of lateral wave modelling in combination with measurement of losses in the walls for this and for waveguide excitation. A suggested laboratory set-up could be used for sloping boundaries or boundaries that are rough or undulating.

A summary and conclusion with recommendations are contained in Chapter 7.

There follows the list of references and supplemental bibliography in Chapter 8.

2. Lithospheric Profiles

2.1 Introduction

Most of the earlier lithospheric waveguide depth profiles were based on the laboratory measurements of samples of rock as functions of temperature and pressure. With few exceptions, emphasis was placed on the depth variation of conductivity σ; this was due probably to the belief that the expected exponential attenuation would be low enough only at low frequencies where the loss tangent $p = 60\ \sigma\ \lambda_o/\varepsilon_r$ is quite large (σ in Si/m, λ_o the free space wavelength in meters, and ε_r the relative dielectric constant). In analyses of these profiles, most investigators had assumed ε_r to be constant with depth in the lithospheric waveguide, with values of 4 to 10.

Earlier analyses assumed the waveguide to have a depth of 10 to 40 km. On top, it was bounded by an overburden or sea of such high loss-tangent that this region was represented by a highly conducting metallic plate in many analyses and models.

At the bottom, the earlier analyses assumed the conductivity towards the hot "Moho" discontinuity to be so high that it again was represented by a highly conducting plate. These earlier analyses assumed a homogeneous parallel plate slab, somewhat idealized, to calculate the fields in the guide. Refinements grew as more complicated profiles of the crust developed. We trace here the profiles from the early one of Wheeler to that of Wait, then to Levin and coworkers, to Keller, to Housley and to the work of Simmons.

2.2 Wheeler's Profile

Wheeler's (1961) early paper, interestingly enough, concerned itself with a means of communicating to a submarine near an ocean floor from a shore based source. A sketch of the concept is shown in Figure 2.1 (a); the transmitter, shown in Figure 2.1 (b), passes through about 1 km of overburden and then extends 2 km in a borehole into the waveguide where it excites a TEM mode. The conductivity profile is shown in Figure 2.1 (c) as a function of depth and temperature. The boundaries are roughly 2 and 20 km deep, where the rock conductivity may be 10^{-6} to 10^{-11} Si/m, a useful value being 10^{-8} Si/m. The relative dielectric constant was 6. The "upper wall", perhaps 1 to several kms thick has a range of 4 Si/m for sea water down to 10^{-4} Si/m in rather dry minerals. The lower region was termed the "inverted ionosphere" or "thermal ionosphere" by Wheeler (1961) with temperatures of 300° to 600° C.

2.3 Mott and Biggs' Profile

A couple of years later, Mott and Biggs (1963) also considered VLF propagation below the sea. Their concept is shown in Figure 2.2 (a) for the communicating region, the upper boundary 1 km thick being the wet, highly conducting continental surface or the ocean. The propagating region was assumed to consist of dry, low-temperature low conductivity granites or basaltic rocks, 20 to 70 km thick. The bottom was formed by ultra-basic rocks, having higher conductivity because of the high temperature.

Propagation takes place between 2 vertical electric dipoles (VED) extending 1 or 2 km into the low conductivity region, with an upper value of 10^{-6} Si/m for long-distance communication.

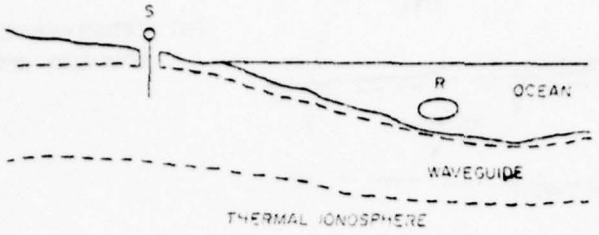

(a) Communication from buried VED source S via deep waveguide under the ocean to receiver R located in the sea.

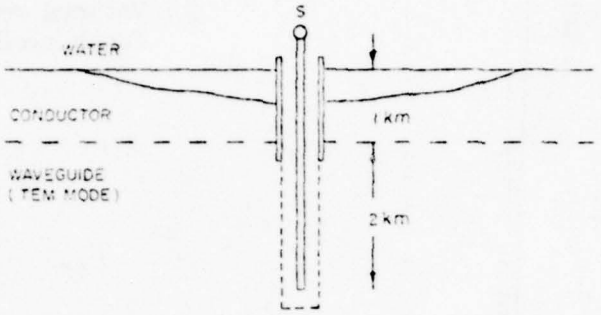

(b) Sketch of VED source antenna S inserted into the waveguide.

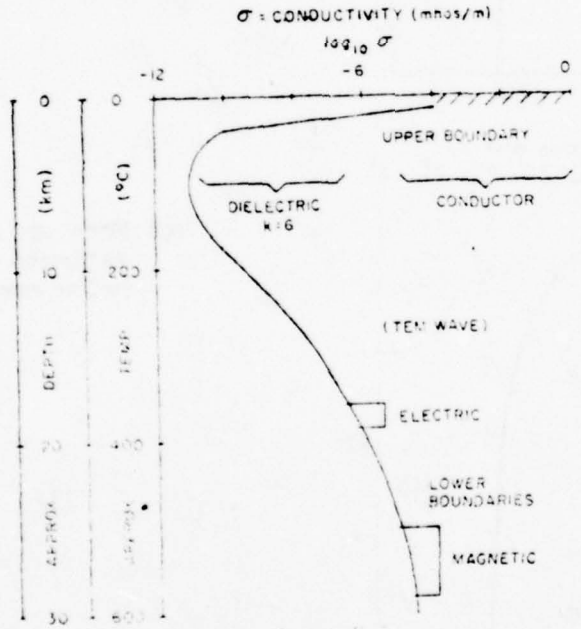

(c) Profile of conductivity and temperature with depth.

Fig. 2.1 Wheeler's concept and conductivity profile for communication under the ocean via a deep waveguide to a submerged receiver. (From Wheeler, 1961).

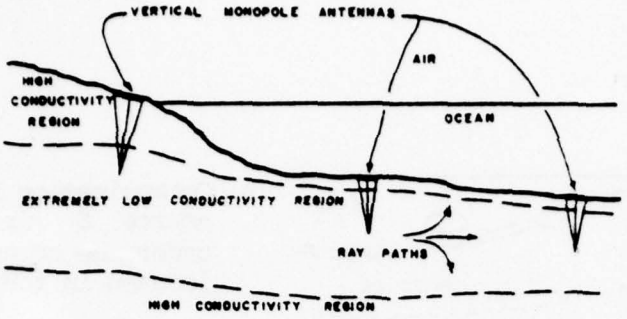

(a) Cross-section sketch showing communication zone

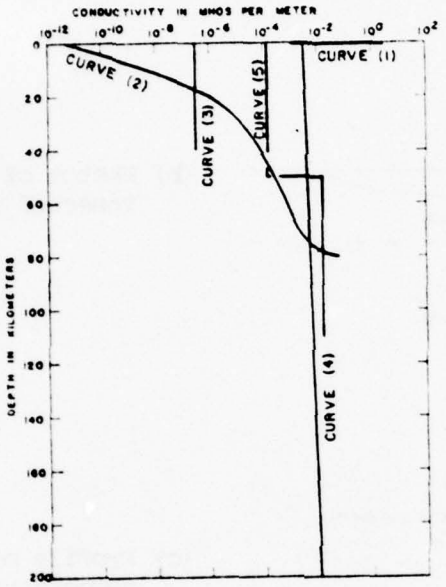

(b) Various conductivity depth profiles.

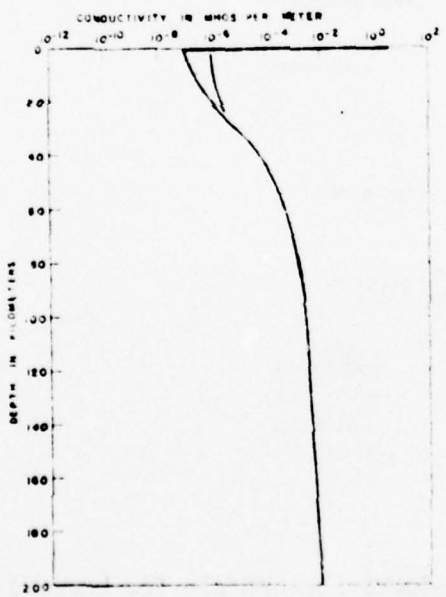

(c) Mott and Biggs' estimate of conductivity below ocean bottom

Figure 2.2 Mott and Biggs' concept of undersea communication, with conductivity profile. (Mott and Biggs, 1963)

Earth conductivity estimates are shown in Figure 2.2 (b). The curve labeled number "1" indicates measured earth conductivities of 10^{-3} for poorly conducting earth to 4 Si/m for sea water. Curve "2" is from Hughes (1953) for olivines, with McDonald's (1959) estimates of temperature distribution. Curve "3" is an estimate of maximum conductivity, by Garland and Webster (1960) for western Canada pre-Cambrian basement rocks. Curve "4" is that of Lahiri and Price (1939) while curve number "5" is due to Cantwell and Madden (1960). Some of these curves are included in a composite one drawn by Iizuka (1968), discussed later on. The final conductivity-depth profile assumed by Mott and Biggs (1963) is shown in Figure 2.2 (c). In essence this is a two-region model, the bottom being 10 - 20 km deep with a bottom region having a conductivity 10^{-6} to 10^{-7} Si/m, and a dielectric constant of 6 with a top region of sea water with 4 Si/m for conductivity, perhaps 1 to 2 km thick.

2.4 The Profile of Brown and Gangi

Brown and Gangi (1962, 1963) and Gangi (1966) gave a diagram of earth conductivity as a function of frequency and depth, as shown in Figure 2.3.

The surface and near surface overburden had conductivities ranging from 10^{-1} to 10^{-4} Si/m, with an average of 10^{-2} to 10^{-3} Si/m. The relative dielectric constant had a wide range of values, with a typical value of 4 to 10 being widely used.

For the crust, the values were inferred from tables in Von Hippel (1954) for the effects of temperature and water content of quartz and silicates (pages 303-314 of his book). The low conductivity value of granite is frequency sensitive and the authors show values for 1, 10 and 100 kHz.

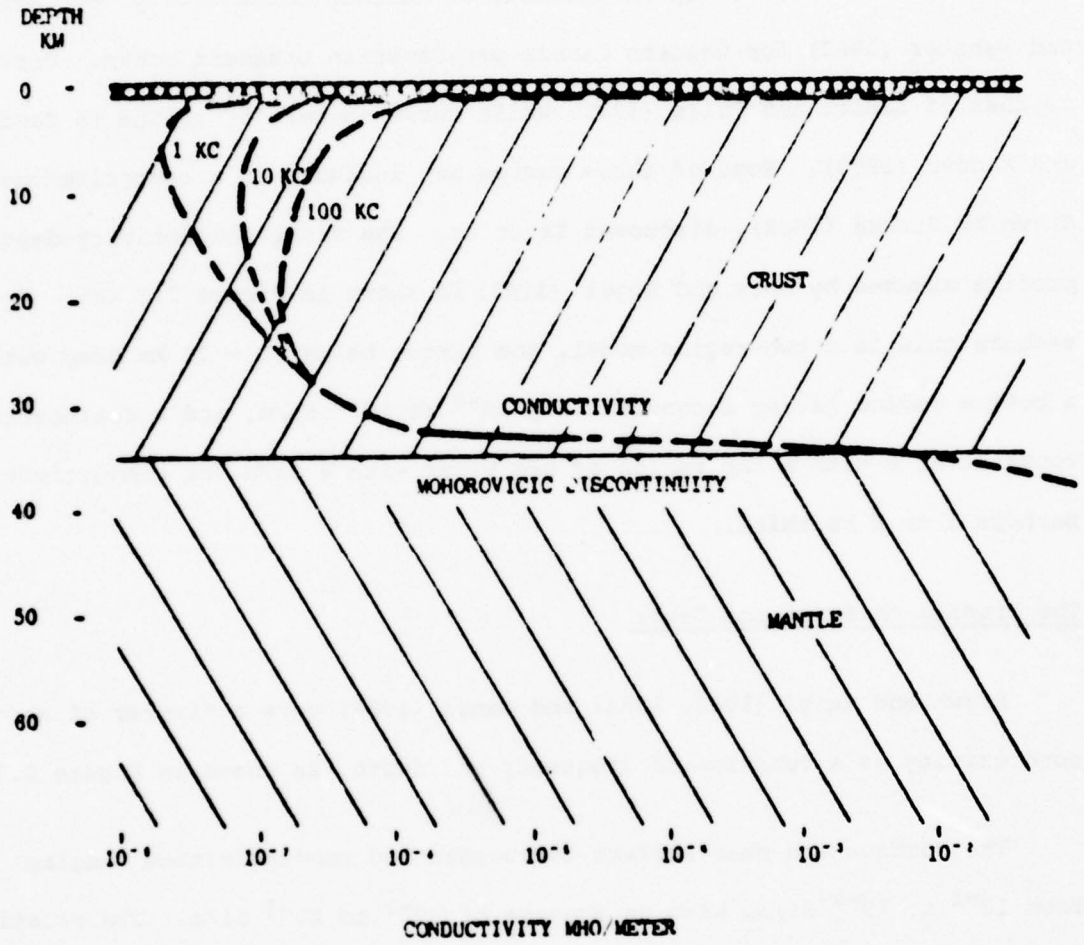

Figure 2.3 Brown and Ganci's inferred conductivity profile. (Brown and Ganci, 1962,1963; Ganci,1966)

At 30 km depth, the conductivity increases rapidly, temperature being about 300^{o} C, relatively independent of frequency. Near the Moho the conductivity is about 4×10^{-3} Si/m. Relative dielectric constant was of the order of 5, down to 30 km.

In their theoretical studies, the "real earth" situation was approximated by a uniform slab between two highly conducting planes (See next Chapter). The conductivities chosen were according to frequency in the low conductivity region.

2.5 Levin's Profile

An idealized cross-section of the earth's crust was delineated and shown by Levin (1966) in Figure 2.4 illustrating the crust under a continent vs. an ocean basin, as well as the continental shelf. Under the continent is granite underlain by basalt down to the Moho. Proceeding through the shelf, the granitic rock disappears leaving basalt under the ocean and volcanoes. The Moho may be 35 km deep under the continent and about 10 km under the ocean.

After a considerable discussion, Levin (1966) showed a trial profile of both conductivity and relative dielectric constant with depth. Levin (1966) cited the measurements of rock characteristics by Acker and Mueller (1966) from 3 km drill holes associated with a full scale propagation experiment. His conductivity profile is summarized in Levin (1971) and shown in Figure 2.5. The variation of dielectric constant is discussed later in the paper by Schwering, Peterson, and Levin (1968), and is overlooked by many authors.

In his AGARD paper, Levin (1966) concluded that "full scale studies of lithospheric propagation must be carried out in boreholes nearly 10 km deep

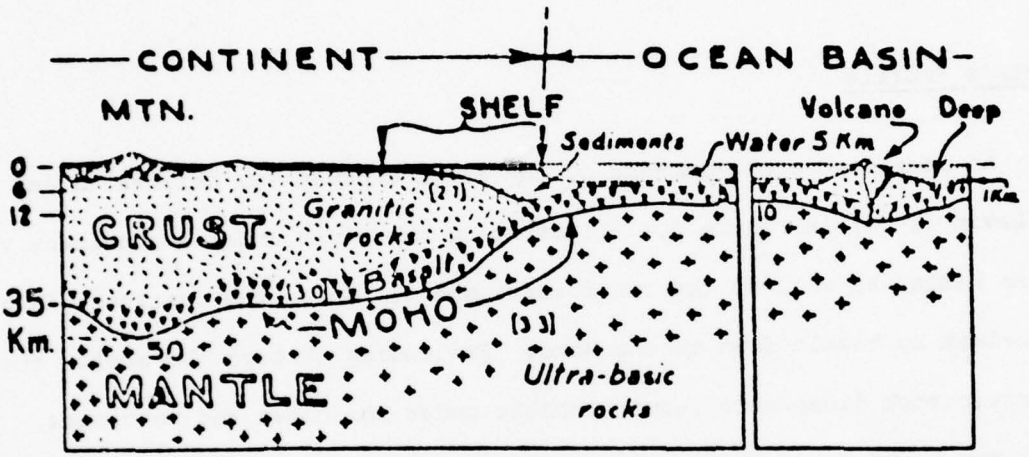

Figure 2.4 Levin's idealized cross-section of the earth's crust (Levin,1966)

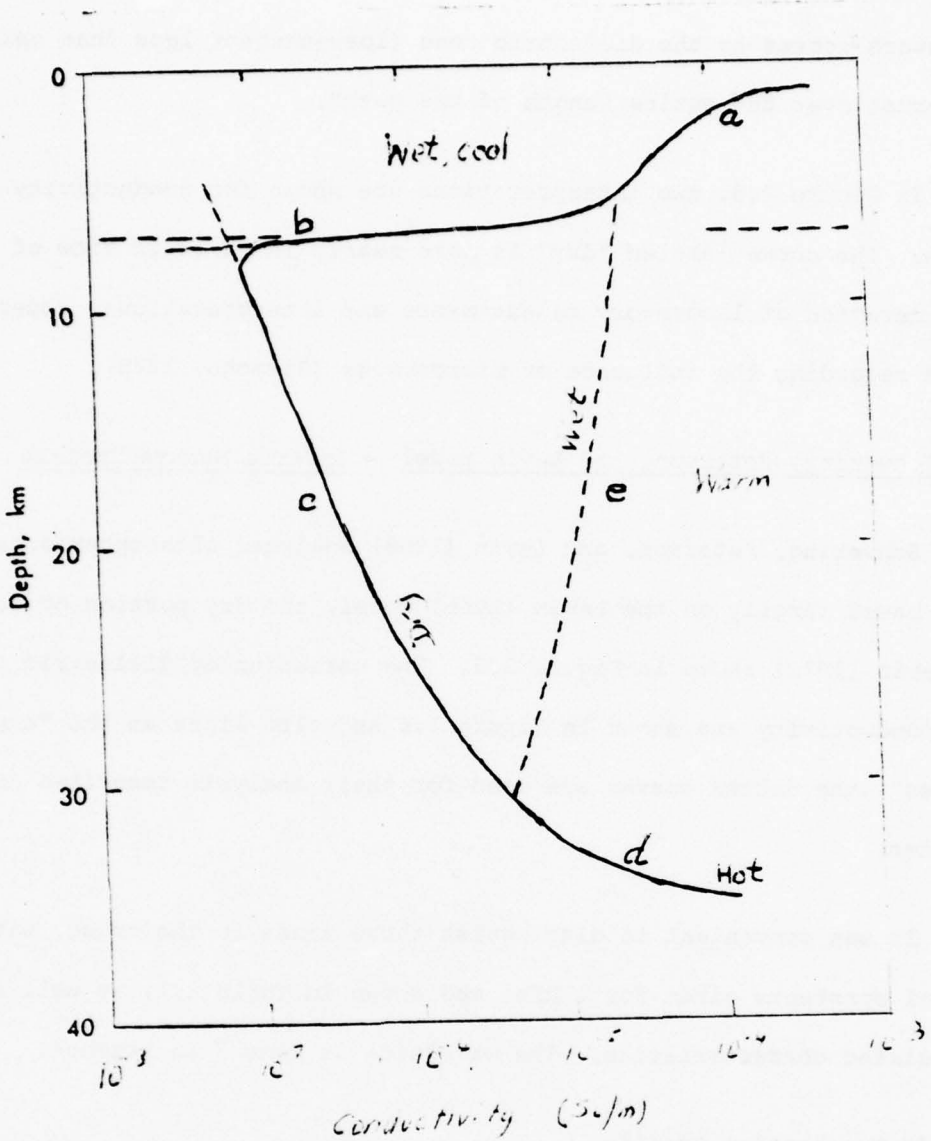

Figure 2.5 Levin's conductivity profiles according to two hypotheses. One profile is abcd; the other is aed. (Levin,1971; see also Levin,1966)

to assure access to the dielectric zone (loss-tangent less than unity) of the crust over the entire length of the path".

In Figure 2.5, two interpretations are shown for conductivity vs. depth. The curve labeled "dry" is more nearly in favor in view of recent consideration of laboratory measurements and interpretations, especially those regarding the influence of microcracks (Simmons, 1978).

2.6 The Schwering, Peterson, and Levin Model - Inverse Square Profile

Schwering, Peterson, and Levin (1968) analyzed lithospheric propagation based largely on the Levin (1966) model, the dry portion of conductivity of Levin (1971) shown in Figure 2.5. The variation of dielectric constant and conductivity are shown in Figure 2.6 as solid lines as the "experimental values"; the dotted curves are used for their analysis described in the next Chapter.

It was convenient to distinguish three zones in the crust, with electrical constants given for 1 kHz, and shown in Table 2.1, as well as other postulated characteristics. The waveguide is Zone 2 in essence.

2.7 Wait's Exponential Profile

After studying the performance of electrical constants in a number of ways, Wait (1966c), offered a unique profile suitable for analysis (Wait 1966a, 1971), to attempt a quantitative result. His model is illustrated in Figure 2.7. In a cylindrical coordinate system, the plane $z = 0$ separates the highly conducting overburden having a complex relative dielectric constant K_g, the overburden top being at $z = -h$. The basement has a relative dielectric constant $K(z)$ which is complex, having a constant relative

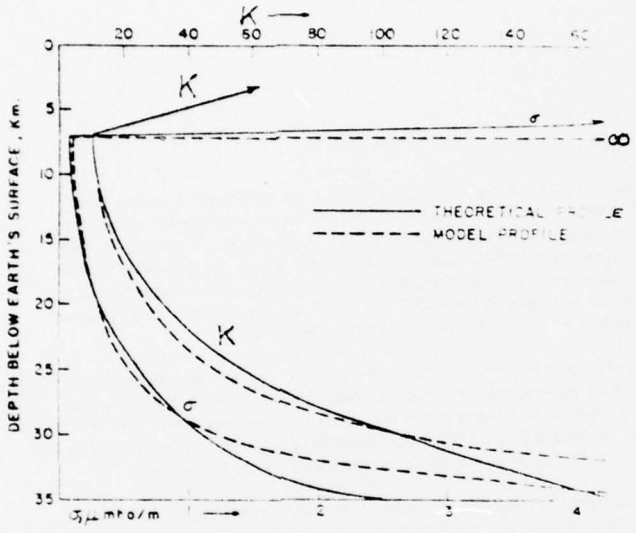

Figure 2.6 Schwering, Peterson and Levin (1968) profiles of relative dielectric constant and conductivity. See also Wait,1971. Dashed curve is the model profile; solid curve is that used for theoretical analysis.

CRUSTAL ZONES

Zone 1 (Upper). Cool but *wet*. Superficial zone of porous and fractured, sedimentary, igneous, and metamorphic rocks (open system) groundwater saturated, climate and terrain permitting. Conductivity and dielectric permittivity controlled by the water distribution, hence characterized by great variability, high to low values, large negative gradient with depth, $\sigma = 10^{-1}$ to 10^{-5} mho m, $\varepsilon = 10^{6}$ to 10^{1}; loss tangent $\delta > 1$. Probable depth extent about 7 km.

Zone 2 (Middle). Warm and *dry*. Zone of tight granitic basement rocks, more homogeneous, relatively closed system, little or no molecular H_2O, typical of silicate dielectric. Low to moderate ($\sigma 10^{-8}$ to 10^{-5} mho m) and ($\varepsilon 10$ to 100), both exhibiting positive exponential gradients with depth; $\delta < 1$. Zone extends to 35 or 40 km depth.

Zone 3 (Lower). Dry but *hot*. Bottom zone of the crust, possibly extending into the mantle. Anhydrous silicate mineral assemblage of plutonic facies. Intrinsic and ionic charge carriers lead to moderate to high conductivity and permittivity ($\sigma > 10^{-5}$, $\varepsilon > 100$), with very large positive gradients, $\delta \geq 1$.

Note: The values of σ, ε and δ apply to a frequency of 1 kHz.

Table 2.1 Descriptions of crustal zones according to Schwering, Peterson, and Levin given in their 1968 article, Schwering, Petersen, and Levin (1968)

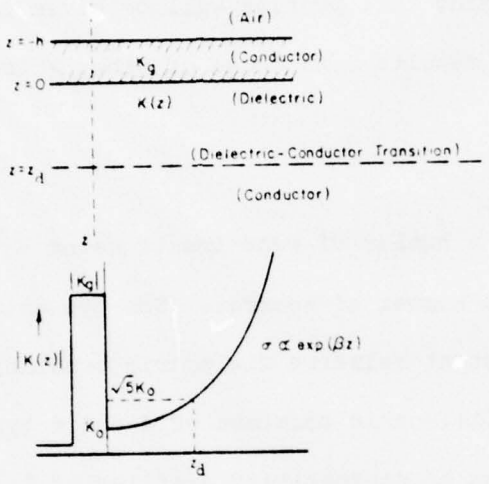

Figure 2.7 Wait's analytical profile. K is the complex appropriate relative dielectric constant; the conductivity profile in the waveguide is exponential in form. See Wait, 1971; also Wait, 1963, 1966a, c.

dielectric constant and a conductivity which increases exponentially with depth. The reference depth was chosen for convenience as that depth z_d where the loss tangent was two; for VLF it appears that z_d is of the order of 30 km. At very great depths, where the loss tangent greatly exceeds unity, K(z) varies exponentially with depth. Near z = 0, the ideal case would have K(0) real.

The results of using this profile will be given in the next Chapter where he compares his results with those of other authors.

2.8 Iizuka's Profiles

Iizuka performed a number of experiments using a "typical" lithospheric profile deduced from a number of sources. The typical case of a profile of loss-tangent with constant relative dielectric constant is shown in Chapter 5, Figure 5.6. for a dielectric constant of 4 and a typical frequency of 5 kHz. The compilation of conductivity profiles of Iizuka (1968) is shown in Figure 2.8. They were deduced from Wait (1963), Wheeler (1961), Mott and Biggs (1963), Keller (1963), Ames, Frazier, and Orange (1963), Cantwell and Madden (1960), Watt, Mathews, and Maxwell (1963), deBettencourt and Frazier (1963), Garland and Webster (1960) among others.

In Figure 2.8, the conductivity is plotted as a function of depth to depths of 40 km or slightly more. The conductivity ranges from 10^{-8} to 10^{-1} Si/m, the larger values being near the earth's surface or at great depths. Since he preferred an analysis based upon loss-tangent, he noted "lower limit of tan δ" near a conductivity of 10^{-8} Si/m and a higher limit near 10 km depth with a conductivity of about 10^{-4} Si/m. (For his "typical"

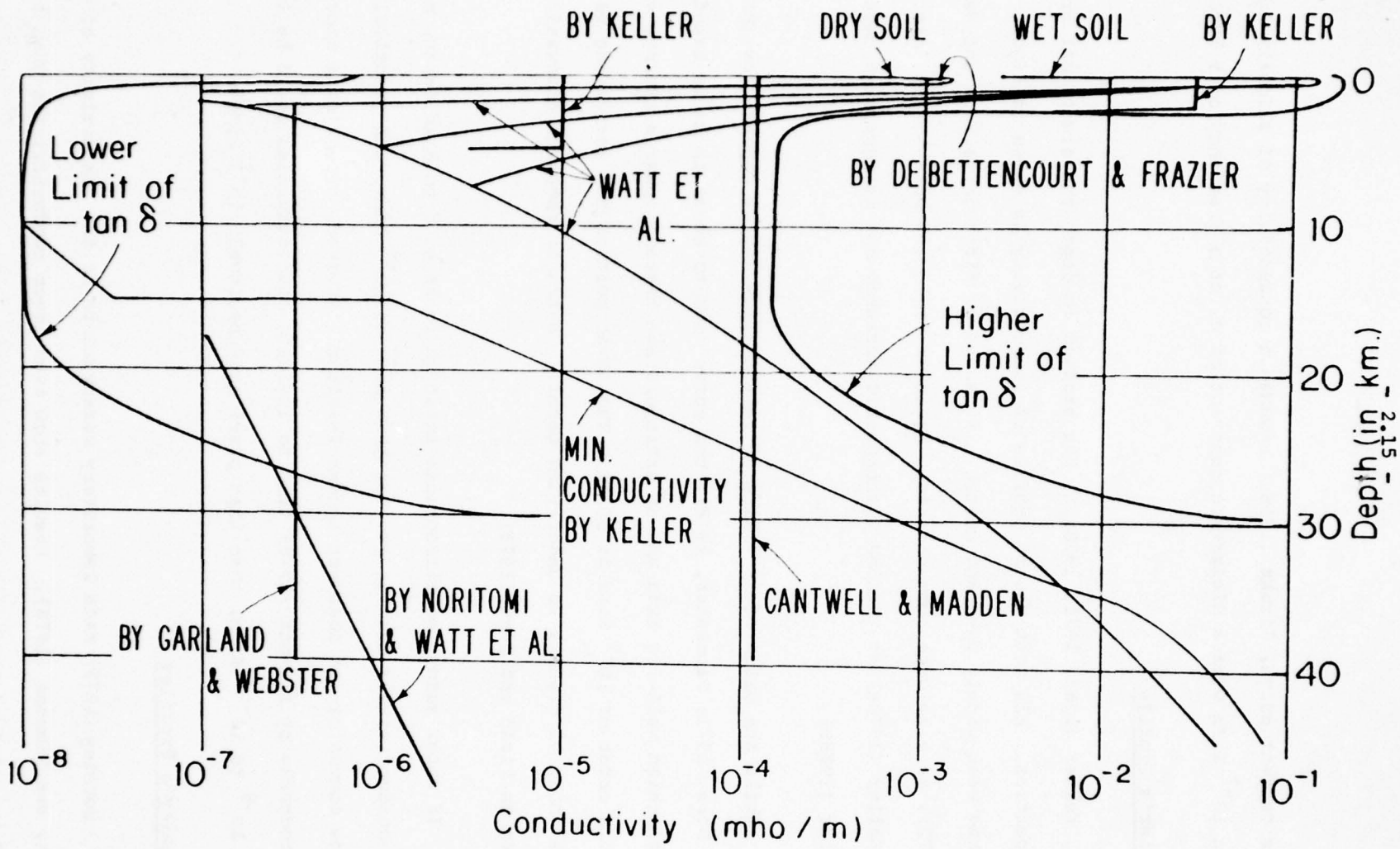

Figure 2.8 Iizuka's summary of conductivity profiles from various sources, circa 1963. Iizuka (1968). See text.

loss tangent curve, Iizuka (1968) assumed a conductivity of slightly less than 10^{-7} Si/m with a dielectric constant of 4, at a frequency of 5 kHz)

2.9 Keller's Profile

Keller (1963, 1971, 1978a,b) has studied in depth the electrical crustal properties. His most recent profile of conductivity is shown in Figure 2.9. It has been widely used and quoted. It appeared first in Gallawa and Haidle (1972), as a private communication, again in Field and Dore (1973), discussed by Keller (1978a) at the ONR Lithospheric Workshop and is reprinted here from Keller (1978b).

While the value of 10^{-4} Si/m at very shallow depths appears low (Field and Dore, 1973; Bannister, 1978), the curve down to about 10 km is based on Appalachian well-log data and an extrapolation thereof towards minimum values of the order of 10^{-7} Si/m at 10 km. The lower portion has increasing values from those of granite to underlying basalt. A rather complete discussion is given in Field and Dore (1973).

If water saturated microcracks exist in rocks at 5 to 8 km depth, minimum conductivities must be greater than 10^{-5} to 10^{-6} Si/m, and practical long range communication does not appear feasible. However, recent data concerning microcracks by Simmons (1978) tend to indicate conductivities could be lower, say 10^{-8} to 10^{-10} Si/m, than that previously believed (10^{-7} Si/m).

2.10 Housley's Profiles

Housley (1973) made laboratory measurements on the conductivity of dry rock, see Simmons (1978). Results show even lower conductivities than those of Figure 2.5 of Levin and Figure 2.9 of Keller. Using the new conductivity

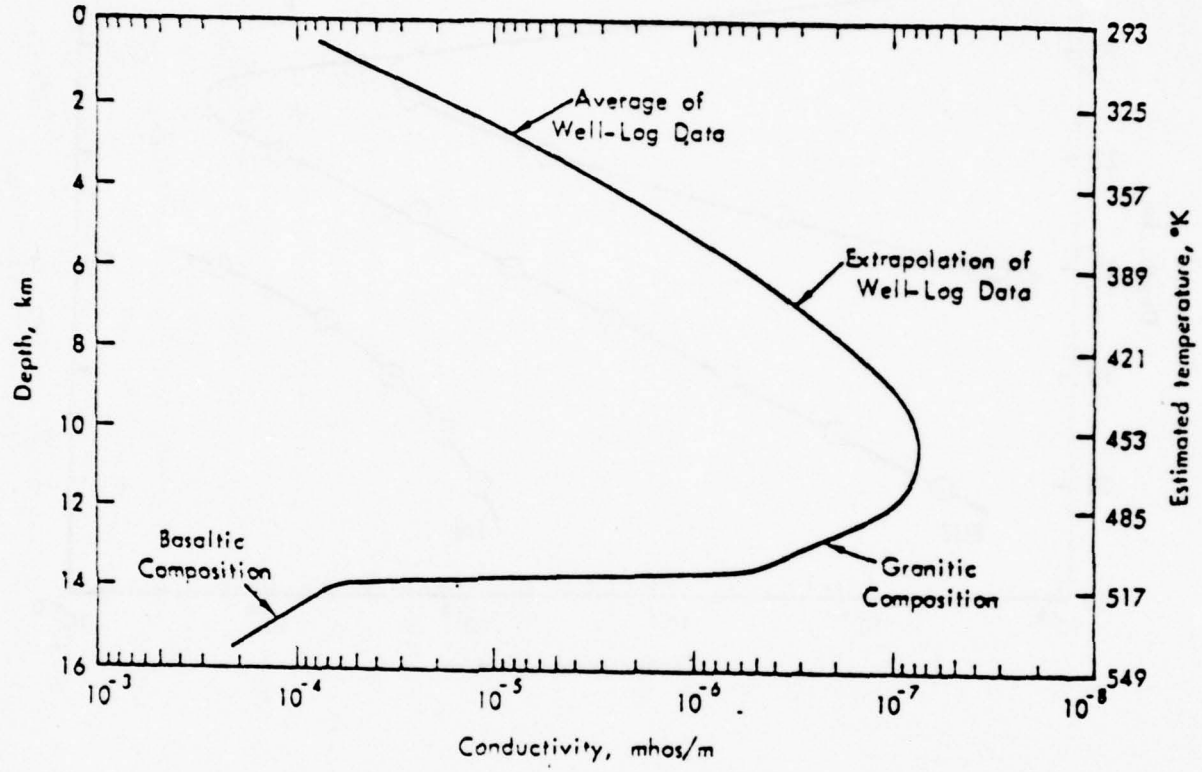

Figure 2.9 Keller's profile of conductivity and temperature vs. depth. From Field and Dore (1973), first as a private communication in Gallawa and Haidle (1972), and discussed by Keller (1978a,b). See also Bannister (1978).

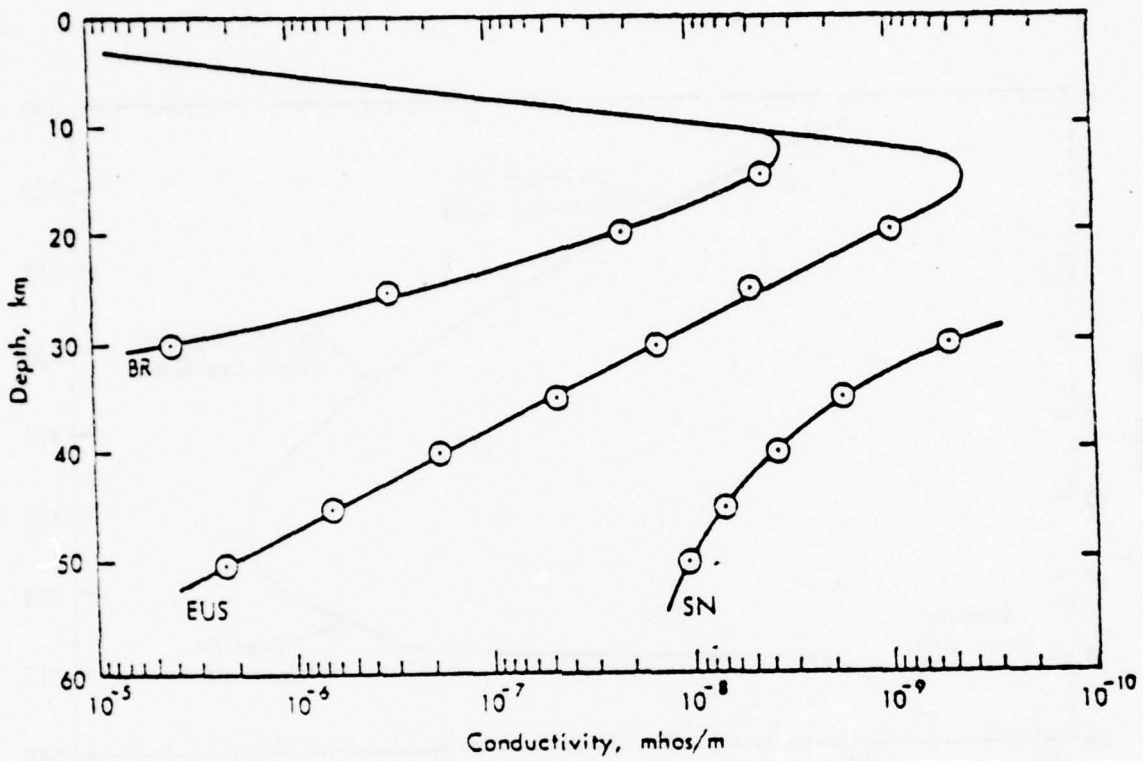

Figure 2.10 Housley's (1973) conductivity profiles, for three heat-flow provinces. From Field and Dore (1973) as private communication. See also Parnister (1978).

data, the profiles are similar to those of Keller in Figure 2.9, for depth less than 10 km, and are shown in Figure 2.10. At greater depths, much lower conductivities are indicated (less than 10^{-8} Si/m).

The three profiles correspond to geotherms in three different heat flow provinces (i.e., BR = Basin and Range; EUS = Eastern United States; SN = Sierra Nevada). The thermal gradients for the Keller model was 16^{o}/km, while for the Housley provinces they were BR (24^{o}/km), EUS (14^{o}/km), and SN (9^{o}/km), where the temperature is in (^{o}C).

2.11 Comment

There are many differing profiles of conductivity vs. depth which are not necessarily definitive. Continued experimental work remains to be done in the laboratory - see Simmons (1978) - and in the field - see Keller (1978a).

3. Summary Review of Theories

3.1 Introduction

When viewing the number of more recent depth profiles of electrical constants in Chapter 2, such as those of Keller in Figure 2.9 and of Housley in Figure 2.10, interest has been revived in the possibility of long-distance communication via a sub-surface waveguide. The minimum conductivities are several orders of magnitude lower than those postulated in the early 1960 era. The lower conductivity values have received support from studies of the effects of microcracks by Simmons (1978).

A number of review papers (Rjanzcev and Shabel'nikov, 1966; deBetten-court, 1966; Levin, 1966, 1971; Wait, 1966c, 1971; Gabillard, 1966; Gabillard, Degauque, and Wait, 1971; and Bannister, 1978) have been published on the various mechanisms dealing with lithospheric propagation, including ground waves, "up-over-and-down," and sub-surface waveguide mechanisms plus communication parameters of antennas, noise, etc. Here we shall briefly summarize those papers dealing principally with the crustal waveguide mechanism. Many focus attention on attenuation of the modes, a few give examples of field strength variations.

3.2 Some Early Works

It is interesting to realize that two of the earliest papers considered the possibility of using the lower-loss region of the crust for the purpose of illustrating a potential mechanism for communication with submarines at great depth.

Wheeler's (1961) very early concept was shown in Figure 2.1. He imagined the existence of a very deep waveguide. With a relative dielectric constant of 6 and a conductivity of 10^{-6} to 10^{-11} Si/m, he obtained a total attenuation of the TEM launched wave of 0.067 dB/km.

Mott and Biggs (1963) also considered undersea communication between two vertical electrical dipoles (VED) both inserted into lower conductivity crustal rock. They envisioned propagation at frequencies of the order of 100 kHz to take place in a plane half space of conductivity 10^{-6} to 10^{-7} Si/m bounded on top by the layer (ocean) having a conductivity of 4 Si/m. They go on to assume the lower region attenuates the wave but does not affect the propagation mechanism - surface wave along the interface like normal surface wave propagation in air above the sea but where the air has been replaced by the rock. See also Carolan and deBettencourt (1963). At lower frequencies, less than 10 kHz for example, the lower region behaves as a waveguide, and "that a TEM waveguide mode will be important", as Wheeler (1961) had postulated. Their conductivity profile is shown in Figure 2.2(c).

3.3 Slabs with Uniform Depth Profiles

For analytical studies of their depth profile shown in Figure 2.3, Brown and Gangi (1962, 1963) and Gangi (1966) assumed the crustal waveguide to be a homogeneous slab bounded by two half-spaces which were highly conducting.* For their analysis, the boundaries were assumed to have effectively infinite conductivity. The waveguide was excited by a vertical electric dipole.A mode series representation was used to obtain the field.

*Reference may be made to Figure 5.1 for a sketch of the guide.

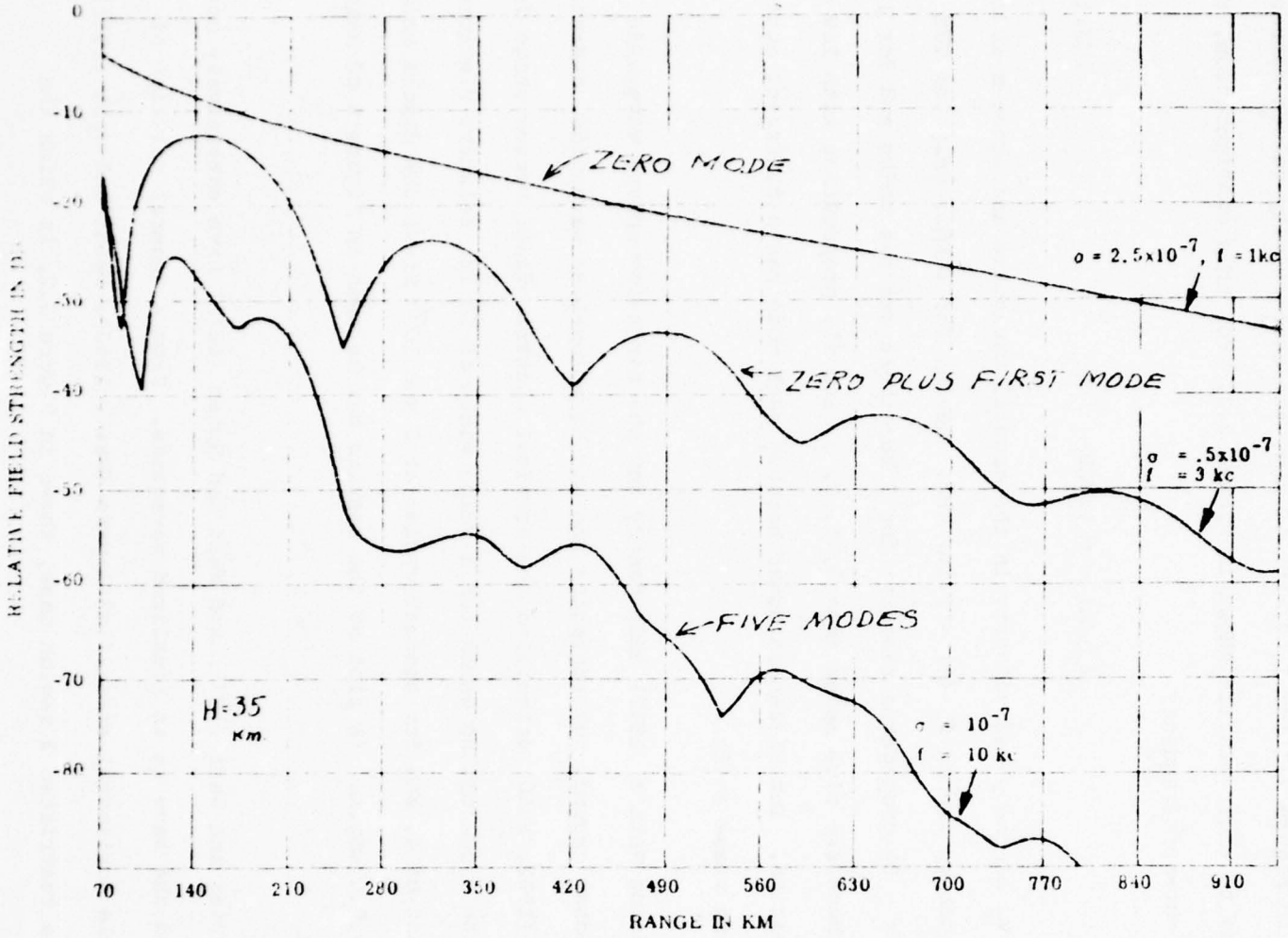

Fig. 3.1 Theoretical Vertical electric field strength vs. Range (Brown and Gangi, 1963)

Calculations were made of the vertical electric field strength versus range for several low frequencies for a guide depth H = 35 km, a relative dielectric constant of 4 and zero antenna depths. A typical result is shown in Figure 3.1 for 1, 3, and 10 kHz, the conductivity values corresponding to their profile shown in Figure 2.3. For this configuration, the modal cut-off frequency

$$f_c\ (m) = m\ v_2/2H \qquad (3.1)$$

where v_2 is the phase velocity in the crustal waveguide and where m is the mode number, whence $f_c\ (m) = 2.1m$, kHz. Hence, for 1 kHz, only the TEM mode (m = 0) propagates readily; for 3 kHz there are two modes and for 10 kHz, there are five modes (m = 0, 1, 2, 3, and 4), propagating with low attenuation. Interferences occur because each mode has a different attenuation and phase shift.

Using Wait's (1957) mode theory for the earth-ionosphere waveguide with lossy ground, but replacing the air by a low-loss waveguide, deBettencourt (1962, 1966) calculated the vertical electric field versus range for infinitely conducting walls for a guide width of 20 km, relative dielectric constant of 4, and for conductivities of 0 and 10^{-6} Si/m; the dipole moment was 16,900 amp.m. (A plot of the results may be seen in Figure 6 of Wait, 1966c).

Spies and Wait (1971) and Wait and Spies (1971) have extensively considered the wave in an idealized waveguide. From a general solution of multiple horizontal stratified layers (Wait, 1962), Spies and Wait (1971) chose a restricted 3 region case, shown in Figure 3.2, in which the

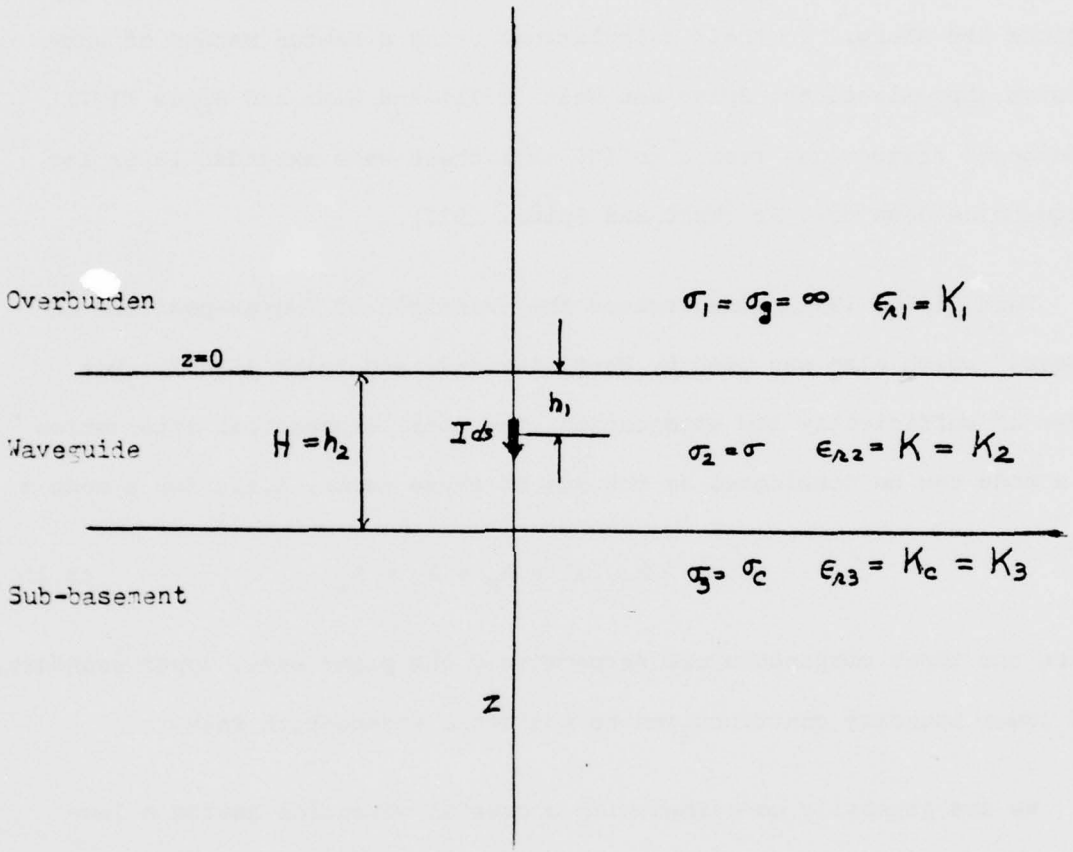

Figure 3.2 Special case of crustal waveguide considered by Spies and Wait (1971) and Wait and Spies (1971, 1972).

"overburden" region had infinite conductivity, the crustal "waveguide" (region 2) had uniform conductivity of $\sigma_2 = \sigma$ and relative dielectric constant K_2, and the "sub-basement" (region 3) had a conductivity $\sigma_3 = \sigma_c$ and relative dielectric constant of K_c, and was infinitively thick. The waveguide has a thickness $h_2 = h = H$. The boundaries of the various regions are sharp. In their calculations using a Newton method of successive approximations, Spies and Wait (1971) and Wait and Spies (1971) considered frequencies from 1 to 100 kHz; these were extended later for frequencies down to 1 Hz (Wait and Spies, 1972).

Wait (1966, 1971) demonstrated the principle of "super-position of losses," which also was used by Watt, Leydorf, and Smith (1966). For modes of sufficiently low attenuation, the total exponential attenuation of a mode can be considered as the sum of three terms, i.e., for a mode m

$$A_t\ (m) = A_p + A_u + A_\ell \qquad (3.2)$$

where the three components are respectively the plane wave, upper boundary, and lower boundary contributions to the total attenuation rate.

We are generally concerned with a crustal waveguide having a low-loss-tangent region whence it can be shown that

$$A_p = 1.64 \times 10^6\ \sigma_2/\sqrt{K_2} \qquad \text{dB/Km} \qquad (3.3)$$

and is independent of frequency if the electrical "constants" are constant. For a given plane slab boundary, the wall attenuation contribution depends upon the guide loss-tangent and whether the boundary is electrically thick or thin. Expressions based on approximation similar to those of Wait (1963)

have been given for several cases by Watt et al. (1966). As aforementioned, we are generally interested in the crustal waveguide which has a low loss-tangent, and the boundary layers have a high loss-tangent, and are electrically thick. For this case, if σ_B is the conductivity of one of the uniform slab boundary layers, then Watt et al (1966) give the boundary attenuation for the TEM (m = 0) mode as

$$A_B\ (0) = 2.29 \times 10^{-2}\ \ (K_2 f/\sigma_B)^{\frac{1}{2}}/H \qquad \text{dB/Km} \qquad (3.4)$$

Whilst for the TM_I Mode (m = 1)

$$A_B\ (1) = 4.58 \times 10^{-2}\ \ (K_2 f/\sigma_B)^{\frac{1}{2}} \left[1-(f_c/f)^2\right]^{-1/2} /H \ \text{dB/Km} \qquad (3.5)$$

where f_c is f_c (m = 1) from equation (3.1)

In Figures 3.3 and 3.4, taken from Spies and Wait (1971), the total attenuation for modes of lowest attenuation are shown as functions of frequency for a guide thickness of H = 20 km, and upper layer of infinite conductivity, the waveguide with a dielectric constant K = 9 and conductivities of 10^{-6} or 10^{-7} Si/m, and the sub-basement layer with a uniform dielectric constant of K_c = 15 and a conductivity of 10^{-2} Si/m (Figure 3.3) or 10^{-3} Si/m (Figure 3.4).

In a manner similar to that of Bannister (1978), we made calculations for a frequency of 10 kHz, the model cut-off frequency being 2.5m kHz. (The loss-tangent of the waveguide region is very small. The plane wave attenuation A_p for $\sigma_2 = 10^{-7}$ Si/m, K_2 = 4 works out to be .0546 dB/Km, whilst for $\sigma_2 = 10^{-6}$, it becomes 0.546 dB/Km. The plane wave attenuation is critically dependent on conductivity.

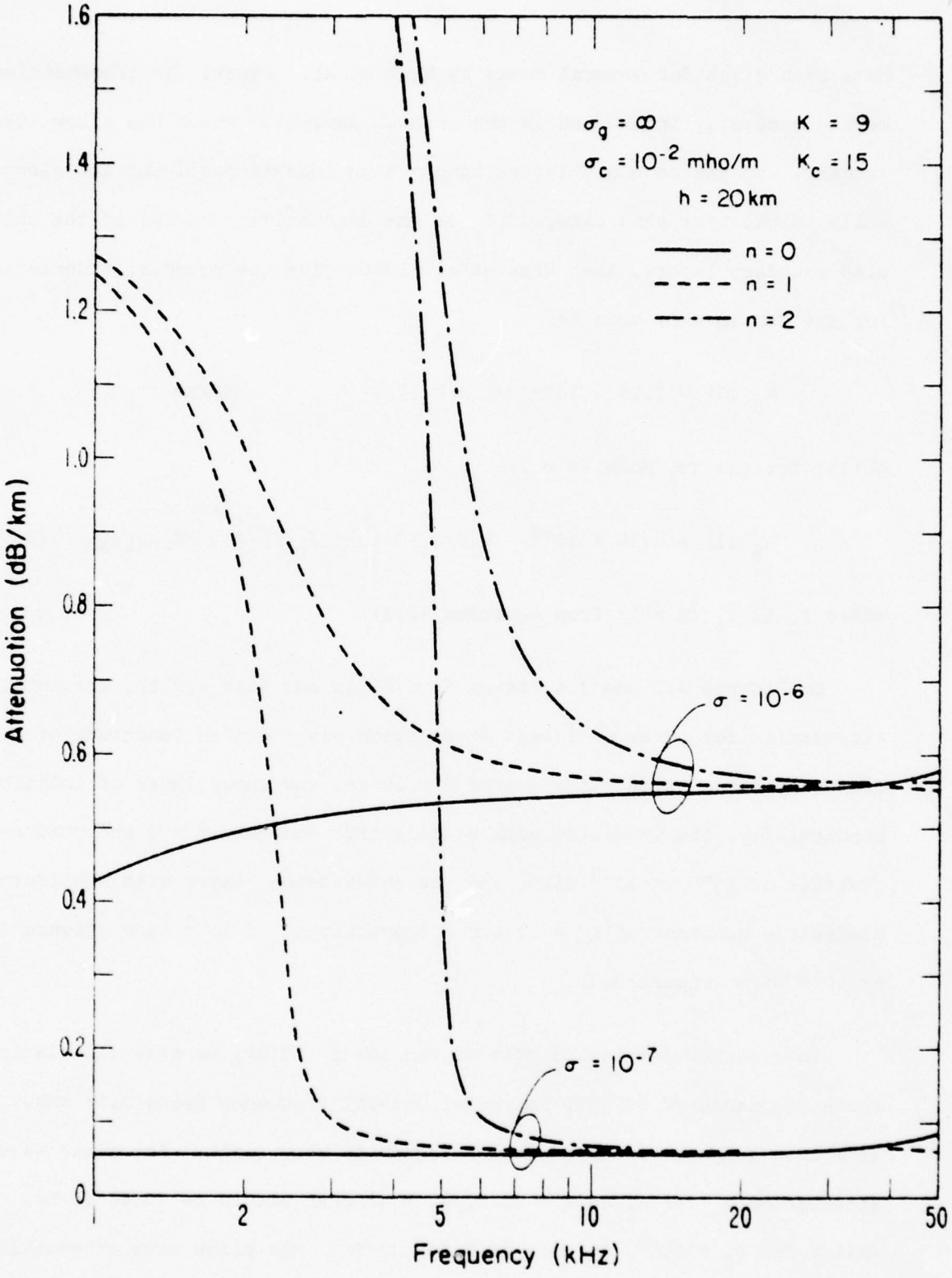

Fig 3.3 Wave guide attenuations for mode n for idealized wave guide shown in Fig. 3.2 (Spies and Wait, 1971)

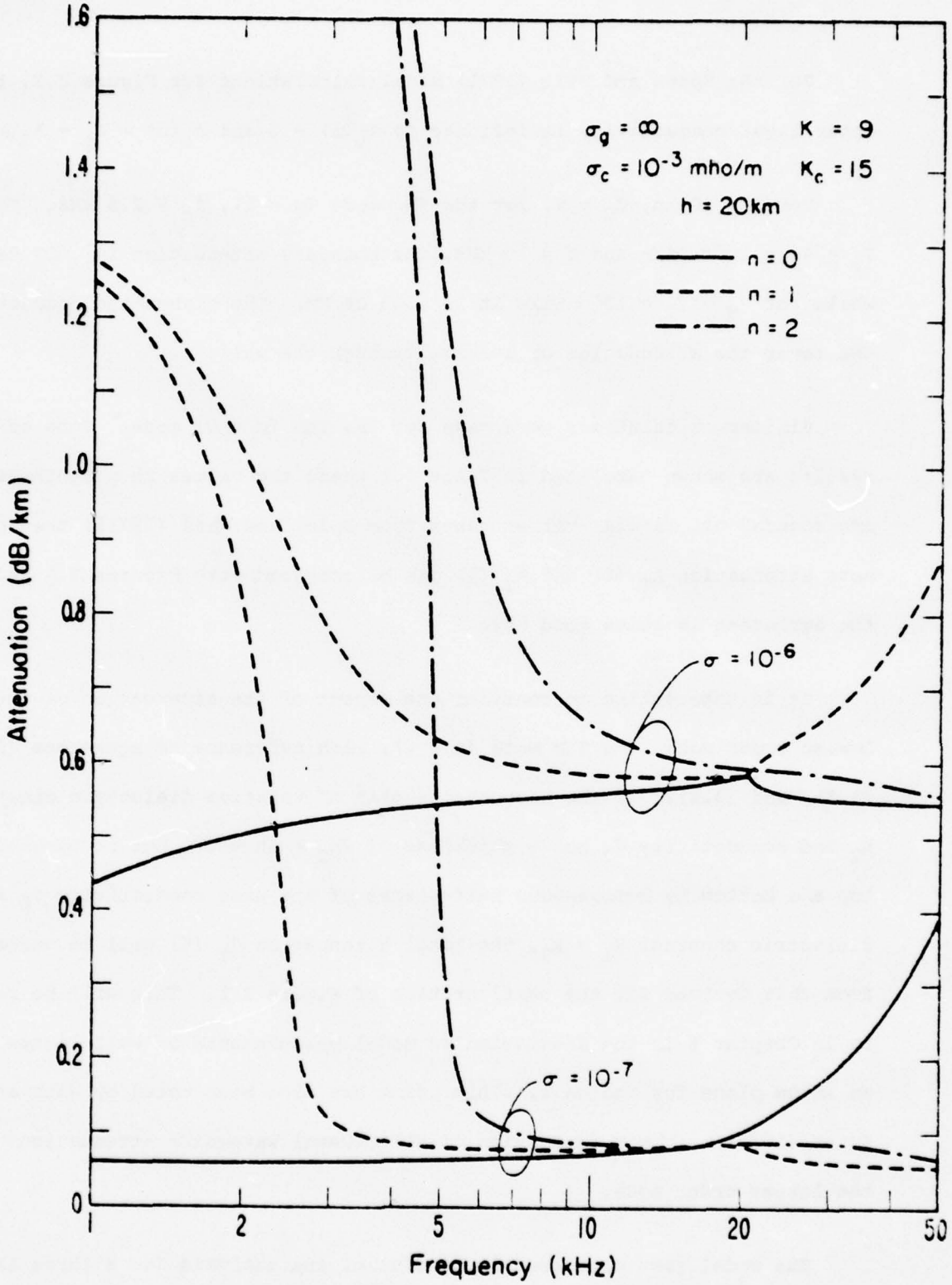

Fig.3.4 Same as Fig.3.3, but for $\sigma_c = 10^{-3}$ Si/m (Spies and Wait,1971)

For the Spies and Wait (1971) model calculations for Figure 3.2, the upper layer conductivity is infinite so $A_u(m) = 0$ and $A_t(m) = A_p + A_\ell(m)$.

For H = 20 km, $K_2 = 9$, for the TM_1 mode (m = 1), $f_c = 2.5$ kHz. For $\sigma_B = \sigma_c = 10^{-2}$ Si/m and f = 10 kHz, the boundary attenuation is .007 dB/Km while for $\sigma_B = \sigma_2 = 10^{-3}$ Si/m it is .023 dB/Km. The higher the conductivity, the lower the attenuation or leakage through the wall.

Similar calculations were made for the TEM (m = 0) mode. Some of the results are shown tabulated in Table 3.1 where the values in parentheses are rounded off tabular values taken from Spies and Wait (1971); the approximate attenuation A_T (0) and A_T (1) can be compared with Figures 3.3 and 3.4; the agreement is quite good here.

It is interesting to consider one aspect of the attenuation of the lowest order mode, the TEM mode (m = 0), with reference to equations (3.2), (3.3), and (3.4). If the homogeneous slab of relative dielectric constant K_2 and conductivity σ_2 has a thickness of $2h_2 = 2h = 2H$, but is bounded on top and bottom by homogeneous half-spaces of the same conductivity σ_B and dielectric constant $K_1 = K_3$, the total attenuation σ_T (0) will be unchanged from that derived for the configuration of Figure 3.1. This will be referred to in Chapter 6 in the discussion of model measurements of wall losses with an image plane for region 1. This point has also been noted by Wait and Spies (1972) in their discussion of ELF crustal waveguide attenuations for the lowest order mode.

The model just discussed is mindful of the analysis for a three layer structure, shown in Figure 3.5(a), as considered by Viggh (1963). His slab

TAPLF 3.1

Approximate versus exact modal attenuations for modes of low attenuation, for for idealized waveguide shown in Figure 3.2

$\sigma_1 = \sigma_g = \infty$ $h_2 = H = 20$ km. $f = 10$ kHz $\epsilon_{r2} = K_2 = 9$ $\epsilon_{r3} = K_3 = 15$

TEM (m=0)				TM_1 (m=1)			
			$\sigma_3 = 10^{-2}$ Si/m				
σ_2	A_p	$A_3(0)$	$A_T(0)$	σ_2	A_p	$A_3(1)$	$A_T(1)$
10^{-6}	.546	.004	.55 (.55)	10^{-6}	.546	.007	.55 (.57)
10^{-7}	.055	.004	.059 (.059)	10^{-7}	.055	.007	.062 (.064)
			$\sigma_3 = 10^{-3}$ Si/m				
10^{-6}	.546	.011	.56 (.56)	10^{-6}	.546	.023	.57 (.59)
10^{-7}	.055	.011	.066 (.071)	10^{-7}	.055	.023	.078 (.080)

For comparison, the figures in parentheses are from Spies and Wait, 1971, tables. The attenuations A are in dB/km.

of depth D with conductivity $\sigma_2 = 10^{-6}$ Si/m was bounded by identical top and bottom half spaces with conductivities $\sigma_1 = \sigma_3 = 10^{-2}$ Si/m; all three regions had the same relative dielectric constant of 10. The slab was electrically thin so that only the TEM mode was considered dominant. An example of the attenuation as a function of thickness is shown in Figure 3.5(b) where frequency is the parameter; both scales are logarithmic.

Waveguides having low loss-tangents but bounded by layers on top and bottom have been considered by Gabillard (1966) and in a review paper given by Gabillard, Degauque, and Wait (1972). Essentially these papers refer to the work in France where they were able to demonstrate the propagation effects in mine galleries and in a uniform gypsum layer.

3.4 Non-homogeneous Depth Profiles

3.4.1 Wait's Exponential Profile

Besides the aforementioned works of Wheeler (1961) and Mott and Biggs (1963) another early paper was that of Wait (1963, 1971)who considered the analysis of the exponential depth profile shown in Figure 2.7 in order to obtain quantitative results. For z positive, the complex relative dielectric constant was chosen for convenience to be exponential in form and given by

$$K(z) = K_o \left[1-j2 \exp B(z-z_d)\right] \tag{3.6}$$

where z_d is the waveguide "depth" which is discussed below.

For z = 0, at the top of the waveguide

$$K(0) = K_o \left[1-j2 \exp (-Bz_d)\right] \cong K_o \tag{3.7}$$

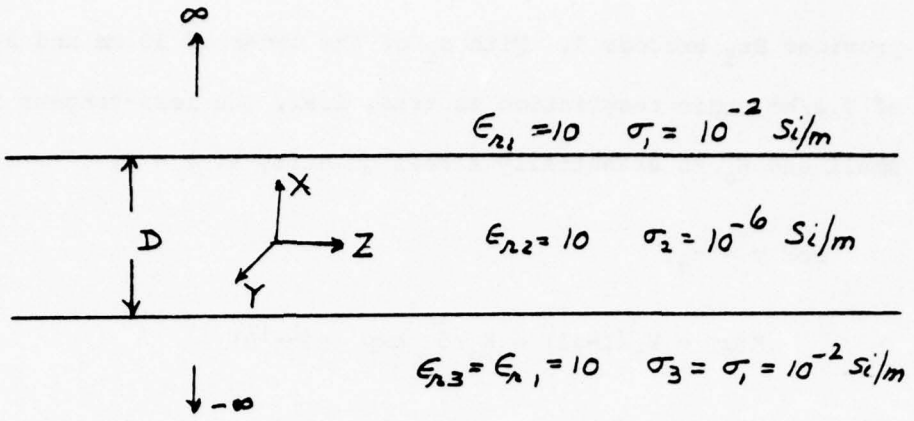

(a) Three-layer structure for analysis

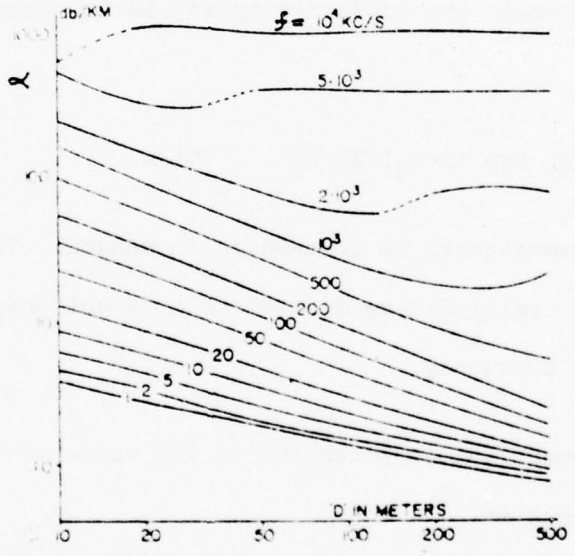

(b)

Fig.3.5 (a) Three-layer structure for analysis: (b) Attenuation α for electrically thin waveguide layer vs. layer thickness D , with frequency as the parameter. (Viggh,1963)

provided Bz_d exceeds 3. With z_d of the order of 30 km and B of the order of 0.2/km, this restriction is true, i.e., the loss-tangent is extremely small and K_o is essentially a real quantity at z = 0.

For $z = z_d$,

$$K(z) = K_o(1-j2) = K_o\sqrt{5} \exp(-j1.11) \tag{3.8}$$

That is, the loss tangent at $z = z_d$ is 2.

For very large depths

$$K(z) \cong -j|K(z)| = -j2K_o \exp B(z-z_d) \tag{3.9}$$

Since K_o is real, the conductivity may be expressed as a function of depth as

$$\sigma(z) = K_o \exp (z-z_d)/30\,\lambda_o \quad \text{(Si/m)} \tag{3.10}$$

where λ_o is the wavelength in free-space in meters. These expressions assume that this real relative dielectric constant and conductivity are not functions of frequency.

At z = 0, where the loss-tangent of the guide is very small, we designate the wavelength as

$$\lambda_2' = \lambda_o/K_o^{\frac{1}{2}} \tag{3.11}*$$

Wait (1963) derives the vertical field strength for a VED in the waveguide from a vertically directed Hertz vector. From the residues at the poles of the denominator in the expression for the latter, he obtains the

---

*Wait uses the quantity λ_o to designate what we have called λ_2'

model resonance condition, finally expressing the field E_z as $E_o W$ where E_o is a reference field. This reference field is that of a vertical dipole in a dielectric half-space erected on a perfectly conducting ground plane of infinite extent. The expression for W is dimensionless and contains all the characteristics of the waveguide modes. Because the lower boundary is not sharply defined, the mode of lowest attenuation is not the TEM (m = 0) mode but one of the TM modes (m = 1, 2 . . .).

For purposes of illustration, Wait (1963, 1971) calculated the attenuations for modes m = 1 and 2 for the special case where the overburden was so largely conducting that K_g was assumed to be infinite. He chose the case where $\lambda_2' = 15$ km. The attenuations A_1 and A_2 for the modes of lowest attenuation are shown plotted as functions of the quantity B in Figure 3.6(a) and (b), respectively. The parameter on the curves is the waveguide depth in "wavelengths" denoted by z_d/λ_2'.

Wait (1963, 1971) shows how these curves can be scaled for other wavelengths, for a given guide thickness in wavelengths. In these articles and another for plane slabs (Wait, 1966), he illustrates how the total attenuation for the lowest order modes may be shown to be the sum of the three terms, the plane wave attenuation plus the losses in the two "walls" as given in equation (3.2), (Wait, 1971).

For the dominant mode attenuation, he notes the comparison of values of Schwering, Peterson, and Levin (1968) for their inverse square profile of 0.256 dB/km compared with that value (0.275 dB/km) they obtained using Wait's (1963) method. Wait's (1963) values, he notes, lead to lower attenuations than those of Schwering et al (1968) because of the steeper gradients.

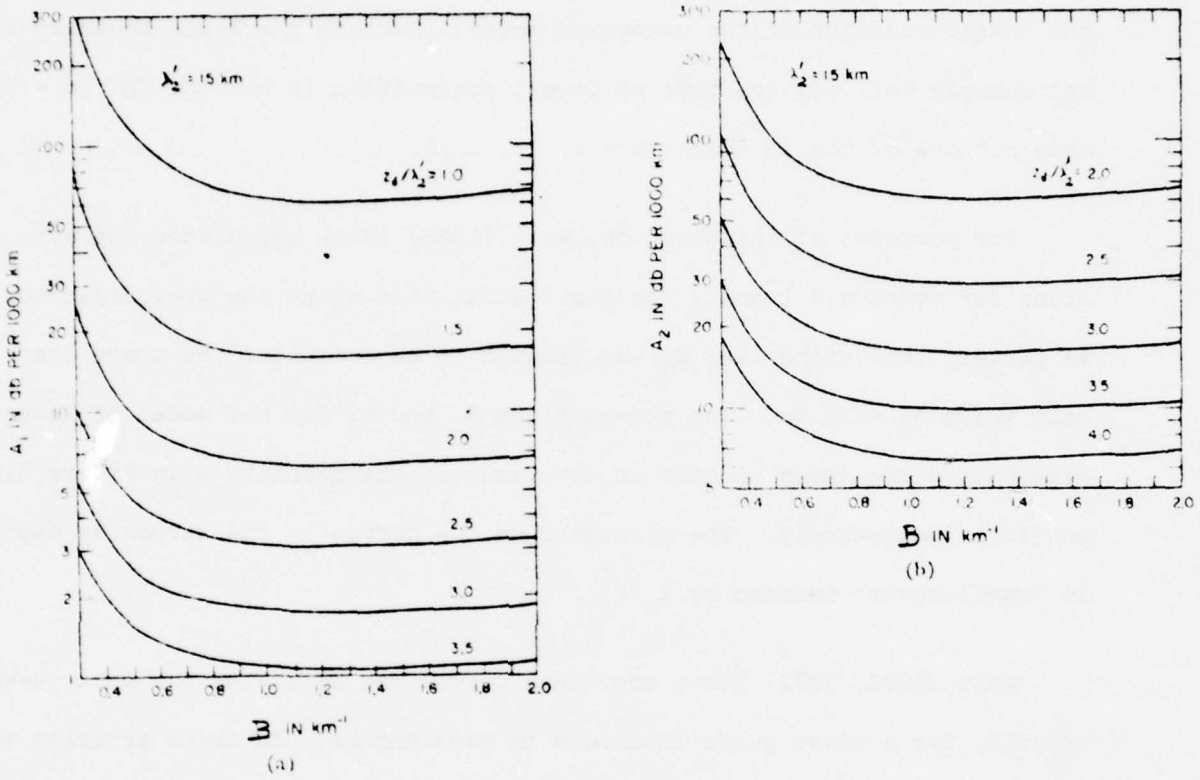

Fig. 3.6 Attenuation rates for an exponential depth profile as a function of B for various values of zd/λ_2', which is the depth of the guide in "wavelengths". (a) Attenuation rate A_1 for the first mode. (b) Attenuation rate A_2 for the second mode. Note that the unit of attenuation is in dB/Mm, and that K_g is infinite. (From Wait,1963).

3.4.2 The Inverse Square Profile of Schwering, Peterson, and Levin

The depth profile of Schwering, Peterson, and Levin (1968) is shown in Figure 2.6, the dashed curves being used for analysis. Both the real relative dielectric constant K and conductivity σ vary as the inverse square of the depth z measured positively downward. The vertical electric dipole (VED) is located in the waveguide at z = 0 at the upper wall. The upper zone (overburden) is assumed to be infinitely conducting. The depth dependence is such that both K and σ become infinite again at a depth y_o = 33km, and the conductivity of the lower zone below 33 km is also infinite.

The complex relative dielectric constant may be written

$$K'(z) = K_o(1-jp)F(y_o,z) \qquad (3.12)$$

where $F(y_o,z)$ is the depth dependence factor

$$F(y_o,z) = \left(\frac{y_o}{y_o-z}\right)^2 = \left(\frac{33}{33-z}\right)^2 \qquad (3.13)$$

for the depth z (in km) lying between 0 and 33 km. The real relative dielectric constant at zero depth is K = 10 and the loss-tangent is p = 0.2, for the values assumed by Schwering et al (1968) at a frequency of 1 kHz. For these assumptions, then, the depth dependencies of the real relative dielectric constant and of the conductivity are

$$K(z) = K_o\, F(y_o, z) \qquad (3.14)$$

$$\sigma(z) = 1.11 \times 10^{-7}\ F(y_o, z) \quad \text{Si/m} \qquad (3.15)$$

respectively. If these electrical constants are independent of frequency,

then the loss tangent at any frequency is

$$p(f) = 0.2/f$$

where f is the frequency in kHz.

Schwering et al (1968) employ a z-directed vector potential to obtain a wave equation for this potential by using cylindrical coordinates and related expressions for E_z, H_ϕ and E_r. The wave equation differs from the usual wave equation by the addition of a term due to the non-homogeneous depth behavior of K'(z). Going through the process of separation of variables for the vector potential, the authors arrive at a modal equation for each field component which includes "depth gain" functions. At the depth z = 0, the radial electric field $E_r = 0$, and the corresponding expressions for E_z and H_ϕ are simplified.

For first three modes m = 1, 2, and 3, the attenuation coefficients at 1 kHz are calculated to be 0.256, 1.17, and 1.99 dB/km (taken from Table II of Schwering et al, (1968), which lists values for the first 10 modes).

The magnitude of the vertical electrical field strength is shown plotted in Figure 3.7 for 1 kHz and for the range 20 to 100 km, using the first eight modes. The first mode is dominant at distances in excess of 50 km; the effect of higher order modes is hardly evident in the range of 20 to 50 km.

In Figure 3.8 are shown the frequency variation of the attenuation rate α_1 and phase velocity v_1 of the dominant mode (m = 1), the latter normalized to the velocity in free space (3×10^8 m/sec). There is resultant dispersion of the signal waves, but it becomes small as the frequency increases.

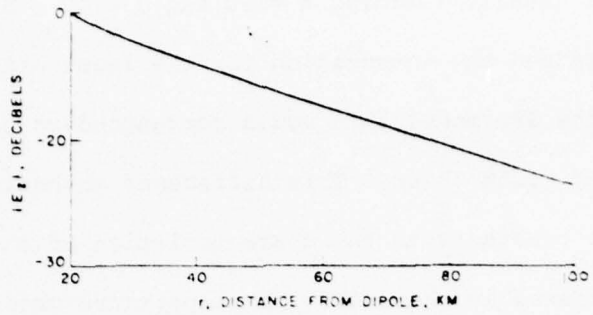

Fig. 3.7 Variation of vertical electric field strength with range at zero depth. (Schwering, Peterson, and Levin, 1968).

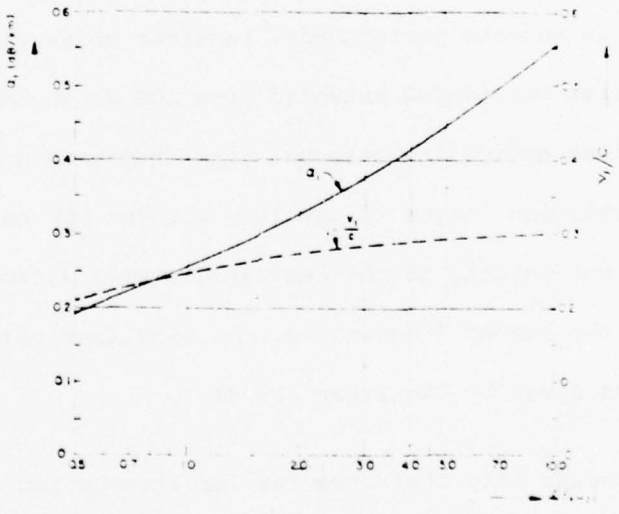

Fig. 3.8 Attenuation rate and normalized phase velocity of dominant mode vs. frequency. (Schwering, Peterson, and Levin, 1968).

Schwering et al (1968) considered the uniform depth profile solution of Brown and Gangi (1963), assuming K = 10 and $\sigma = 10^{-7}$ Si/m for a frequency of 1 kHz; they obtained the attenuation for the least attenuated mode as 0.052 dB/km. In the SPL model this would correspond to the dominant (m = 1) mode attenuation of 0.256 dB/km. This difference emphasizes the sensitivity of the propagation constants to the characteristics of the assumed depth profile. Of importance is the effect of temperature gradient; it is zero for the Brown and Gangi model and about 20^{o}C/km of depth for the SPL model.

3.4.3 Theoretical Results of Field and Dore for More Recent Profiles

Concerned with the possibility of lithospheric waveguide communication systems as a whole, Field and Dore (1973) considered the fields propagated via the more recent non-homogeneous profiles discussed in Chapter 2 plus the effects of depth attenuation of atmospheric noise and other system parameters such as antenna performance, receiver noise figure, and data rates. Frequencies considered extended from 100 Hz to 100 kHz. Using conceptual profiles having dry basement rock indicated more favorable communication transmission ranges in the 30 - 100 kHz VLF band. Presumably this effect was due largely to the heavier downward attenuation of atmospheric noise at the higher frequencies. An excellent review of their system analysis work was given by Bannister (1978).

We shall discuss only their results for attenuation rates, and calculations of field strength versus range and depth.

Field and Dore (1973) used full-wave calculations for the inhomogeneous conductivity depth profiles. Rectangular coordinates were employed for

plane TM waveguide modes propagating in the x-direction for a vertical electric dipole lying along the z-axis. Expressions were developed for the E_x and E_y electric field strength components and a "voltage" normalized magnetic field component $H'_y = 120\pi H_y$ where H_y is the usual magnetic field strength. While their formulations accounted for the depth variation of the real relative dielectric constant, their calculations assumed a constant value of 10 for all depths and profiles.

Presented in Figure 3.9 are the calculated attenuation rates for the modes of least attenuation as a function of frequency for the depth conductivity profiles of Levin (1966) shown in Figure 2.5, of Keller (1972) in Figure 2.9, and Housley (1973) BR profile shown in Figure 2.10. The least attenuated modes are TEM modes for frequencies less than about 2 kHz and the lowest order TM mode for higher frequencies.

In Figure 3.9 it is seen that the attenuation depends markedly on both the minimum conductivity and the gradient of the depth profile. The lowest attenuation occurs for the Housley BR profile, having a minimum conductivity of about 5×10^{-9} Si/m. The Levin (wet) model with a minimum of 10^{-5} Si/m has the highest attenuation. While the Levin (dry) and Keller models have similar minimum conductivities of 10^{-7} Si/m, the attenuation rates at 1 kHz are 0.28 dB/km for the Levin (dry) model but only 0.18 dB/km for the Keller profile. For the latter, the lower value is due in part to the sharp transition in conductivity near a 14 km depth, according to Field and Dore (1973).

Note that for the uniform ideal waveguide treated by Spies and Wait (1971) and Wait and Spies (1971), with a conductivity of 10^{-7} Si/m for the

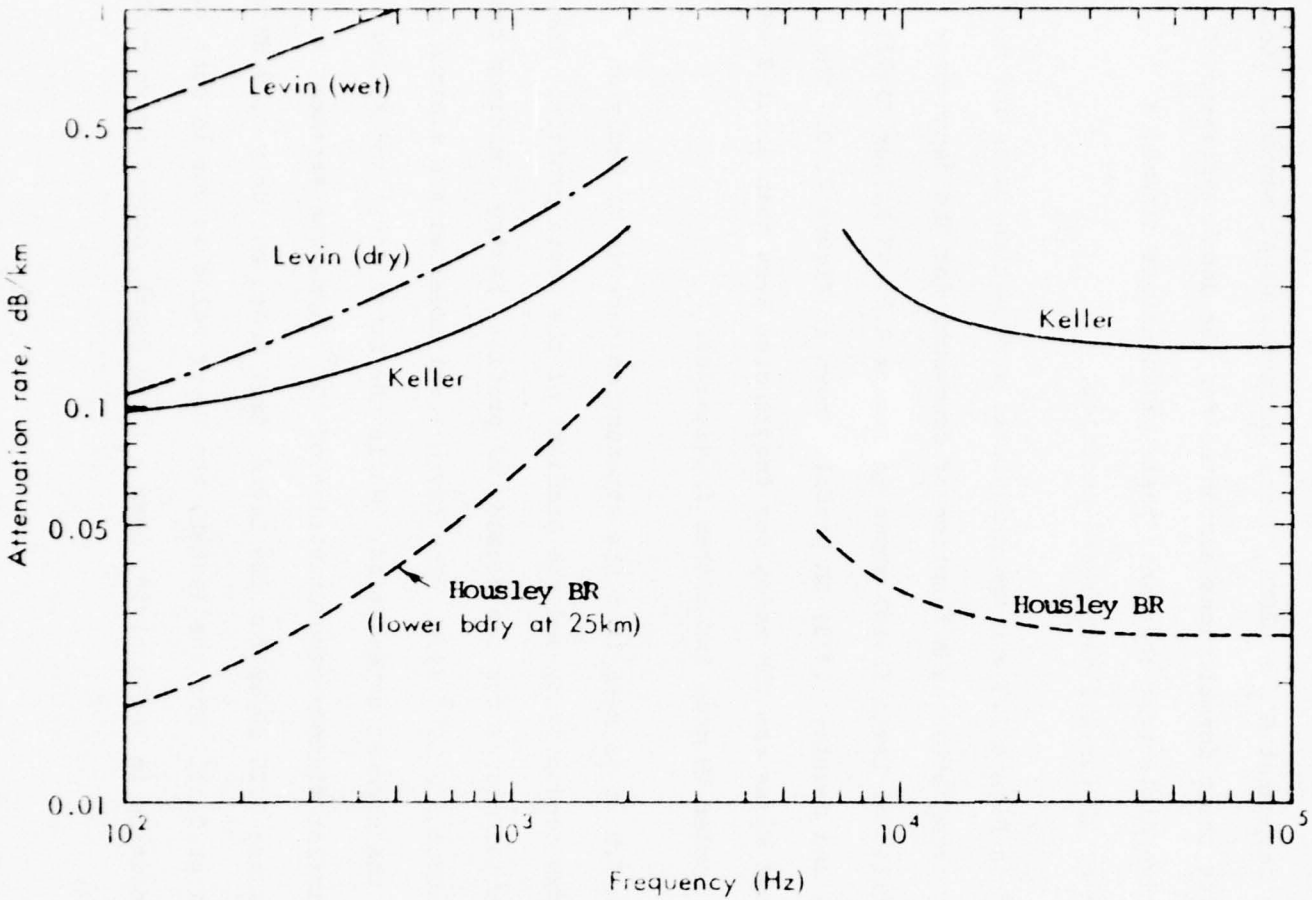

Fig. 3.9 Frequency variation of attenuation rates for four model conductivity profiles. (Field and Dore, 1973)

waveguide, the resulting attenuations are 2 or 3 times lower than the values shown in Figure 3.9 for the Levin (dry) and Keller models. These models have more gradual "boundaries" than the sharp boundaries in the depth profiles of Spies and Wait. If we averaged the Keller profile over some range of depth, an average might be 5 or 6 x 10^{-7} Si/m; such a value in the Spies and Wait case would result in a higher attenuation value.

In Figure 3.10 are presented the normalized magnitudes of the three field components versus depth for the Keller profile at 1 kHz. The normalization is such that the value of the "voltage normalized" magnetic field H'y is unity at the depth of minimum conductivity at 10 km. For the VED receiver, the magnitude of E_z has a broad maximum near a depth of 10 km. Note that E_x has a maximum magnitude at a 6 km depth, 14 db below the maximum value of E_z; E_x is less than E_z at depths below a 4 km depth but E_x exceeds E_z at smaller depths.

Considering the vertical field itself, the relative vertical strength versus frequency for several depths is shown in Figure 3.11 for the Keller profile. The values are normalized to that value at 10 km depth irrespective of the frequency. From these curves, one notes the relative decrease in vertical electric field strength as the receiving antenna is moved toward the surface, for a given frequency. Thus, at a frequency of 1 kHz, the relative field strengths are 13, 32, and 44 dB below that at 10 km depth, for depths of 4, 2, and 1 km, respectively. At 20 kHz, the degradations are 16, 36, and 52 dB for those same depths, respectively. Field and Dore have made similar calculations for the Housley BR model. For depths below 10 km, the degradations in vertical electric field strength

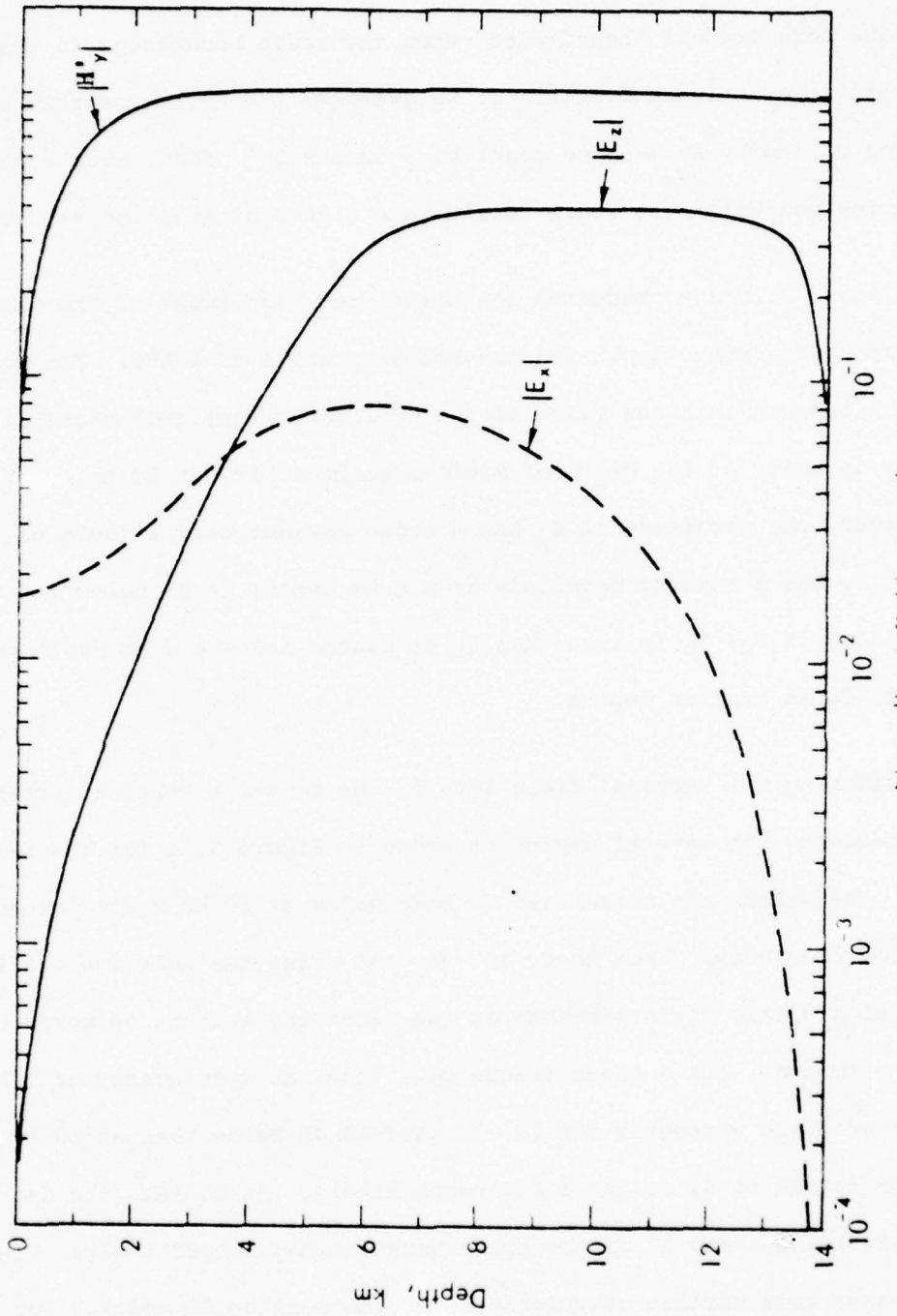

Fig. 3.10 Normalized field strengths vs. depth - Keller profile, 1 kHz. (From Field and Dore, 1973).

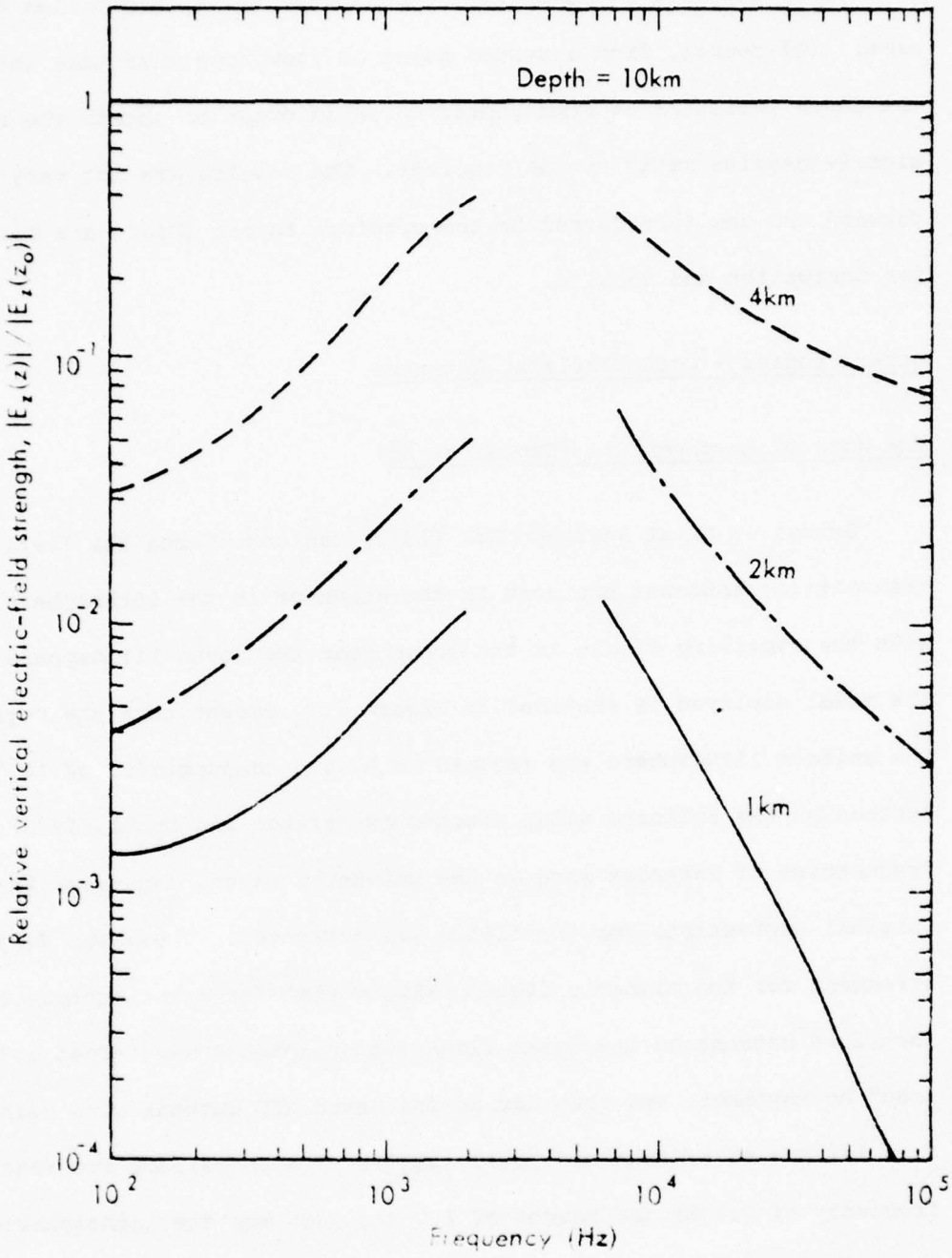

Fig. 3.11 Relative vertical electric field strengths vs. frequency at several depths (Keller profile). (From Field and Dore, 1973).

are nearly the same because the two conductivity depth profiles are the same. (Of course, from a system point of view, one must take into account the depth variation of atmospheric noise in order to obtain the resulting signal-to-noise ratio at the receiver. The results are not very straightforward and one is referred to the original report (Field and Dore, 1973) for derivation and results.

3.5 Other Studies - Ocean Emplaced Antennas

3.5.1 The Work of Raytheon Co. (Grossi et al)

Grossi et al at Raytheon Co. (1973) had considered the fields from transmitting antennas emplaced in the ocean or in the lithosphere below, with the receiving dipole in the ocean near the ocean-lithosphere interface. The model employed is sketched in Figure 6.2, except that the region below the uniform lithosphere was assumed to have a conductivity of 10^{-2} Si/m instead of the infinite value assumed by Frieman and Kroll (1973). Frequencies of interest were in the sub-Hertz range. An error in the original expressions for the fields was corrected. There was very good agreement for the magnetic fields between that for a horizontal, long, insulated antenna on the ocean floor (which antenna was termed a "phantom loop" by Raytheon) and that for an insulated HED antenna when using the formulations of Frieman and Kroll (1973). The comparison was made at a frequency of 0.1 Hz and ranges of 100 and 1000 km; the lithospheric region had a conductivity of 10^{-6} Si/m.

3.5.2 The Work of Frieman and Kroll

Frieman and Kroll, 1973, determine the modes and the mode excitation in a flat, stratified region for both vertical and horizontal current

distributions. The region of interest lies between perfectly conducting plane boundaries at $z = -d_\ell$ and $z = h$ where d_ℓ is the depth of the lithosphere and h is the height of the ionosphere, both measured from the ocean floor.* The depth of the ocean is d_w. The parameters used are $\sigma_w = 4$ Si/m, $\sigma_\ell = 10^{-6}$ Si/m. With frequencies in the range between f = 0.1 and 10 Hz, the propagation constants are, for the lithosphere $\gamma_\ell = (j\omega\mu\sigma_\ell)^{\frac{1}{2}}$, for the sea water, $\gamma_w = (j\omega\mu\sigma_w)^{\frac{1}{2}}$ and for the air, $\gamma_a = (-\omega^2\mu\varepsilon_o)^{\frac{1}{2}}$. By confining their attention to modes that propagate to distances large compared to both d_ℓ and h, Frieman and Kroll require only two modes. These are the lithospheric mode which is large in the lithosphere and the air mode which is large in the air. Solutions for the magnetic field of these modes are obtained with both vertical and horizontal electric dipoles located on the floor of the ocean. Their results indicate "that at large distances the HED is more effective than the VED by a factor $(\sigma_w/\sigma_\ell)^{\frac{1}{2}} = 2\text{x}10^3$". They go on to show that the contribution from the terms that involve the depth d_w of the ocean are essentially the same as for an ocean of infinite depth. Finally, in the range where the thickness d_ℓ of the lithosphere is effectively infinite, the magnetic field reduces to that obtained by Banos, 1966, or Kraichman, 1970, for the problem of two half-spaces. This is given by the near-field formula

$$H_\Theta = \frac{jI\Delta\ell}{2\pi\gamma_w} \frac{\cos\Theta}{\rho^3}$$

In a specific example, the magnetic field is calculated for a terminated insulated antenna 10 km long and 4 cm in diameter lying on the ocean floor.

---

*See Figure 6.2 for geometry employed.

4. The Two-Half-Space Model and Lateral-Wave Transmission

4.1 Introduction

In their modal analysis of electromagnetic wave propagation in a lithosphere composed of granitic rock ($\sigma = 10^{-6}$ Si/m) and bounded above by sea water ($\sigma = 4$ Si/m) and below by the mantle ($\sigma = \infty$) Frieman and Kroll [1973] concluded that with horizontal-electric-dipole excitation and reception at points on the ocean floor, the received field was very little affected by the thickness of the lithosphere ($d_\ell \sim 10$ km) or by the depth of the water ($d_w \sim 5$ km) in the frequency range from 0.1 to 10 Hz. This means that the electric field at the point of reception is governed by a single dominant mode which corresponds to the solution for transmission along the boundary between two half-spaces, the ocean and the lithosphere. This conclusion is confirmed by the careful interpretation by Bubenik and Fraser-Smith [1978] of their analysis of the field of a vertical magnetic dipole located in sea water midway between the air above and the sea floor (lithosphere) below. Bubenik and Fraser-Smith compared the contributions to the total field by direct transmission through the sea as if this were infinite in all directions with those by air-surface and sea-floor lateral-wave modes. They concluded that for a dipole near the air surface, the air-surface mode dominates; for a dipole near the sea floor, the sea-floor mode dominates. Since a vertical magnetic dipole is equivalent to four horizontal electric dipoles arranged in a square, its field is a superposition of the fields of the four dipoles, each like the field of a single horizontal electric dipole. The superimposed fields of the very closely spaced dipoles lead to a large reduction in the resultant field due to cancellation but this in no way alters the nature of the field with respect to its modal structure. This means that if the sea-floor lateral-wave mode dominates for a vertical magnetic dipole in sea water near the sea floor, the same is true for a horizontal electric dipole at the same location.

Extensive numerical calculations by King and Sandler [1977] based on the exact general theory of Baños (1966] have shown that transmission between horizontal electric dipoles in a dissipative half-space near its boundary with air is predominantly by the so-called lateral waves. This is true for a dissipative half-space that has the properties of sea water, lake water, or dry earth over a frequency range from 1 to 10^9 Hz. For radial distances from ρ = 1 m to 100 km and more, the dominant component of the electric field at a depth z in the medium due to a transmitting dipole at the depth d is the radial one, i.e., E_ρ . While there are short ranges where the component E_ϕ is somewhat greater than E_ρ , this difference is never large. On the other hand, there are large ranges including especially the greater distances where E_ρ greatly exceeds E_ϕ . It follows that for practical transmission over large distances E_ρ is the only satisfactory component. It has also been shown by direct comparison of the numerical calculations from the exact integrals with a set of approximate formulas due to Baños [1966] that these latter are roughly correct at least in order of magnitude far beyond the ranges of validity specified by Baños. Specifically, the graphs of the electric field as a function of distance at a given frequency as calculated from Baños' near-, intermediate-, and far-field formulas can be extended to points of intersection. The sequential combination of the three graphs provides a continuous curve of $|E_\rho|$ against distance from the source ρ (but with discontinuities in slope at the intersections of the near- and inter-

mediate-field graphs and of the intermediate- and far-field graphs) that follows fairly closely the smooth graph computed from the exact integrals. This general agreement is very significant because it justifies the use of Baños' simple formulas to gain an understanding of the physical nature of the waves propagating from the source to the receiver and of the significance of the numerous parameters and variables that combine to determine the field at the point of observation.

4.2 Baños' Approximate Formulas and Their Interpretation

The coordinates and parameters used in the representation of the field in a region consisting of a half-space of sea water (Region 1, $z \geq 0$) and a half-space of the lithosphere (Region 2, $z < 0$) are shown in Fig. 4.1 . The wave number in sea water with the time dependence $e^{-i\omega t}$ is*

$$k_1 = \beta_1 + i\alpha_1 = (\omega^2\mu_0\varepsilon_1 + i\omega\mu_0\sigma_1)^{1/2} \doteq (i\omega\mu_0\sigma_1)^{1/2} \tag{4.1}$$

The wave number for the lithosphere is

$$k_2 = \beta_2 + i\alpha_2 = (\omega^2\mu_0\varepsilon_2 + i\omega\mu_0\sigma_2)^{1/2} \tag{4.2}$$

As indicated, the sea water behaves like a good conductor over all useful frequencies. The same is true for the lithosphere at low frequencies. At high frequencies the lithosphere may behave like a dielectric so that the more general formula for the wave number is retained.

Baños' approximate formulas for the electric field of a horizontal electric dipole at the location shown in Fig. 4.1a are given by (7.10), (7.32) and (7.45) in his book [Baños, 1966]. With small changes in the notation and the substitution of $k_1^2/i\omega\mu_0$ for σ_1, the formulas for the radial component of the electric field are:

Near Field:
$$E_{1\rho} \doteq \frac{i\omega\mu_0}{2\pi k_1^2} \frac{\cos\phi}{\rho^3} e^{i[k_2\rho + k_1(d+z)]} \tag{4.3}$$

Intermediate Field:

---

*The form on the right in (4.1) assumes $\sigma_1/\omega\varepsilon_1 \gg 1$ for sea water.

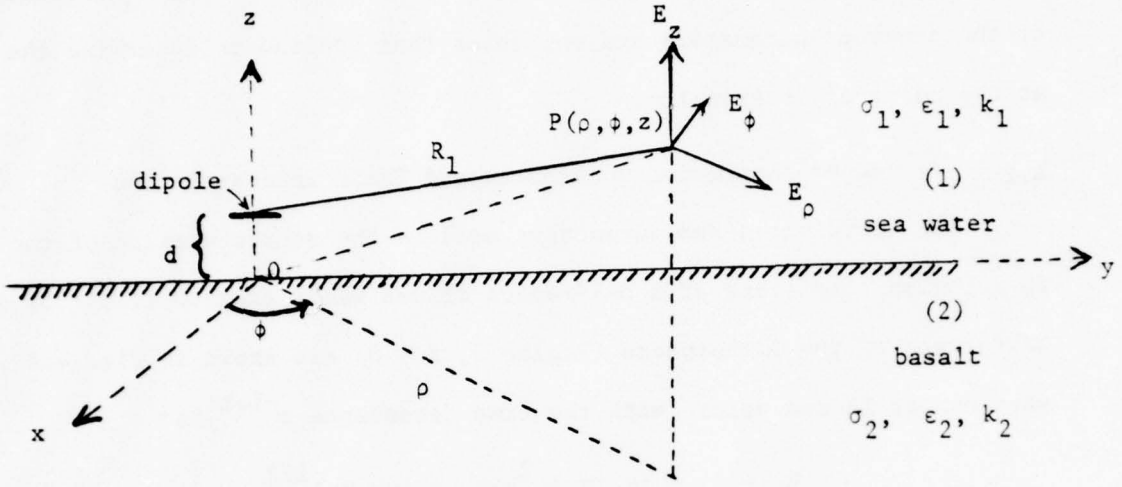

Fig. 4.1a Two-half-space Model for Lateral-Wave Transmission

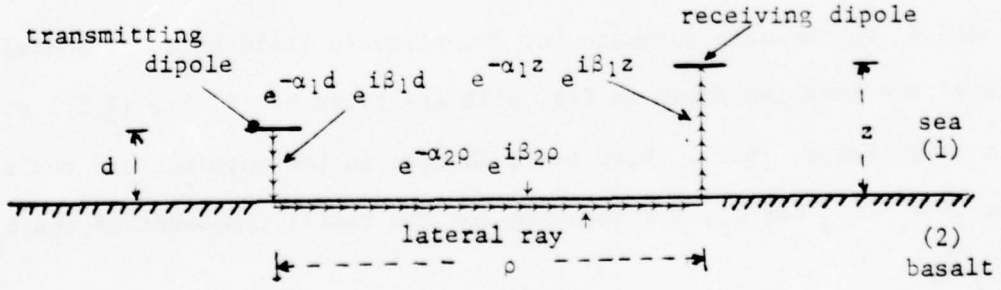

Fig. 4.1b Schematic Diagram of a Ray in Lateral-Wave Transmission and its relation to the Mathematical Representation:

$$e^{-[\alpha_2\rho+\alpha_1(d+z)]}\ e^{i[\beta_2\rho+\beta_1(d+z)]}$$

$$E_{1\rho} \doteq -\frac{i\omega u_0 k_2^2}{2\pi k_1^2}\frac{\cos\phi}{\rho}\left[1 + i\frac{k_2}{k_1}(i\pi k_2\rho/2)^{1/2}\right] e^{i[k_2\rho + k_1(d+z)]} \tag{4.4}$$

Far Field:

$$E_{1\rho} \doteq \frac{\omega u_0}{2\pi k_2}\frac{\cos\phi}{\rho^2} e^{i[k_2\rho + k_1(d+z)]} \tag{4.5}$$

The formulas for the other components are similar, but since $E_{1\rho}$ is the only generally useful one, it is sufficient to consider it. The ranges in which each of the three formulas is a good approximation have been specified by Baños. For sea water they are extensive, but even for this they do not actually join. Numerical calculations from the exact integrals have shown the three formulas may be used successively as the radial distance is increased with the transition from the one to the other occurring where the magnitudes of the field are equal. At and near these transitions from the one formula to the other the approximations are quantitatively inadequate but qualitatively correct.

The lateral-wave nature of the field is evident in all three formulas. Note that they all have the same exponential term which is readily interpretted. It indicates a traveling wave originating at the source dipole, (ρ=0, ϕ=0,z=d), traveling downward in the sea water to the boundary surface , then traveling radially outward in the lithosphere a distance ρ , and finally traveling upward from the surface to the receiver at the point of observation at $P(\rho,\phi,z)$. This involves travel in the sea water (Region 1) over a total distance z + d and travel in the lithosphere (Region 2) over the distance ρ (Fig. 4.1b). In the sea the attenuation and phase constants are, respectively, α_1 and β_1; in the lithosphere they are α_2 and β_2. If the real and imaginary parts of the exponents are separated, the common exponential term has the expanded form

$$e^{-[\alpha_2\rho + \alpha_1(d+z)]}\, e^{i[\beta_2\rho + \beta_1(d+z)]} \tag{4.6}$$

Clearly there is attenuation in both regions but since the conductivity of the lithosphere (Region 2) is much smaller than that of the salt water (Region 1) it follows that $\alpha_2 << \alpha_1$. For a given range ρ an important quantity in determining the amplitude is the total vertical distance $z + d$. The closer the transmitting and receiving antennas are to the boundary, the larger will be the amplitude of the field. However, if $\alpha_1(d+z) < 1$, $e^{-\alpha_1(d+z)} \doteq 1$ even for large values of $d + z$. This can be accomplished by choosing a low enough frequency so that α_1 is small even though σ_1 is as large as 4 S/m. Insofar as the exponential term is concerned, small distances z and d are desirable as well as a frequency that is not too high. For a specified range the contribution to the attenuation by the factor $e^{-\alpha_2\rho}$ can be reduced only by making α_2 smaller. With a given conductivity of the lithosphere α_2 can be decreased only by lowering the frequency.

If the exponential term does not dominate, a significant field can be maintained at great distances. In order to understand its dependence on the distance and frequency it is necessary to examine the other factors that determine the amplitude. The radial distance appears in all three formulas (4.3) - (4.5) but in a different manner in each. In the near-field formula the amplitude decreases as $1/\rho^3$, a prohibitively rapid rate of decrease. In the far-field formula the rate of decrease is as $1/\rho^2$, a great improvement over the near field. Finally, in the intermediate range the rate of decrease with radial distance varies between $1/\rho$ and $1/\sqrt{\rho}$ - which is by far the most favorable. The comparable dimensionless quantities for the three ranges are: $(k_1\rho)^{-3}$, $k_2^2/k_1^3\rho$, and $1/k_1k_2\rho^2$ in the order near field, intermediate field, and far field. With a proper choice of frequency for the parameters of the media involved, the largest magnitude of the radial electric field should be obtained when ρ is in the intermediate zone near its boundary with the far zone. This clearly excludes very low frequencies for which the near-field formula is applicable for the relevant radial range.

A better understanding of the complete picture including the exponential

and inverse distance dependences can be obtained from Fig. 4.2 which displays contours of constant $|E_\rho|$ (in dB referred to 1 volt per meter) as a function of the radial distance and the frequency for a horizontal electric dipole at a depth d = 15 cm in water. The point of observation is at the depth z = 30 cm in the water. The half-space bounding the water is air filled. In the previous notation, the water is Region 1, the air is Region 2. In this case $\alpha_2 = 0$ and $\beta_2 = 2\pi/\lambda_2$ where λ_2 is the wavelength in air. The real effective permittivity of the water is $\varepsilon_{er1} = 80$; the real effective conductivity in Siemens per meter is $\sigma_{e1} = 0.004$, 0.04, 0.4 and 4 in the diagrams from left to right. The diagram on the left applies when the antennas are in lake water of high purity, the diagram second from the left is for polluted lake water, the diagram on the extreme right for sea water, The contours were obtained from numerical computations of the electric field using the exact integrals.

In the diagram on the left the conductivity is sufficiently low so that the exponential attenuation, $e^{-\alpha_1(z+d)}$, is not dominant at any frequency with z + d = 45 cm. In terms of the approximate formulas of Baños, the right-hand third of the diagram is for low frequencies and the near-field formula with its $1/\rho^3$ amplitude factor, the left-hand third is for high frequencies and the far-field formula with its $1/\rho^2$ amplitude factor. The transition between them at intermediate frequencies is for the intermediate-field formula. Note that at any fixed distance, for example ρ = 8 km, $|E_{1\rho}|$ is very much greater at the high frequencies than at the low ones. Specifically, at the high frequencies $|E_{1\rho}| \doteq -120$ dB, in the low-frequency range $|E_{1\rho}| \doteq -200$ dB. In the second diagram from the left the conductivity of the water is ten times greater but still small enough to make the exponential attenuation unimportant. The contours of constant electric field are quite similar to those on the left with only a small decrease in amplitude in the high-frequency range, a somewhat larger one in the low-frequency range. In the third diagram from the left the conductivity is multiplied by another factor ten and this makes it large enough so that the

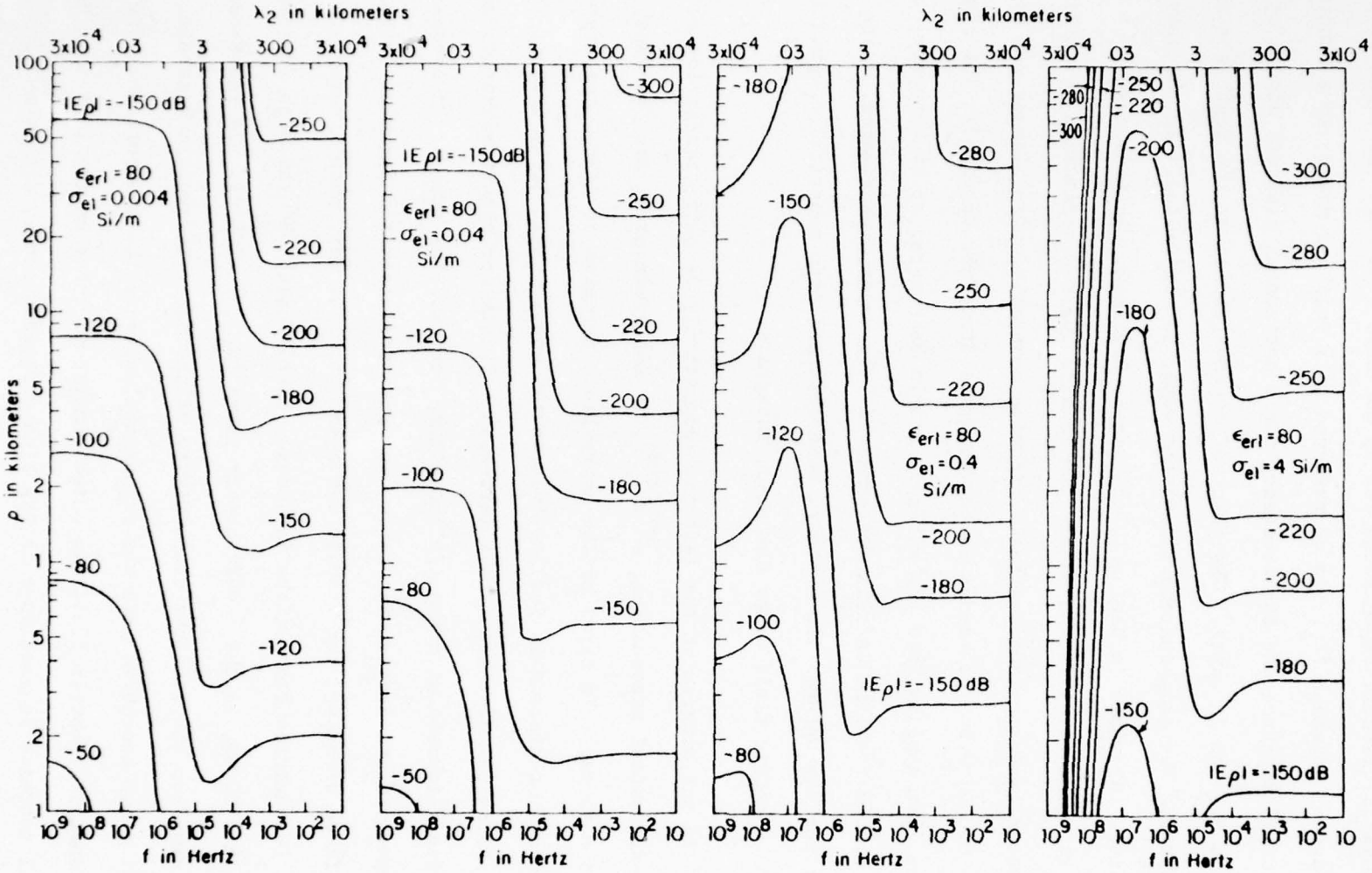

Fig. 4.2 Contours of constant $|E\rho|$ for water as functions of frequency f and radial distance ρ; d = 15 cm; z = 30 cm.

exponential attenuation begins to play a significant role, but only at the higher frequencies. The rapid decrease in amplitude at frequencies above 10^7 Hz is due to the exponential factor $e^{-\alpha_1(z+d)}$ with z+d = 45 cm. Note, however, that even with the exponential attenuation significant, the field in the high frequency range is still much greater at any fixed distance than in the low frequency range. The optimum frequency is clearly in the vicinity of 10^7 Hz where the contours show a maximum distance for any specified value of $|E_\rho|$. In the graph on the right for sea water the exponential attenuation has become the major factor at the higher frequencies. The radial electric field decreases to extremely small values at all distances when the frequency is increased to 10^8 Hz or higher. However, at any fixed distance the field has a maximum near $f \approx 10^7$ Hz and this maximum is significantly greater than the field at the same distance at any of the lower frequencies. Thus, when z + d = 45 cm the field at any radial distance ρ is greater at a frequency between 5×10^6 and 5×10^7 than at any frequency below $f = 10^5$ Hz.

If the total distance of travel in the sea water is increased from z + d = 45cm the maximum field at any fixed radial distance moves toward lower frequencies. When this reaches about 10^5 Hz the exponential attenuation will effectively eliminate the maxima in the high frequency range and the field in the low-frequency range will be larger than that anywhere in the high-frequency range. The choice of frequency for lateral wave transmission is seen to depend critically on the quantity $\alpha_1(z + d)$ and the exponential $e^{-\alpha_1(z+d)}$. When the region of low conductivity is not air with $\sigma_2 = 0$ but the lithosphere with $\sigma_2 = 10^{-8}$ to 10^{-4}.the additional exponential attenuation by the factor $e^{-\alpha_2\rho}$ must also be considered. This requires a complete recalculation. However, the basic properties of wave propagation with horizontal-dipole excitation near an interface are best understood from the simpler case with a perfect dielectric like air as the half-space with small conductivity.

Before proceeding to a study of lateral wave propagation along the

surface of two half-spaces with the properties of sea water and the lithosphere, it is well to point out that the simple picture illustrated in Fig. 4.1b of lateral waves traveling vertically downward from the source dipole a distance d to the boundary surface, along the surface a radial distance ρ to the point below the receiver, and then vertically upward a distance z to the receiving dipole, is an idealization that is an excellent approximation with a highly conducting medium like sea water. With poorer conductors the optimum angle downward from the source to the surface is the critical angle at which the incident wave is neither transmitted nor totally reflected but travels along the surface. With sea water this angle is very close to 90°; for media with lower conductivities and permittivities the angle can be considerably smaller than 90°. A discussion and determination of this angle is given by Staiman and Tamir [1966]. For a maximum transmitted signal the dipole should not be parallel to the interface but perpendicular to the direction of the critical angle. With sea water the difference between the two orientations is negligible.

4.3 Lateral-Wave Transmission Along the Lithosphere-Ocean Boundary

Lateral-wave transmission along the boundary between air and water involves exponential attenuation only along the two vertical parts of the path, both in the salt water. This has the form $e^{-\alpha_1(z+d)}$ where d is the depth of the horizontal dipole in the sea water and z is the depth of the point of observation. When the transmission is along the boundary in air it is loss free since $e^{ik_2\rho} = e^{i\beta_2\rho}$ with $k_2 = \beta_2 + i\alpha_2$ and $\alpha_2 = 0$. When the half-space of air is replaced by a half-space of rock with the real effective permittivity ε_{e2} and the real effective conductivity σ_{e2}, the wave number $k_2 = \beta_2 + i\alpha_2$ is complex so that $e^{ik_2\rho} = e^{-\alpha_2\rho}\, e^{i\beta_2\rho}$. Thus there is exponential attenuation along the main path of propagation in the lithosphere in addition to the decrease in amplitude governed by the complicated functional dependence on the inverse powers of the radial distance ρ.

Computations have been made from the exact integrals for lateral-wave transmission from a horizontal electric dipole with unit moment, $Id\ell = 1$. The dipole is at the depth d in the sea water and the field is calculated at the radial distance ρ at the depth $z = d$. (Note that in the computations for air and sea water, $z = 2d = 0.3$m) . The material parameters used in the calculations of the electric field are $\varepsilon_{e1} = 80\varepsilon_0$ and $\sigma_{e1} = 4$ Si/m for Region 1, the sea. For the lithosphere, Region 2, $\varepsilon_{e2} = 16\varepsilon_0$ and σ_{e2} ranges from 4×10^{-8} Si/m to 4×10^{-3} Si/m. Initially $z = d = 0.15$m . Computations of $|E_\rho|$ (which is the dominant component in lateral-wave transmission) have been made over radial distances from $\rho = 0.1$ to $\rho = 100$km at frequencies from 10 to 10^9 Hz. Graphs showing $|E_\rho|$ as a function of the radial distance with the frequency as the parameter are shown in Fig. 4.3a for $\sigma_{e2} = 4 \times 10^{-8}$ and 4×10^{-7} Si/m and in Fig. 4.3b for $\sigma_{e2} = 4 \times 10^{-6}$, 4×10^{-5}, 4×10^{-4}, and 4×10^{-3} Si/m. From these graphs the contours of constant $|E_\rho|$ shown in Figs. 4.4a - 4.4c have been constructed. These show $|E_\rho|$ as a function of both the radial distance and the frequency in the manner carried out in the comparable Fig. 4.2 for air and water.

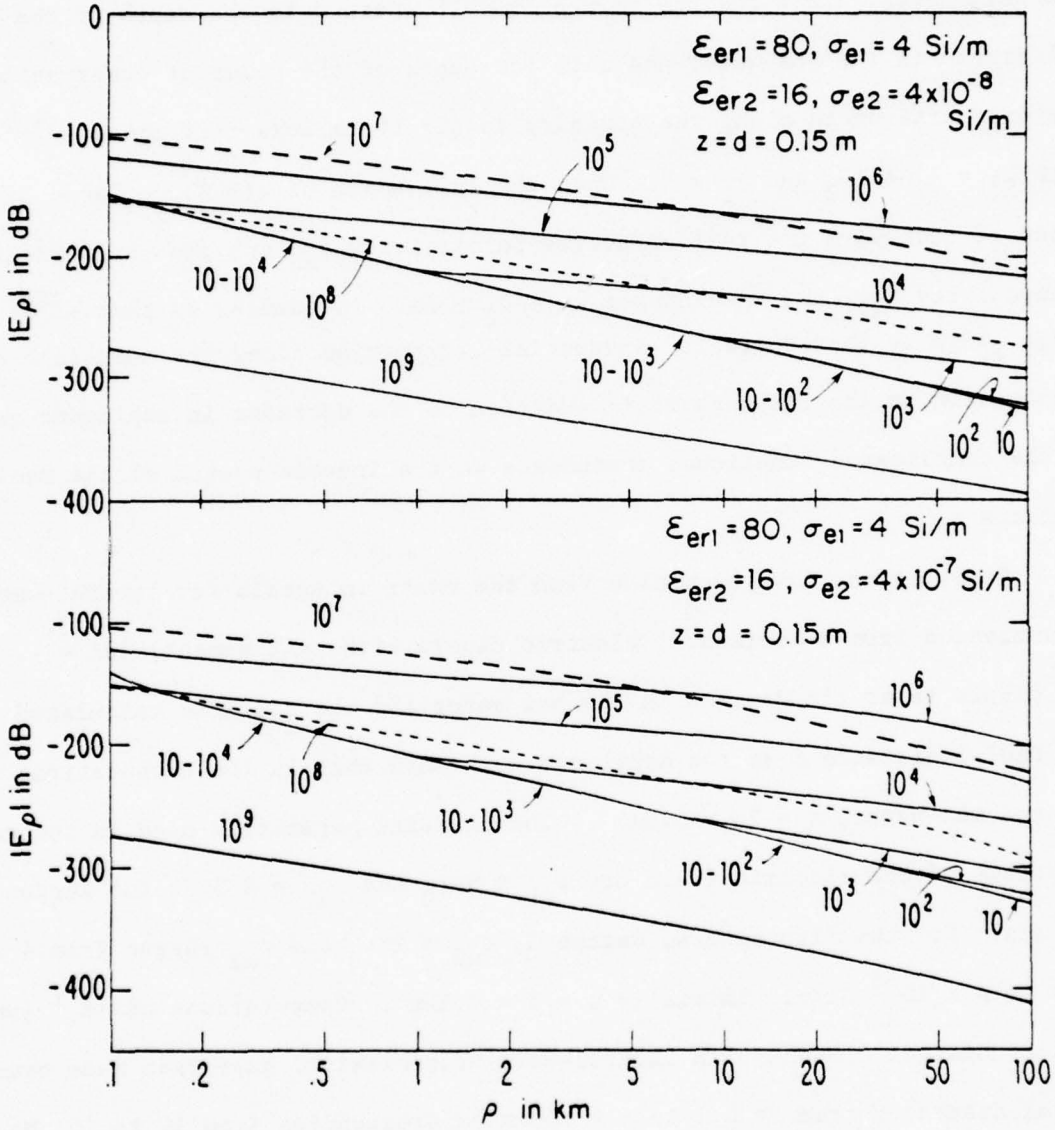

FIG. 4.3a MAGNITUDE OF E_ρ IN SEAWATER BOUNDED BY THE LITHOSPHERE, z = d = 0.15 m.

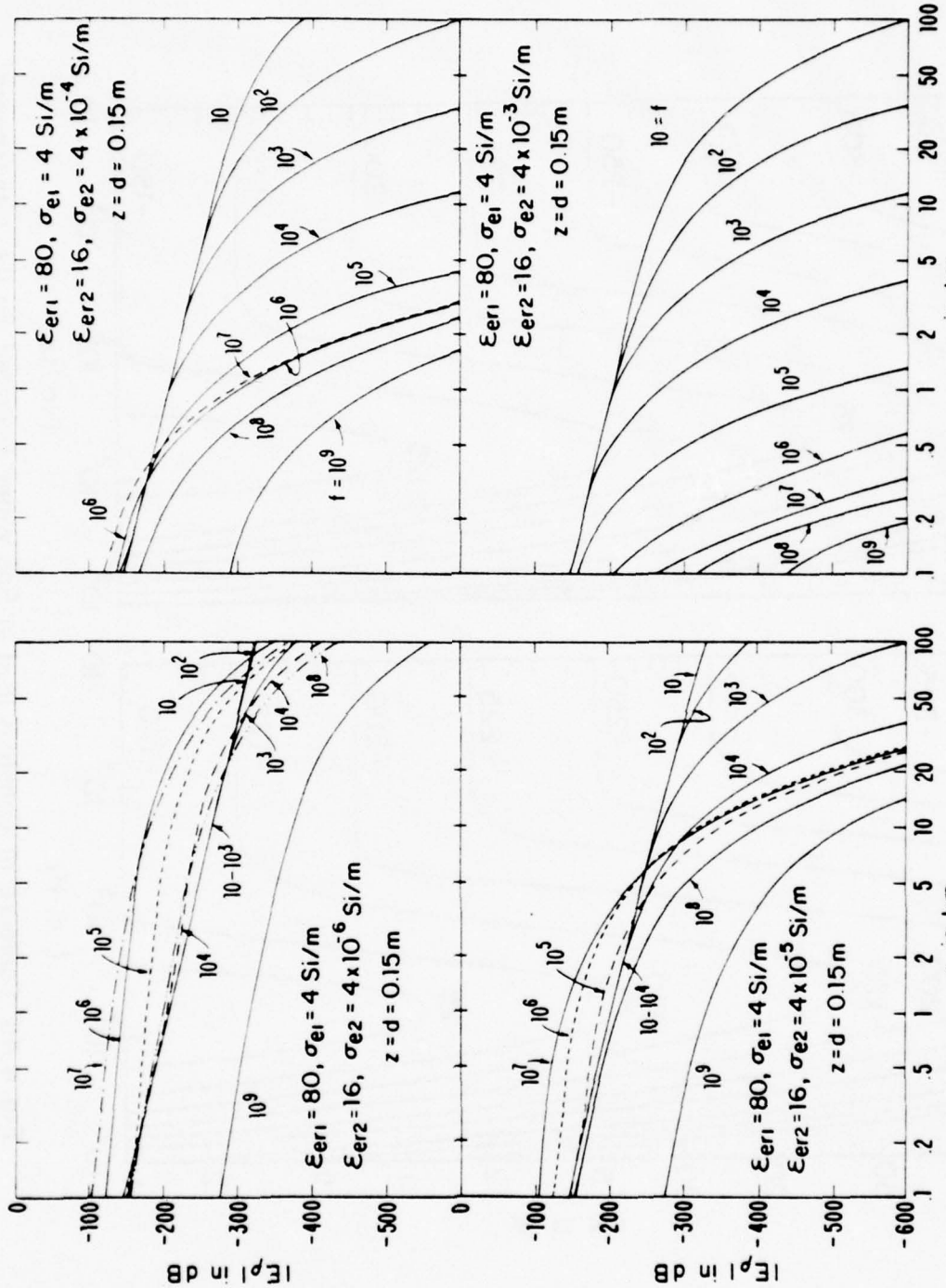

Fig 4.3b Magnitude of E_ρ in Sea Water Bounded by the Lithosphere; z = d = 0.15m

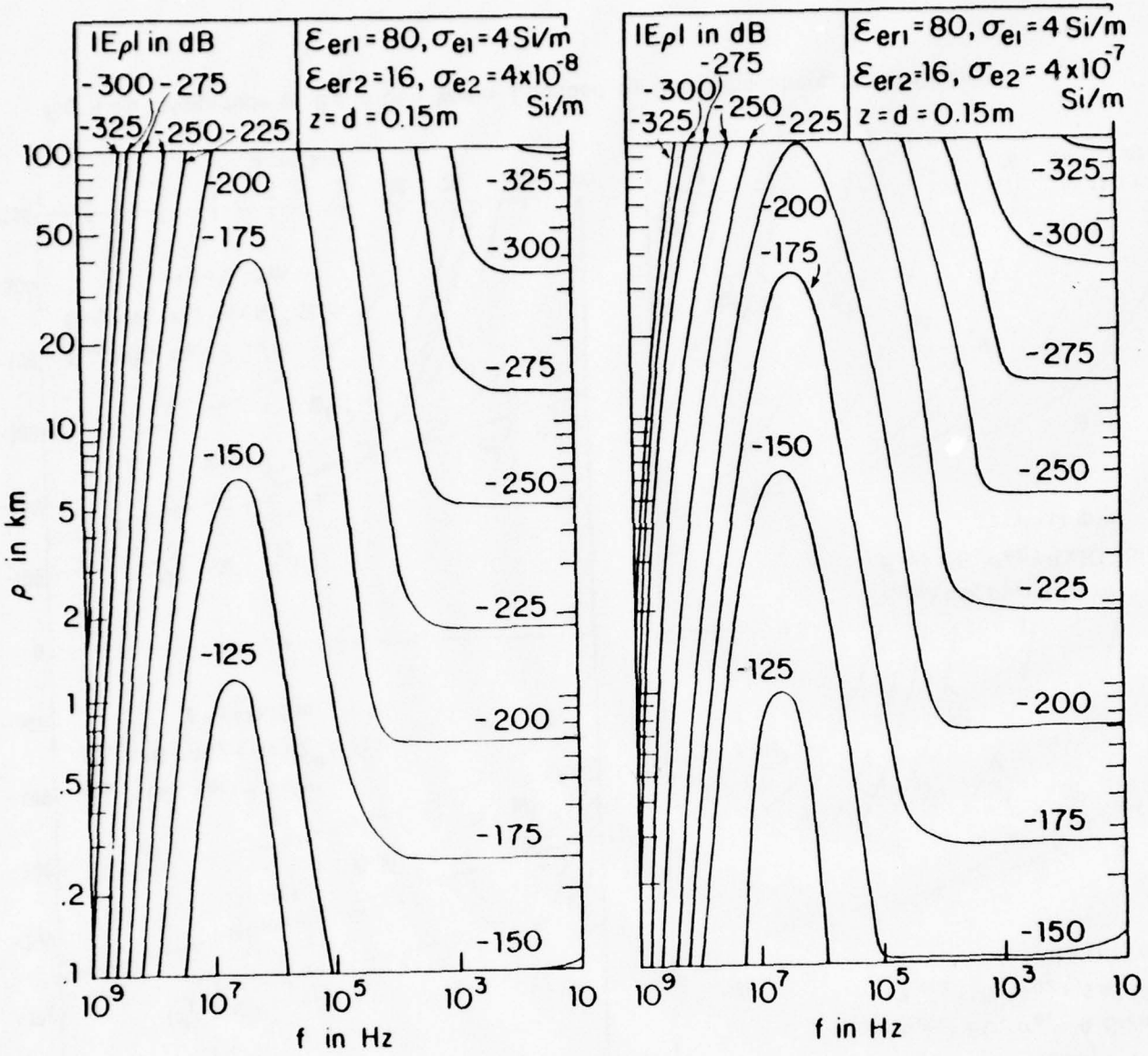

Fig. 4.4a Contours of Constant |Eρ| in Sea Water Bounded by the Lithosphere; z = d = 0.15m

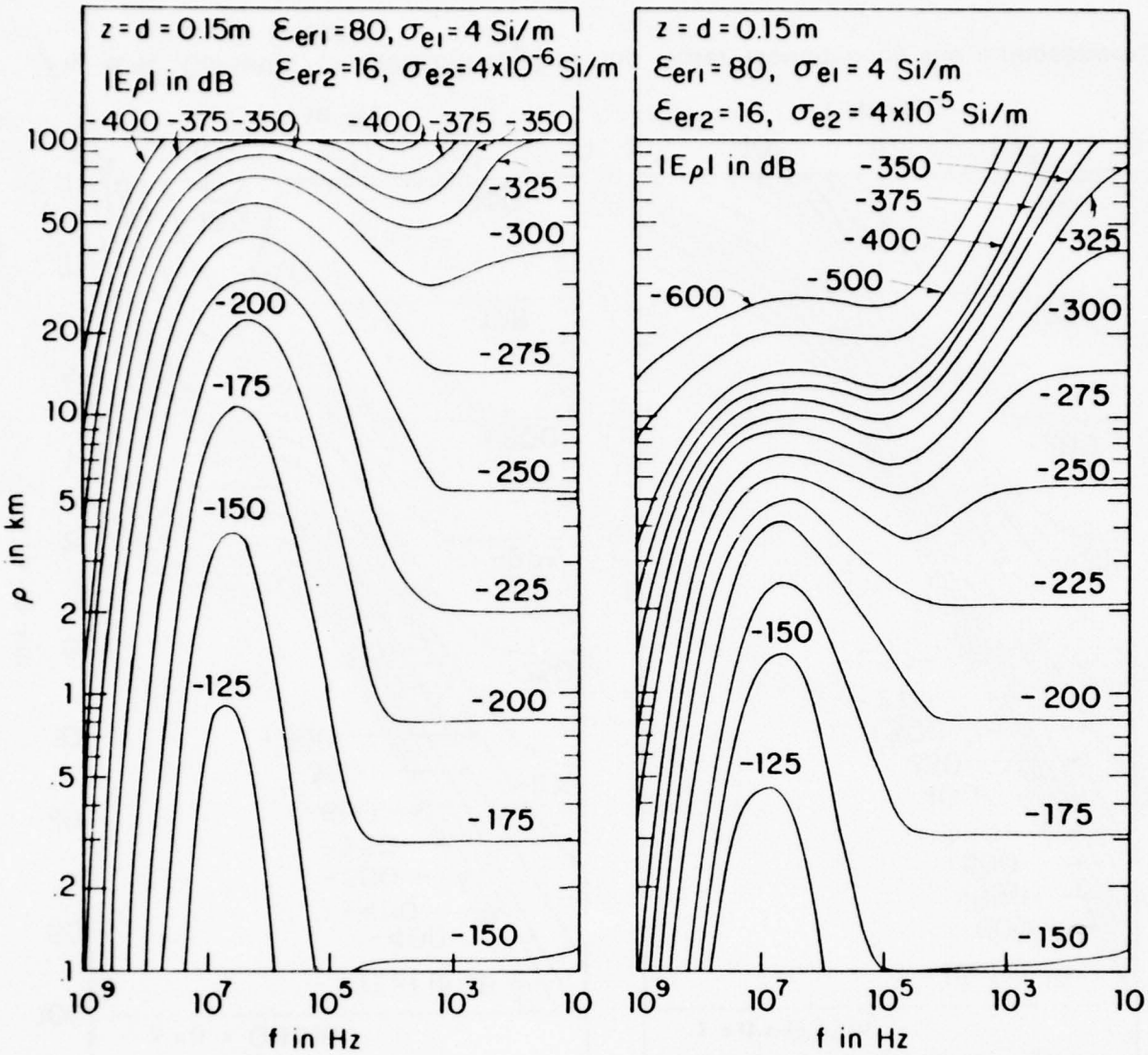

Fig 4.4b Contours of Constant |Eρ| in Sea Water Bounded by the Lithosphere; z = d = 0.15m

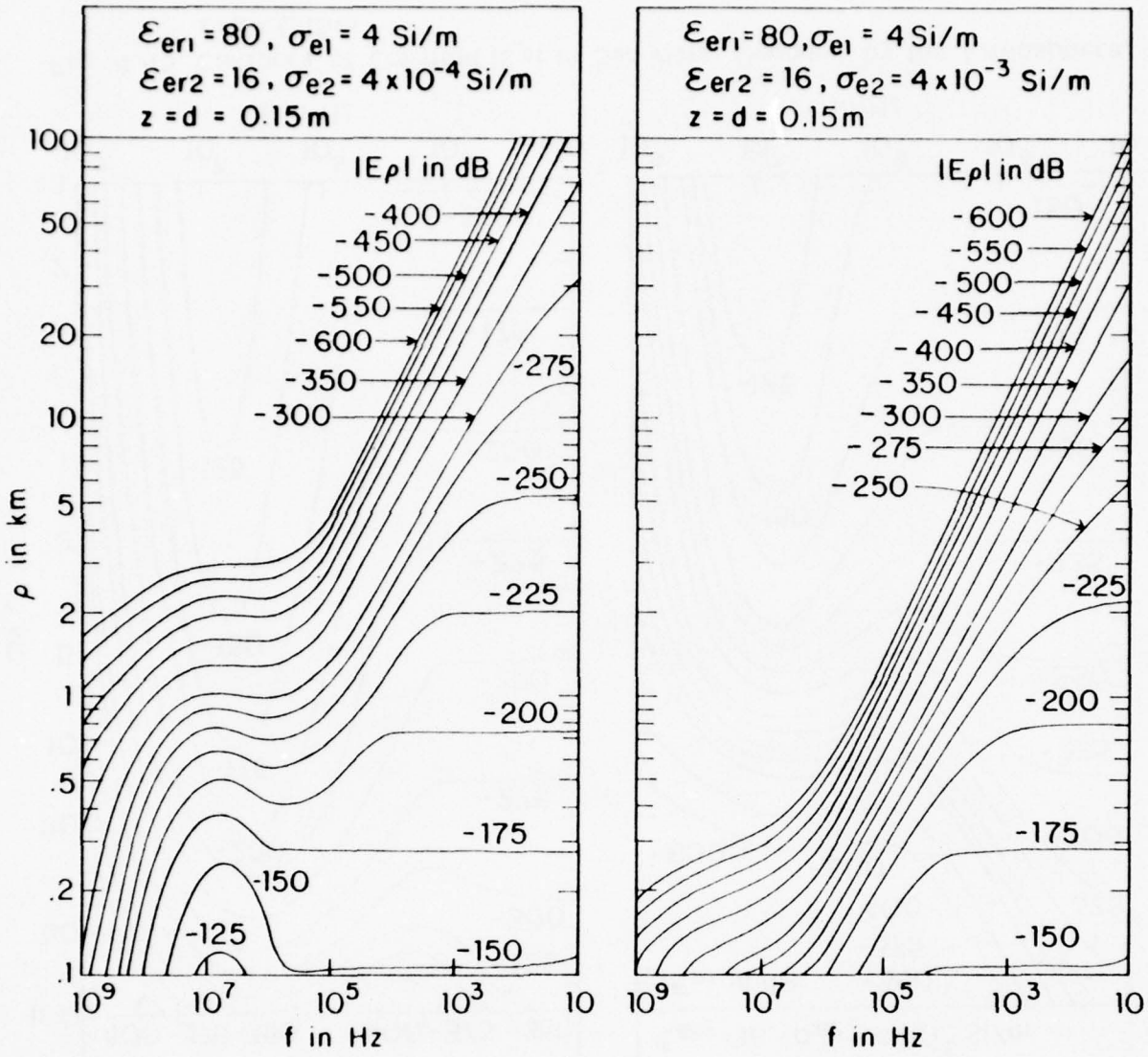

Fig. 4.4c Contours of Constant |Eρ| in Sea Water Bounded by the Lithosphere; z = d = 0.15m

The set of contours on the left in Fig. 4.4a is for sea water and a lithosphere with the low conductivity $\sigma_{e2} = 4 \times 10^{-8}$ Si/m. It resembles the corresponding set of contours on the extreme right in Fig. 4.2 for sea water and air with the conductivity $\sigma_{e2} = 0$. In both sets of graphs the exponential attenuation $e^{-\alpha_1(z+d)}$ dominates the high-frequency quarter on the left. Here the graphs show a rapidly decreasing radial range for any given value of $|E_\rho|$ as the frequency is increased. The rate of decrease for sea water and air is even more rapid than that for sea water and the lithosphere because (z+d) = 0.45m with the former, 0.3m with the latter. On the other hand, attenuation by $e^{-\alpha_1(z+d)}$ is insignificant in the low-frequency third of the contours on the right in each diagram. This is because at low frequencies α_2 is very small. For air, $\alpha_2 = 0$, $e^{-\alpha_2\rho} = 1$, and the contours for fixed values of $|E_\rho|$ are virtually horizontal in the low-frequency third of the right-hand set of contours in Fig. 4.2. This indicates that the radial range for a specified field is almost independent of the frequency in the low-frequency range. For the lithosphere, $\alpha_2 \neq 0$ and $e^{-\alpha_2\rho}$ varies significantly with both the frequency and the radial distance. As a consequence, the contours for given values of $|E_\rho|$ at low frequencies range from horizontal lines when σ_{e2} is small to steeply increasing graphs when σ_{e2} is large. The increase in radial range as the frequency is reduced and the conductivity increased is clearly shown in the sequence of graphs in Figs. 4.4b and 4.4c.

Perhaps the most significant characteristic of the contours of constant $|E_\rho|$ for sea water and air (on the extreme right in Fig. 4.2) and for sea water and the lithosphere (Figs. 4.4a - 4.4c) is the relative maximum in the radial range which occurs in all diagrams at frequencies between f = 1 and 10 MHz so long as $\sigma_{e2} < 4 \times 10^{-3}$ Si/m. Particularly notworthy is the fact that the relative maximum value of ρ for a given $|E_\rho|$ is much greater than the corresponding distance for the same value of $|E_\rho|$ at very low frequencies when $\sigma_{e2} < 4 \times 10^{-5}$ Si/m. This can be seen from Figs. 4.4a and 4.4b for both $\sigma_{e2} = 4 \times 10^{-8}$ and $\sigma_{e2} = 4 \times 10^{-7}$ Si/m. For example, when $\sigma_{e2} = 4 \times 10^{-8}$ Si/m, the value

$|E_\rho|$ = -175 dB occurs at ρ = 40 km when the frequency is between 10^6 and 10^7 Hz but ρ < 0.3 km for all frequencies from 10 to 10^4 Hz. Similarly $|E_\rho|$ = -225 dB occurs at ρ near 500 km when the frequency is between 10^6 and 10^7 Hz but at 2 km for all frequencies between 10 and 10^4 Hz. When $\sigma_{e2} = 4 \times 10^{-7}$ Si/m the graphs are very similar to those with $\sigma_{e2} = 4 \times 10^{-8}$ Si/m with a reduction to ρ = 100 km in the radial range at the maximum between f = 10^6 and 10^7 Hz and virtually no change in the short range at low frequencies. However, when σ_{e2} is as large as 4×10^{-6} Si/m the maxima in the radial range near f = 10^7 Hz are substantially depressed but the radial distance for the same values of $|E_\rho|$ at very low frequencies remains smaller so long as ρ < 75 km. Thus, $|E_\rho|$ = -225 dB occurs at ρ = 33 km at the maximum with the frequency between 10^6 and 10^7 Hz and drops to ρ = 2 km at f = 10 to 10^3 Hz. For radial distances greater than about 100 km, a given value of $|E_\rho|$ is found at substantially greater distances at the very low frequencies than at the relative maximum between f = 10^6 and 10^7 Hz. This is a consequence of the radial exponential attenuation factor $e^{-\alpha_2 \rho}$ which is small enough at frequencies as high as 10^6 and 10^7 Hz to depress the relative maximum more and more as ρ is increased. This effect is dramatically shown in the four sets of graphs in Figs. 4.4b and 4.4c in which the conductivity of the lithosphere increases from 4×10^{-6} on the left in Fig. 4.4b to 4×10^{-3} Si/m on the right in Fig. 4.4c. It is seen that $|E_\rho|$ at the maximum near f = 10^7 Hz is reduced more and more while $|E_\rho|$ at very low frequencies and sufficiently great radial distances is increased.

The contour diagrams in Figs. 4.4a,b lead to the following general conclusions regarding lateral-wave transmission along a plane boundary between sea water and the lithosphere when the source is a horizontal electric dipole in the sea at the small distance d = 15 cm from the bounding surface and the point of observation is at the same distance z = d from the surface at a radial distance ρ :
a) If the conductivity of the lithosphere is greater than $\sigma_{e2} = 4 \times 10^{-6}$ Si/m, transmission over distances greater than 50 km experiences the lowest possible

attenuation at frequencies below 1 kHz. This is true for any values of z = d $\geq$ 15 cm.

b) If the conductivity of the lithosphere is significantly smaller than 4×10^{-6} Si/m, there is an optimum frequency between 1 and 10 MHz at which the radial range has a relative maximum that may be substantially greater than the radial distance for any value of $|E_\rho|$ at other frequencies including the very low. Furthermore, an effective directional array with significant gain can be constructed for both the transmitter and the receiver for use at frequencies in the 1 to 10 MHz range.

c) The conclusion under b) assumes the transmitting and receiving antennas to be in the sea water but very near the boundary surface with the lithosphere (d = z = 0.15m). It is to be expected that as the distances d and z from the antennas to the surface is increased, the exponential attenuation $e^{-\alpha_1(z+d)}$ will become dominant at lower and lower frequencies. This must simultaneusly depress the relative maximum which occurs between f = 1 and 10 MHz when (z+d) = 30 cm and move it to lower frequencies. In order to investigate this effect quantitatively,computations were made of $|E_\rho|$ with z = d = 1.5 m over the same range of conductivities for the lithosphere as used in Figs. 4.3a and 4.3b. These results are shown in Figs. 4.5a and 4.5b. From them the contour diagrams in Figs. 4.6a - 4.6c were constructed. They correspond to the diagrams in Figs. 4.4a - 4.4c. It is seen that when $\sigma_{e2} \leq 4 \times 10^{-5}$ Si/m the relative maxima in the radial range have moved from near $f = 10^7$ Hz with z = d = 0.15m to near $f = 10^5$ Hz with z = d = 1.5m and that they are substantially smaller. For example, with $\sigma_{e2} = 4 \times 10^{-8}$ Si/m the maximum range for $|E_\rho|$ = -225 dB is ρ = 10 km with z = d = 1.5m instead of $\rho \sim 500$ km with z = d = 0.15m. There is no corresponding decrease in the range at low frequencies since there the exponential attenuation is small. It follows that unless both the transmitting and receiving antennas are very close to the ocean-lithosphere boundary, the greatest radial range is achieved at low frequencies.

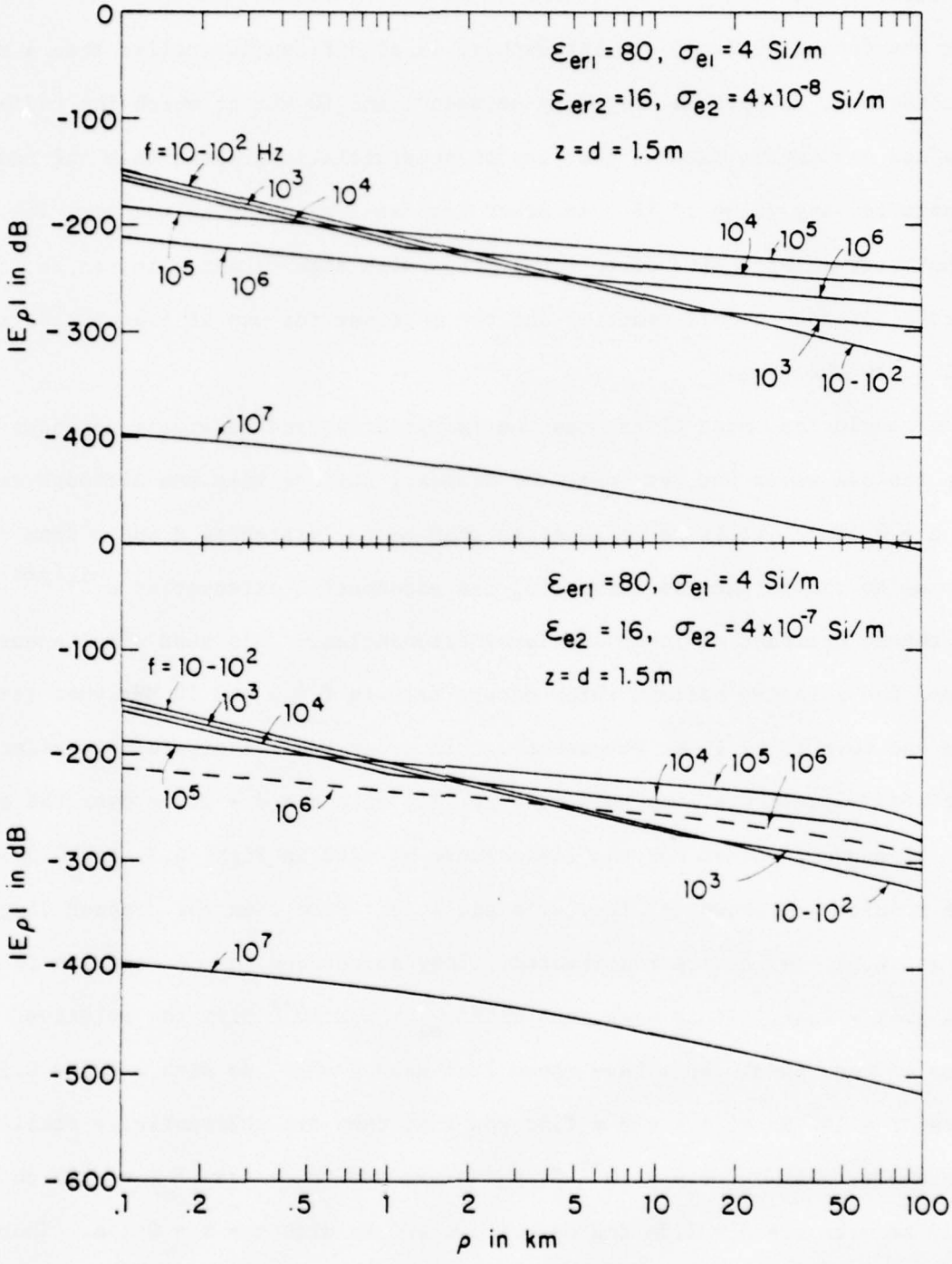

Fig. 4.5a Magnitude of $E\rho$ in Sea Water Bounded by the Lithosphere; z = d = 1.5 m

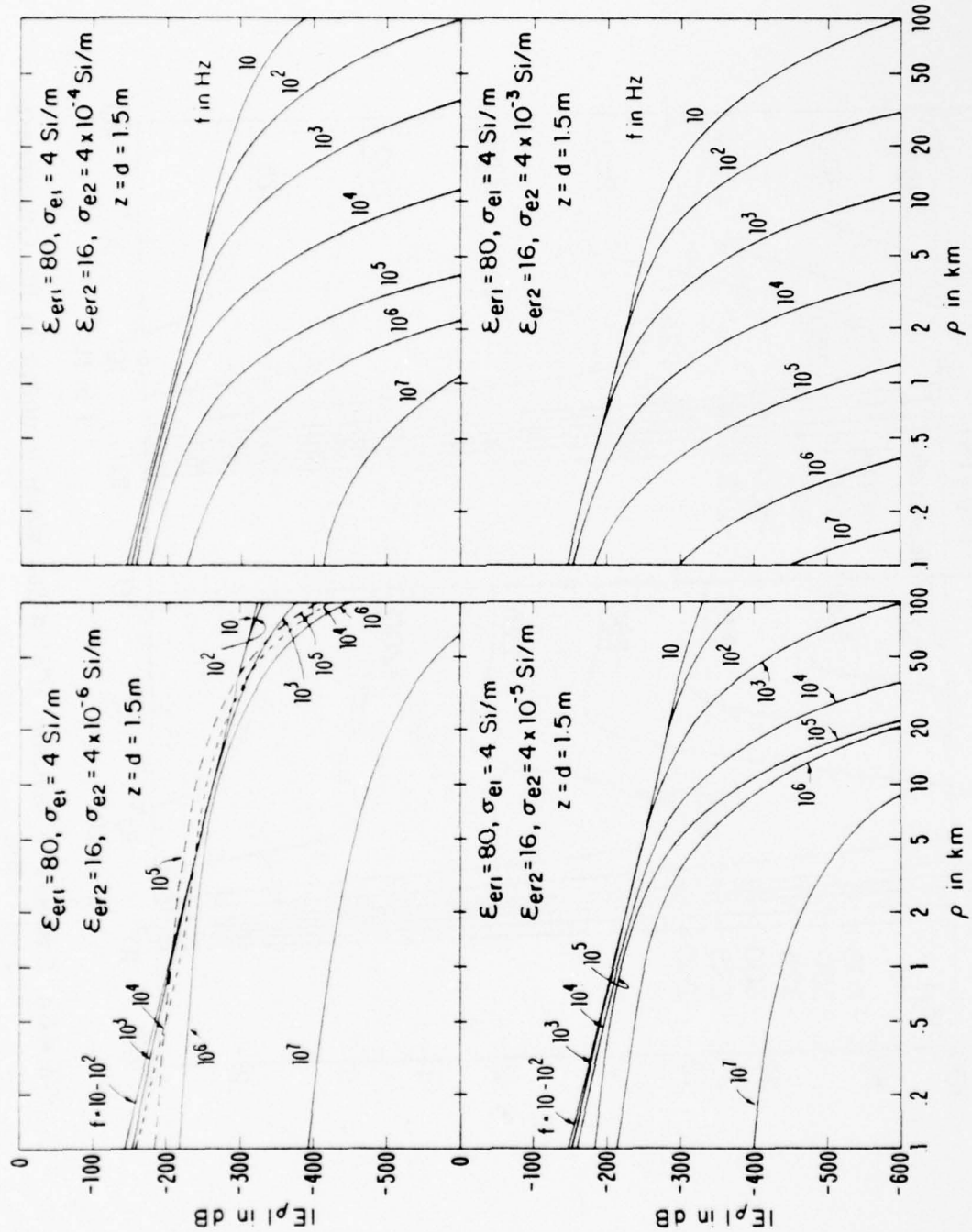

Fig. 4.5b Magnitude of E_ρ in Sea Water Bounded by the Lithosphere; z = d = 1.5 m

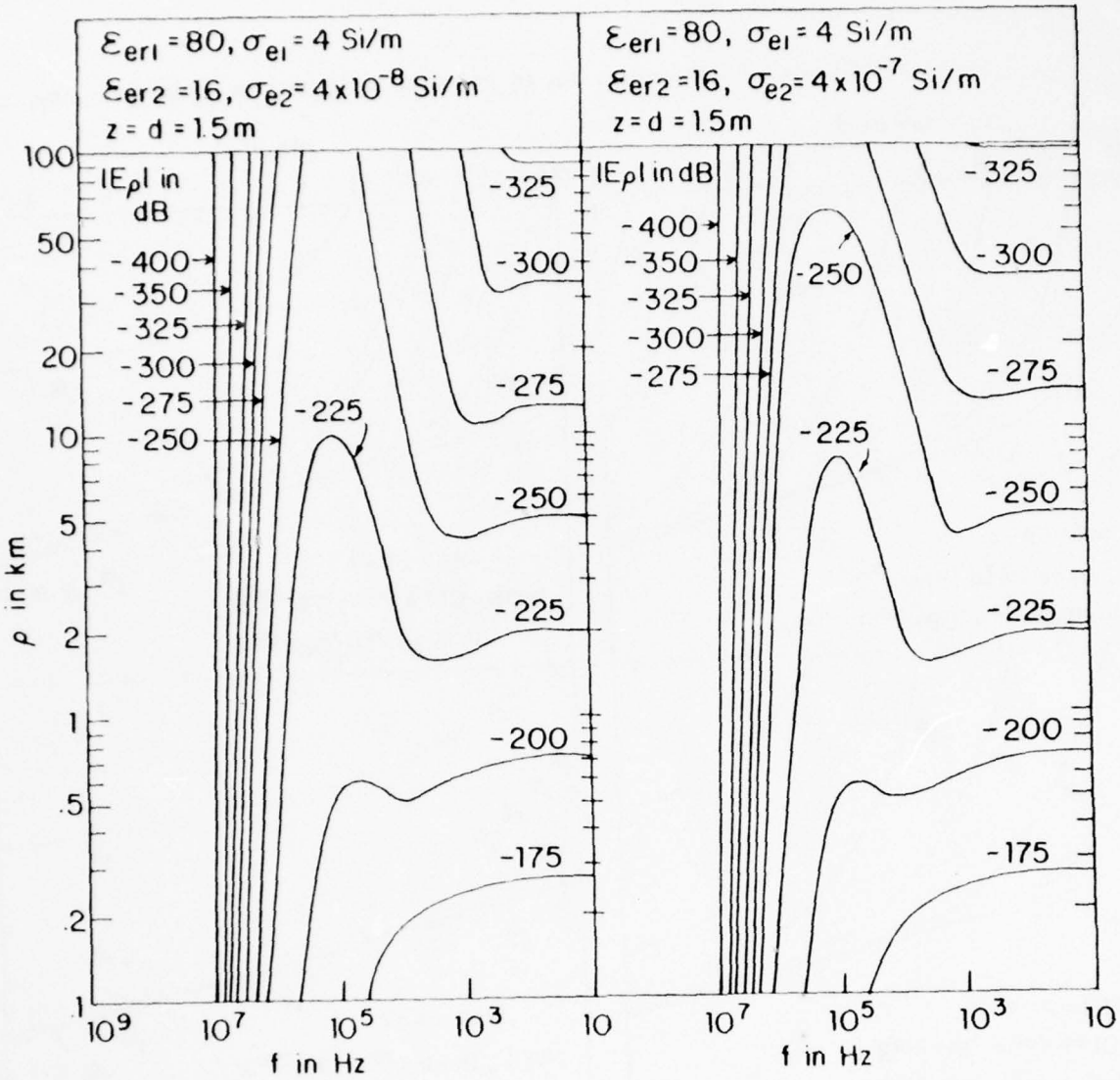

Fig. 4.6a Contours of Constant |Eρ| in Sea Water Bounded by the Lithosphere; z = d = 1.5 m

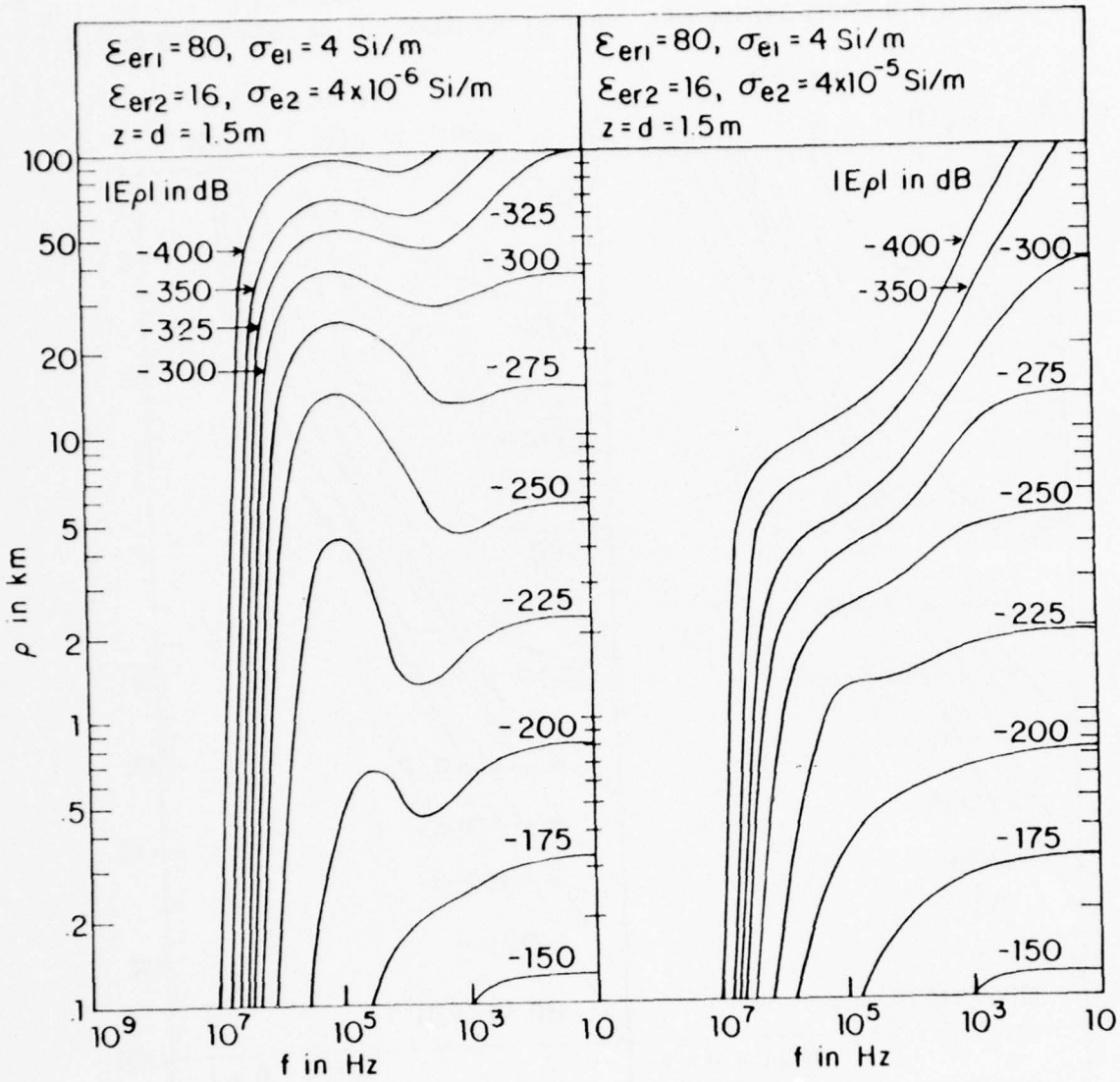

Fig. 4.6 b Contours of Constant |Eρ| in Sea Water Bounded by the Lithosphere; z = d = 1.5 m.

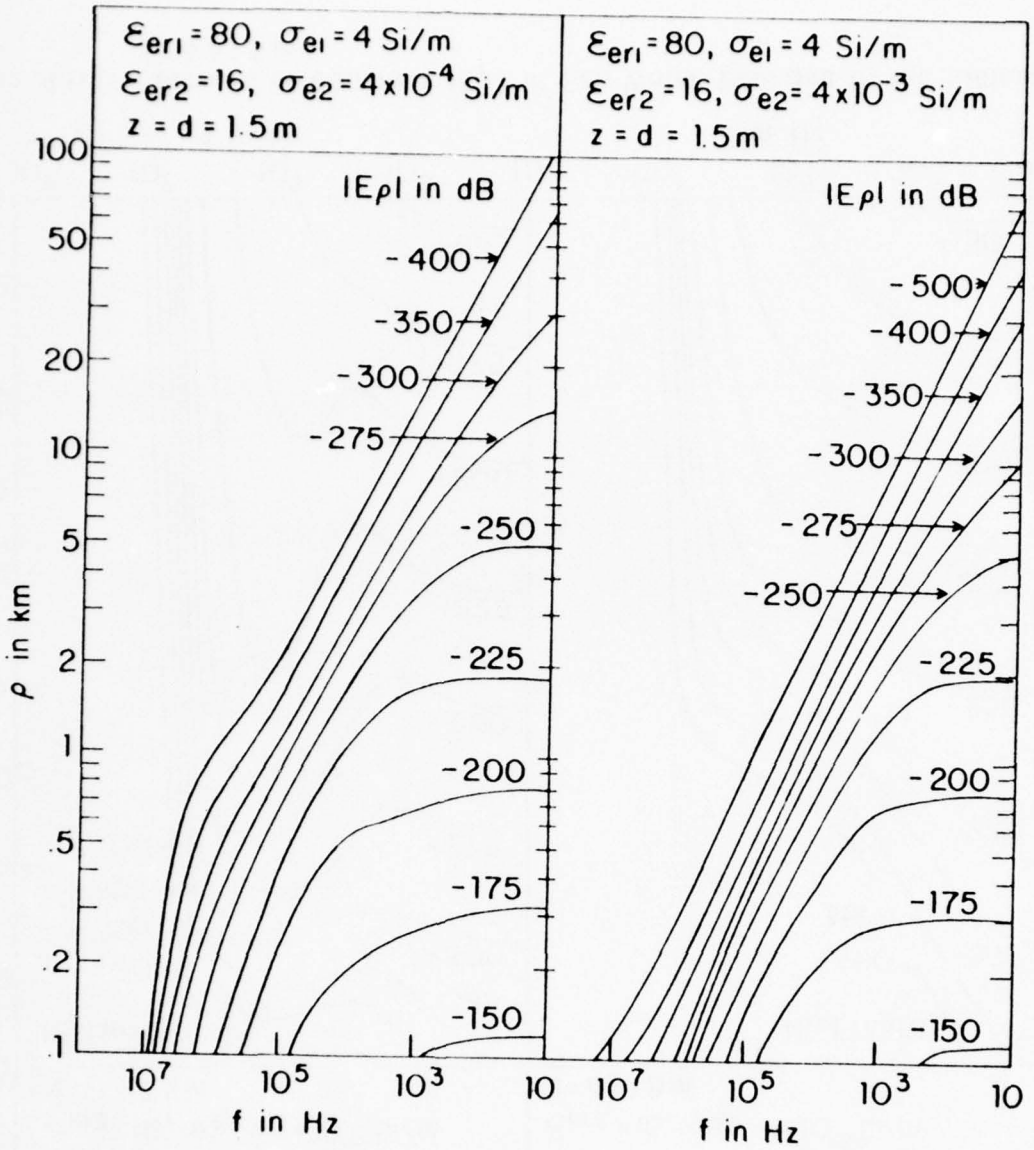

Fig. 4.6c Contours of Constant |Eρ| in Sea Water Bounded by the Lithosphere; z = d = 1.5 m

d) There is a potentially useful low-attenuation window in the frequency range between 0.1 and 10 MHz. It exists only when the conductivity of the lithosphere is sufficiently low, $\sigma_{e2} < 4 \times 10^{-6}$ Si/m. Furthermore, it is available only when the transmitting and receiving antennas are very close to the interface between the ocean and the lithosphere. When $(z+d) \leq 0.3$m the maximum radial range occurs when the frequency is near 10^7 Hz. As the distance from the boundary is increased the frequency for the maximum range decreases. It is near $f = 10^5$ Hz when $(z+d) = 3$ m. The magnitude of the maximum range also decreases as $(z+d)$ is increased.

5. LABORATORY MODELLING AND ELECTRODYNAMIC SIMILITUDE

5.1 Introduction

Laboratory modelling has been used to simulate or demonstrate the behavior of large scale electromagnetic systems by scaling dimensions and frequencies while keeping the same shape of the model and the system it is to simulate. For example, a full scale linear antenna of length L_e operating in air at a frequency f_e can be simulated by measurements on a similar shaped antenna of length $L_m = L_e/n$ provided the model is operated at a frequency $f_m = n\, f_e$ in air. For more general lossy media, a knowledge of the principles of electrodynamic similitude and limitations is needed for the use of models and interpretation of data. We examine relations for application to some propagation problems.

Millington (1948, 1949a,b) discovered the "recovery effect" on the amplitude of LF and VLF ground waves as they traversed a land-sea boundary. A simple model was used to demonstrate the effect, wood to represent the land and copper sheeting to represent the sea. A small microwave source was moved on a small cart away from the source on wood onto the metal whence the signal amplitude increased markedly at the "coast-line," (recovery) and then attenuated slowly along the copper "sea". Quasi-empirical relations were developed in his publications.* Pressey (1956) developed quasi-empirical relations for the phase shift. The matter was studied theoretically and experimentally by King and Maley (1966) and King, Maley, and Wait (1967).

---

*A group of us in February, 1950, witnessed Millington's demonstration at Marconi's arranged through the courtesy of the late Sir Robert Watson Watt.

The model was a tank filled with water to represent land and aluminum sheets to represent the ocean; data were obtained at 4 GHz. While scaling was not exact, the measured electric field strength was reasonably well in accord with prediction.

Model studies of propagation in an idealized crustal waveguide were made experimentally and theoretically by Brown and Gangi (1962, 1963) and Gangi (1966). We shall discuss their results, arranged to demonstrate similitude, a bit later, for a uniform slightly lossy guide represented by saline water.

Iizuka (1967, 1968, 1969) studied the impedance of an antenna and the field variations of waves propagated in a lithospheric waveguide for a guide having variable conductivity with depth. A gel of agar-agar with diffusion of sodium chloride was arranged to provide the desired profile. Similitude in size, frequency, etc., was accomplished and results will be discussed a bit later, also. Others have developed the similitude relations.

5.2 Principles of electrodynamic similitude

The principles of electrodynamic similitude were developed by Stratton (1941) and more completely delineated by Sinclair (1948). Brown and Gangi (1962, 1963) and Gangi (1966) gave the resulting equations, based on Stratton (1941) relating the scaling of frequency, sizes, and electrical parameters of the model system in terms of those quantities of the original system. Keller and Fritschkneckt (1966) gave a brief discussion for scaling media of large loss tangent. Iizuka (1968) developed the relations while employing generalized orthogonal coordinates for the identities of

Maxwell's equations in the original and model systems. Fritschkneckt (1971), basing his work in part on that of Sinclair (1948), used rectangular coordinates as did Sinclair (1948).

Since we are dealing with systems immersed in the earth, such as the lithosphere, we use the subscript "e" on related quantities; the subscript "m" will denote those quantities for the model.

The original and model media are characterized as isotropic, homogeneous, or inhomogeneous, with electrical constants of permittivity $\varepsilon = \varepsilon_o \varepsilon_r$ (where ε_o is approximately $10^{-9}/36\pi$ F/m and ε_r is the relative dielectric constant, a permability μ (which we will ultimately assume to be that of free space $\mu_o = 4\pi \times 10^{-7}$ H/m) and a conductivity σ in Si/m. The unit of length is r. In order that Maxwell's equations remain invariant from the original to model system, we shall scale the electric field strength E, the magnetic field strength H, and time. Thus, for the fields:

$$E_m = q_E E_e \tag{5.1}$$

$$H_m = q_H H_e \tag{5.2}$$

By showing the invariance of Maxwell's equations, we arrive at the relations for μ_m, ε_m and σ_m.

$$\mu_m = \frac{q_E}{q_H} \frac{r_e}{r_m} \frac{\tau_m}{\tau_e} \mu_e \tag{5.3}$$

$$\varepsilon_m = \frac{q_H}{q_E} \frac{r_e}{r_m} \frac{\tau_m}{\tau_e} \varepsilon_e \tag{5.4}$$

$$\sigma_m = \frac{q_H}{q_E} \frac{r_e}{r_m} \sigma_e \tag{5.5}$$

where τ is the unit of time such that $\tau_m/\tau_e = f_e/f_m = \omega_e/\omega_m$ where f is the

wave frequency and ω the angular frequency. The equations (5.1 through 5.3) are cast in the form of Iizuka (1968)*; as mentioned by Fritschkneckt (1971), they are termed by Sinclair (1948) as "absolute" models, for which q_E and q_H are known separately and not merely their ratio. If a specific value is not assigned to q_E or q_H, the model is termed "geometric" by Sinclair (1948).

Multiplying equation (5.3) by (5.4), one obtains:

$$r_m \omega_m \sqrt{\mu_m \varepsilon_m} = r_e \omega_e \sqrt{\mu_e \varepsilon_e} \tag{5.6.a}$$

$$k_m' r_m = k_e' r_e \tag{5.6.b}$$

$$r_m/\lambda_m' = r_e/\lambda_e' \tag{5.6.c}$$

where $k_m' = \omega_m \sqrt{\mu_m \varepsilon_m} = 2\pi/\lambda_m'$ and $k_e' = \omega_e \sqrt{\mu_e \varepsilon_e} = 2\pi/\lambda_e'$; i.e., the k_m' and k_e' are the wave numbers in loss-less dielectrics.**

From (5.4) and (5.5):

$$\frac{\sigma_m}{\omega_m \varepsilon_m} = \frac{\sigma_e}{\omega_e \varepsilon_e} \tag{5.7.a}$$

or

$$p_m = \frac{60\sigma_m \lambda_o}{\varepsilon_{rm}} = p_e = \frac{60\sigma_e \lambda_o}{\varepsilon_{re}} \tag{5.7.b}$$

where $p_{m,e}$ is also known as the loss-tangent $\tan \delta_{m,e}$ and λ_o is the free space wavelength (meters).

---

*i.e., equations (IV-13) through (IV-15) of Iizuka (1968).

**Equations (5.6) through (5.9) correspond to Iizuka's (1968) equations (IV-16) through (IV-19).

Again, from equation (5.3):

$$\frac{q_H}{q_E} \; r_m \omega_m \mu_m = r_e \omega_e \mu_e \tag{5.8}$$

which can be changed,* by using (5.6), to show:

$$\frac{q_E}{q_H} = \sqrt{\frac{\varepsilon_e}{\varepsilon_m}} \sqrt{\frac{\mu_m}{\mu_e}} = \sqrt{\frac{\varepsilon_{re}}{\varepsilon_{rm}}} \sqrt{\frac{\mu_m}{\mu_e}} \tag{5.9}$$

This relation is used when showing the scaled impedance relation of original and modelled antennas.

Iizuka (1968) preferred as convenient to express the similitude conditions as follows: equation (5.6) states the identity of electrical sizes in terms of the loss-less wavelength between original ("e") and model ("m") systems, and equation (5.7) states the identity of loss-tangents of the two systems.

Brown and Gangi (1962, 1963) and Gangi (1966) gave relations similar to those above, viz.:

$$f_m^{\,2} \, \mu_m \, \varepsilon_m \, r_m^{\,2} = f_e^{\,2} \, \mu_e \, \varepsilon_e \, r_e^{\,2} \tag{5.10}$$

$$f_m \; \mu_m \, \sigma_m \, r_m^{\,2} = f_e \; \mu_e \, \varepsilon_e \, r_e^{\,2} \tag{5.11}$$

If one takes the ratio of (5.11) to (5.10), the identity of loss-tangents in equations (5.7) result.

---

*Equations (5.6) through (5.9) correspond to Iizuka's (1968) equations (IV-16) through (IV-19).

With the assumption that $\mu_m = \mu_e = \mu_o$, they go to show:

$$\frac{\sigma_m}{\sigma_e} = \frac{f_m}{f_e}\sqrt{\frac{\varepsilon_{rm}}{\varepsilon_{re}}} = \frac{D_e}{D_e}\sqrt{\frac{\varepsilon_{rm}}{\varepsilon_{re}}} \tag{5.12}$$

$$\frac{f_m}{f_d} = \frac{D_e}{D_m}\sqrt{\frac{\varepsilon_{re}}{\varepsilon_{rm}}} \tag{5.13}$$

where D_e is the depth of the original lithospheric waveguide, and D_m that for the model. While they do not give expressions similar (5.9), Brown and Gangi in their published article (1963) do note that scaling keeps the number of wavelengths between scaled distances constant, which is equivalent to equation (5.6.c), i.e., loss-less wavelengths.

In practice, there are severe restrictions on using these relations in a simulator model. Paraphrasing Iizuka (1968):

(a) the values of ε_r and loss tangent for the model are limited

(b) the dimension scale factor has to be such that the model is not too small or too bulky

(c) ranges of ε_r and loss-tangent by mixing materials is limited

(d) changing loss-tangent or ε_r is complex, it being possible to minimize one while changing the other

(e) materials must not be noxious, explosive or too costly.

5.3 Laboratory lithospheric models and similitude

5.3.1 Idealized waveguide with electrical constants uniform with depth

Brown and Gangi (1962, 1963) and Gangi (1966) made laboratory measurements with a simulated waveguide, the simulation representing an "average"

set of conductivity values deduced from their proposed profiles (See Chapter 2).

The model of the lithosphere to be simulated is shown in the Figure 5.1. In their measurements, the earth model was assumed to have a depth D_e = 35 km, with $\varepsilon_{r2} = \varepsilon_{re} = 4$. Since their conductivity depth model (Chapter 2) showed a conductivity $\sigma_2 = \sigma_m$ that might vary with frequency, appropriate scaling ratios were employed.

An aluminum (or carbon) plate represented the overburden or upper crust and an aluminum plate was used for the lower crustal boundary (Moho). The crustal waveguide was a salt water solution whose conductivity could be varied. A frequency scale factor of $f_m/f_e = 10^5$ was chosen for simplicity in the models. The value of ε_{rm} for water was 80. Since waveguide distances of 1000 km were desired to be simulated, and a conveniently-sized tank was desired for the laboratory, a distance (or depth D_m/D_e) scale factor works out to be 4.47×10^5; thus if D_e were 35 km, a tank depth of 7.82 cm or 3.08 inches results. Distances were plotted in units of H_e or H_m ($H_e = D_e$, $H_m = D_m$).

5.3.1.1 Sample results

In Figure 5.2 is shown measurements on the model at 300 MHz, in the tank 3.08 inches in depth, of the vertical (relative) electric field strength over a range of 2H to 17H (when H is H_m or H_e, the conductivity σ_m being 0.07 Si/m. The loss tangent p_m = .0525 which is small; the corresponding plane wave attenuation is then $\alpha_m = 60\pi\sigma_m\lambda_o/\varepsilon_{rm}^{1/2} = 3.30 \times 10^{-6}$ n/m = 0.28 dB/km. These values of loss-tangent for the earth p_e and σ_e work out to be the same, since they are scaled.

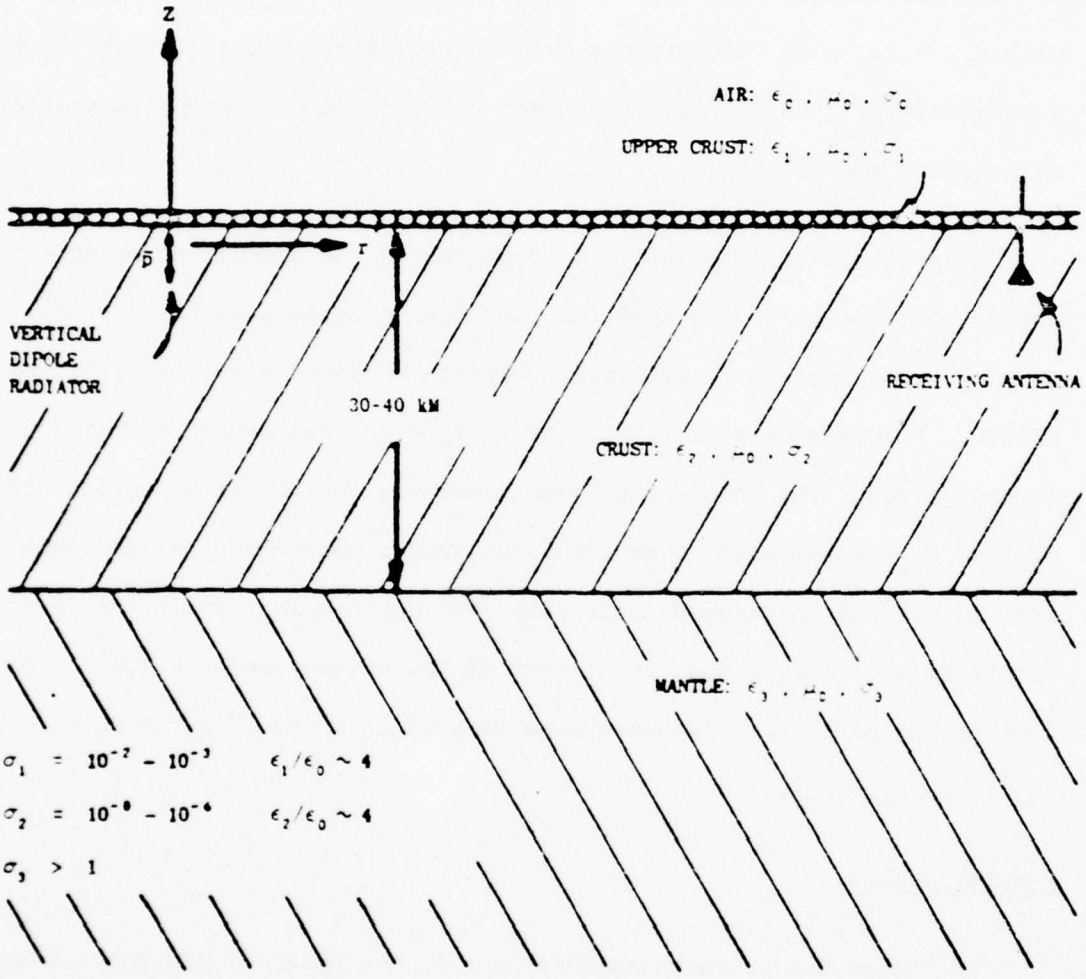

Fig. 5.1 Brown and Gangi model of earth for lithospheric analysis (from Gangi,1966)

In comparison with theory, Figure 5.2 shows bracketing calculations as dots or crosses; the dots correspond to σ_m = .05 Si/m for which the loss tangent p_m is 0.0375 for f_m = 300 MHz just as it is for the scaled value of $\sigma_e = 2.5 \times 10^{-8}$ Si/m at a frequency of 3KHz. The crosses are for calculations for σ_m = 0.10 Si/m for which the loss-tangent p_m = 0.075 at 300 MHz, corresponding to the earth values $\sigma_e = 5 \times 10^{-8}$ Si/m at 3 KHz. The calculations bracket well the measured curve.

Brown and Gangi (1962, 1963) and Gangi (1966) show the effects on field distributions when simple inhomogeneities were introduced. These included (a) a step barrier in the lower boundary to correspond to the shallower depth of the Moho under the sea at the continent-sea boundary; (b) a bar in the upper boundary to represent a geologic fault zone, and (c) a cylinder to correspond to a lens or intrusion of mountains into the granite. While idealized, the results showed potential interference patterns compared with those when no discontinuity was present. (See the original papers for detailed results). It should be noted that the ocean crust may differ markedly in electrical properties from that of the continental crust (Cox, 1971, 1978).

5.3.2 Lithospheric waveguide with constants varying with depth (inhomogeneous)

An inhomogeneous lithospheric waveguide, i.e., a waveguide whose electrical parameters vary with depth has been investigated theoretically in the past seven or eight years but relatively little has been reported on simulation experiments. While the depth variations may be represented by thin horizontal slabs, it is a bit more satisfying to simulate the smooth (sic) depth profiles by suitable materials whose properties may be smoothly

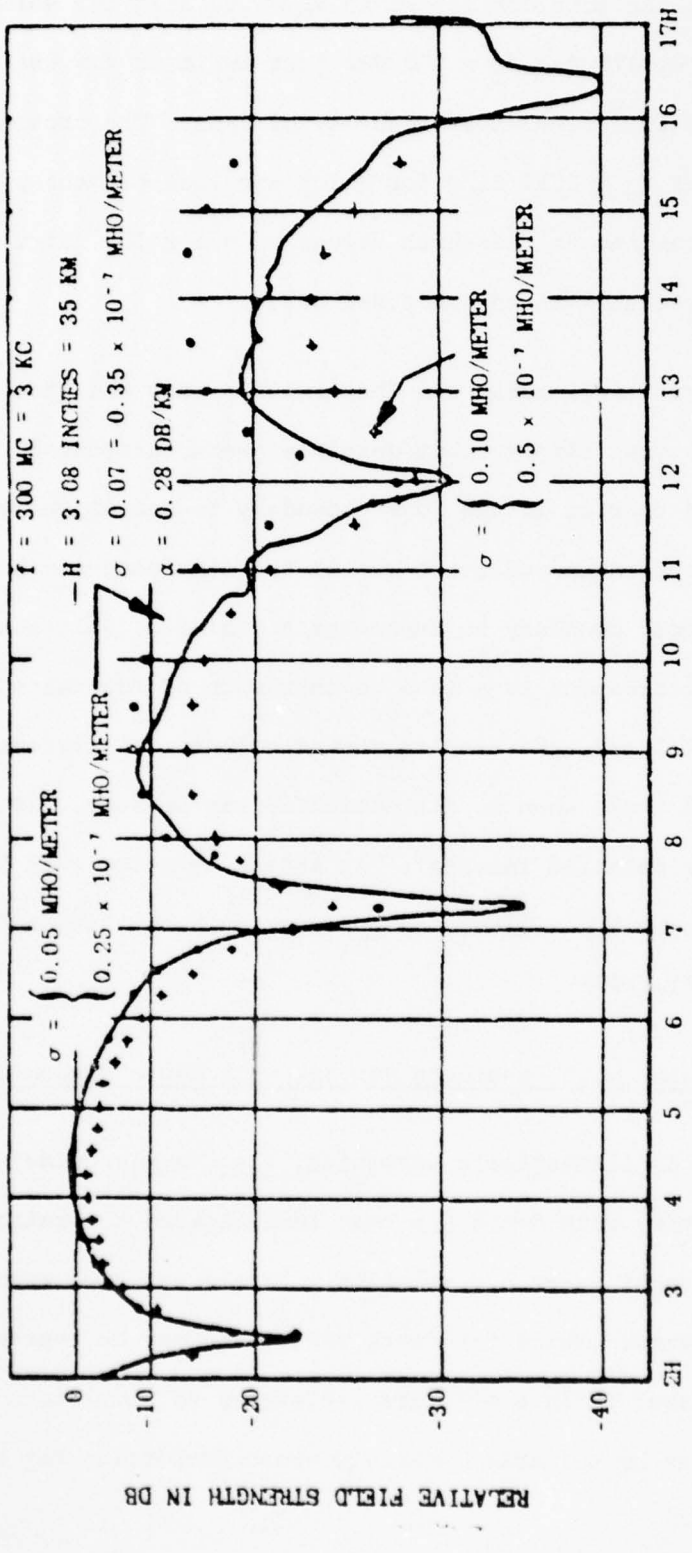

Fig. 5.2 Brown and Ganci similitude model measurements, 300 MHz. Solid curve, measurements; dots and crossestheory with bracketing conductivities.(from Ganci,1966)

AD-A070 531 DEBETTENCOURT (JOSEPH T) NEWTON MA* F/G 20/14
LITHOSPHERIC RADIO PROPAGATION MODELLING A FEASIBILITY STUDY.(U)
APR 79 J T DEBETTENCOURT, R W KING N00014-78-C-0668
UNCLASSIFIED DBK-2 NL

2 OF 2
AD
A070531

END
DATE
FILMED
8-79
DDC

changed. About the only extended model investigations reported are those of Iizuka (1967, 1968, 1969, 1971, 1972). I have found no theoretical comparisons with his measurements. His results extend earlier ones on antenna impedance with stratified films of Iizuka and King (1962 a,b).

The simulator chamber used an agar-agar solution (gel) into which a solution of sodium chloride (NaCl) could diffuse to change the concentration. Two chambers were built, one for antenna impedance measurements and a second larger one for field strength measurements. The technique of fabricating inhomogeneous media was described in Iizuka's 1967 paper; a summary of the work on impedance and field strength appears in his 1972 paper.

The variation of loss tangent and relative dielectric constant as a function of frequency are shown in Figure 5.3 for various media such as agar-agar, agar-agar with ethyl alcohol, tap water, 0.1 mol NaCl solution and ethyl alcohol. For agar-agar NaCl affects loss tangent; ethyl alcohol affects ε_r.

Agar-agar has a high dielectric constant and for simulation use it can reduce the dimensions of the simulation chamber. For various reasons (See Iizuka 1968, Chapter III), a modelling frequency of 114 MHz was chosen. The properties of agar-agar with concentration of NaCl at 114 MHz are shown in Figure 5.4. On the Figure equations for least squares fit are given for ε_r and tan δ, as a function of the concentration C of the NaCl. The agar-agar solution was 1.3% agar-agar and 98.7 tap water. The concentration of NaCl was the weight in grams in 1000 cu cm of agar-agar. If this concentration C is less than 3, then the approximations simplify to:

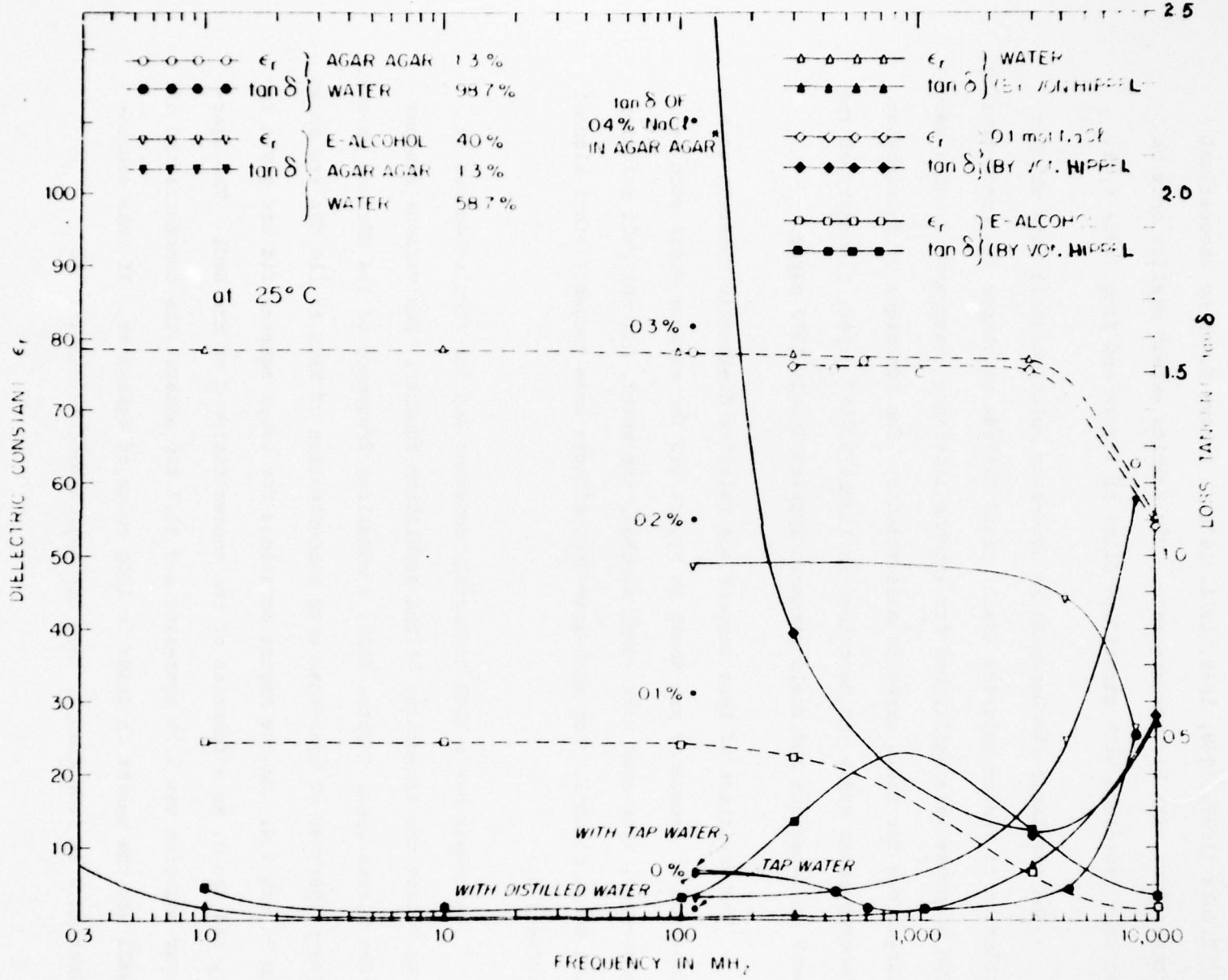

Fig. 5.3 Dielectric constant and loss-tangent vs. frequency for various media, especially agar-agar (from Iizuka, 1968)

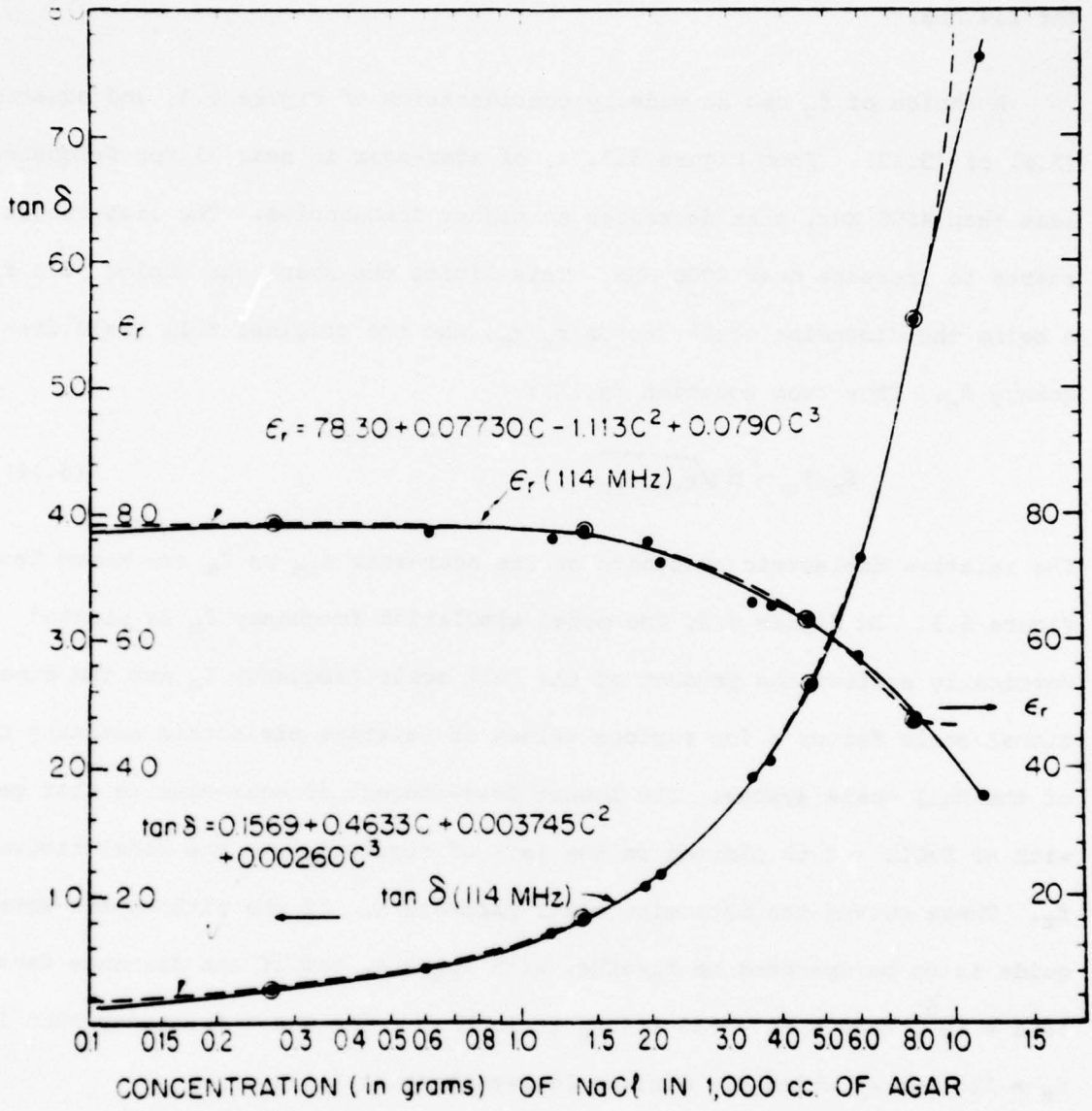

Fig. 5.4 Dielectric constant and loss-tangent of agar-agar as a function of concentration of sodium chloride (NaCl) at 114 MHz. (From Iizuka, 1968)

$$\varepsilon_r = 78.30 + 0.073\ C \tag{5.14}$$

$$p = \tan \delta = 0.1569 + 0.4633\ C \tag{5.15}$$

for 114 MHz.

A choice of f_m can be made by consideration of Figure 5.3, and equation (5.6) or (5.13). From Figure 5.3. ε_r of agar-agar is near 78 for frequencies less than 4000 MHz, then decreases at higher frequencies. The loss-tangent starts to increase near 4000 MHz. This limits the agar-agar choice of n f_m, n being the dimension scale factor r_e/r_m, and the original full scale frequency f_e. Thus from equation (5.13):

$$f_m/f_e = n\sqrt{\varepsilon_{re}/\varepsilon_{rm}} \tag{5.16}$$

The relative dielectric constants of the agar-agar ε_{rm} vs f_m are known from Figure 5.3. In Figure 5.5, the model simulation frequency f_m is plotted vertically against the product of the full scale frequency f_e and the dimensional scale factor n for various values of relative dielectric constant E_{re} of the full scale system. The lowest loss-tangent of agar-agar is that get with no NaCl. It is plotted on the left of Figure 5.5 vs the model frequency f_m. These curves can determine model parameters. If the lithosphere waveguide is to be operated at f_e=5KHz, with ε_{re} = 4, and if the distance factor is $n = 10^5$, then n f_e = 500 (if f_e is in Mhz). The model frequency then is f_m = 114 MHz at which the minimum loss-tangent is 0.13.

Various profiles of the lithosphere itself were deduced from values published up to about 1965 and combined into one plot from Iizuka (1968) and are shown in Chapter 2. A typical simulated profile is shown in Figure 5.6 for a frequency f_e of 5 KHz for loss tangent, the relative dielectric constant

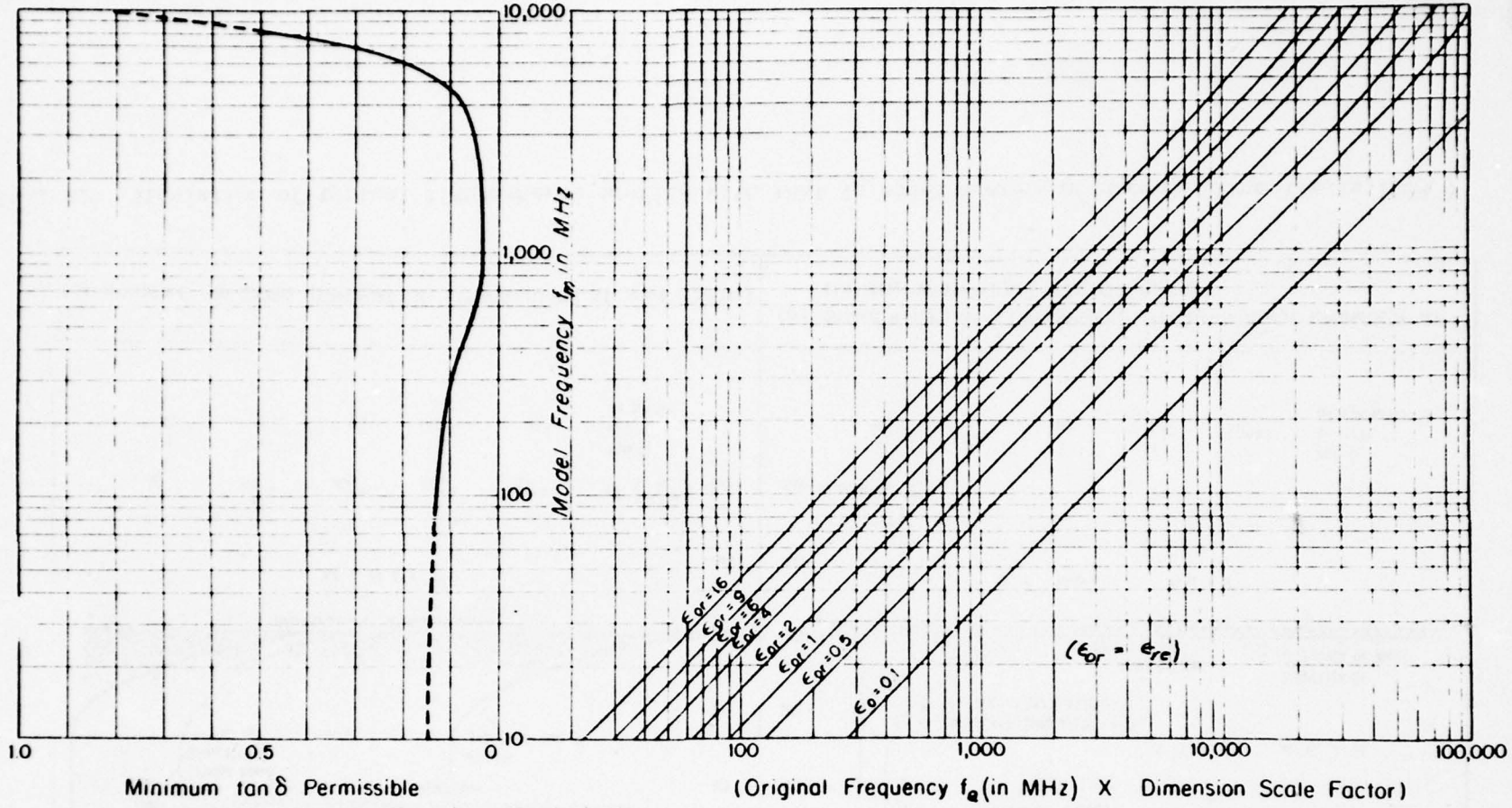

Fig. 5.5 Cross graphs showing relation between model frequency and the product (of original "earth" frequency times dimension factor) and curve of minimum loss-tangent for agar-agar (From Iizuka, 1968).

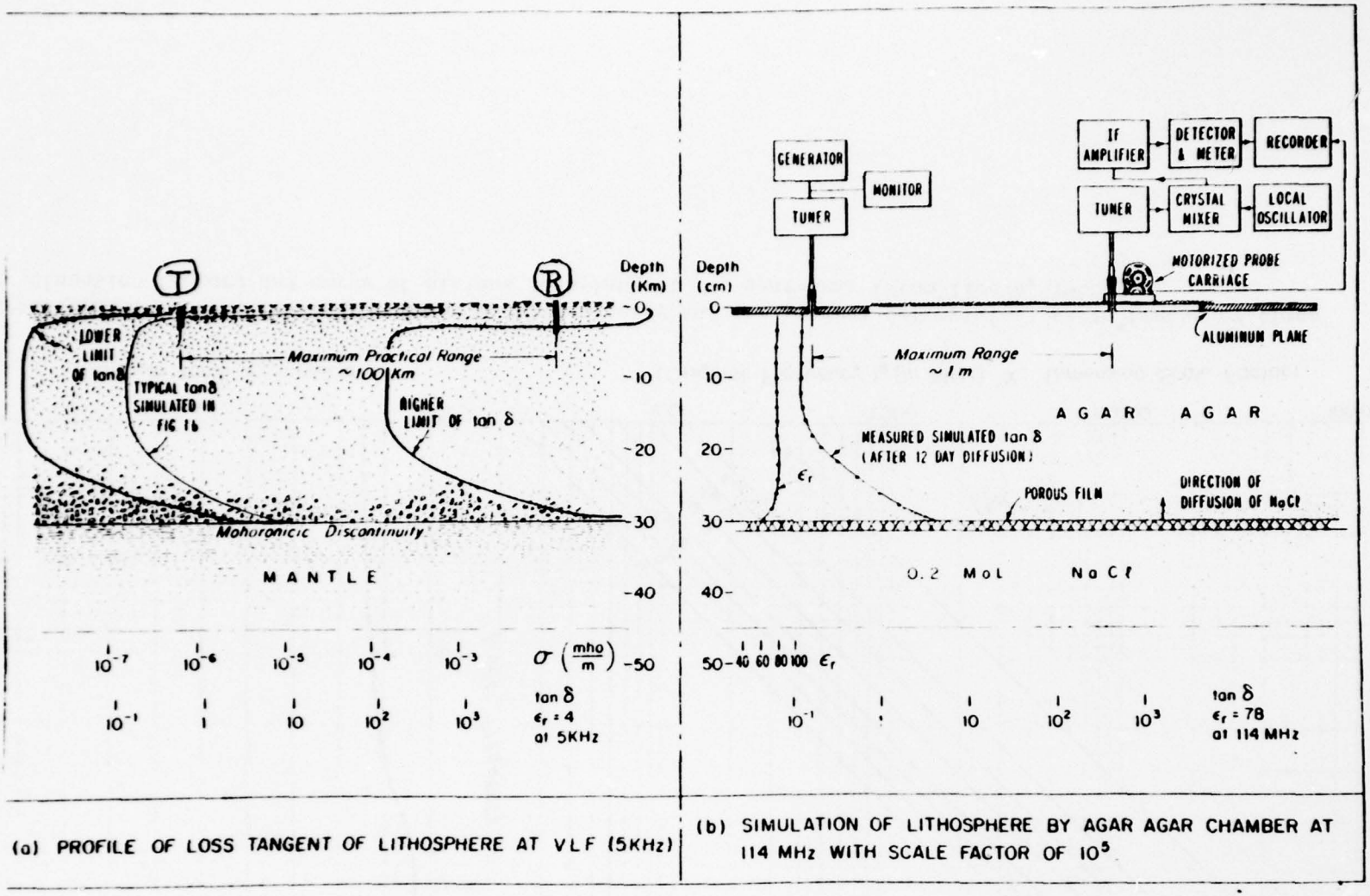

(a) PROFILE OF LOSS TANGENT OF LITHOSPHERE AT VLF (5KHz)

(b) SIMULATION OF LITHOSPHERE BY AGAR AGAR CHAMBER AT 114 MHz WITH SCALE FACTOR OF 10^5

Fig. 5.6 Simulation of typical lithospheric profile with that in model agar-agar chamber (From Iizuka, 1968)

ε_{re} being 4 and constant with depth. The depth of the lithosphere D_m was 30 km, and a modelling scaling factor of 10^5 was used so that the simulation chamber was 30 cm deep, D_m = 0.3 meters. An aluminum plane represented the large loss-tangent upper crust, and a water solution of 0.2 mol NaCl represented the mantle. The simulated profile of the conducting layer was obtained by diffusion of the NaCl, through a porous film into the agar-agar at the bottom.

Iizuka (1968, Chapter IX) describes how to fabricate profiles of various shapes including (a) complimentary error function, (b) error function, (c) linear profile, (d) periodic profile, and (e) miscellaneous profiles.

5.3.2.1 Field strength measurements

It should be mentioned that the experimental modelling chamber of Iizuka could be arranged also with non-parallel top and bottom, a vertical step profile (similar to Brown and Gangi, 1963), a vertical slant profile, or with simultaneous horizontal and vertical profiles.

5.3.2.1.1 Non-parallel plate region with homogeneous medium

The geometry is shown in Figure 5.7. Table I shows the dimensions and electrical properties of the medium for various geometers. Note that for loss tangents of 0.036, 0.23 and 0.88, the corresponding conductivities are 0.073, 0.47 and 1.78 Si/m, the latter approaching that for sea water.

The resulting electric field strength E in Figure 5.8 is shown plotted as $E\ R$ vs the range R for a quarter-wave monopole radiator. Note maxima and minima for the lowest loss-tangent. The smaller the angle the smaller

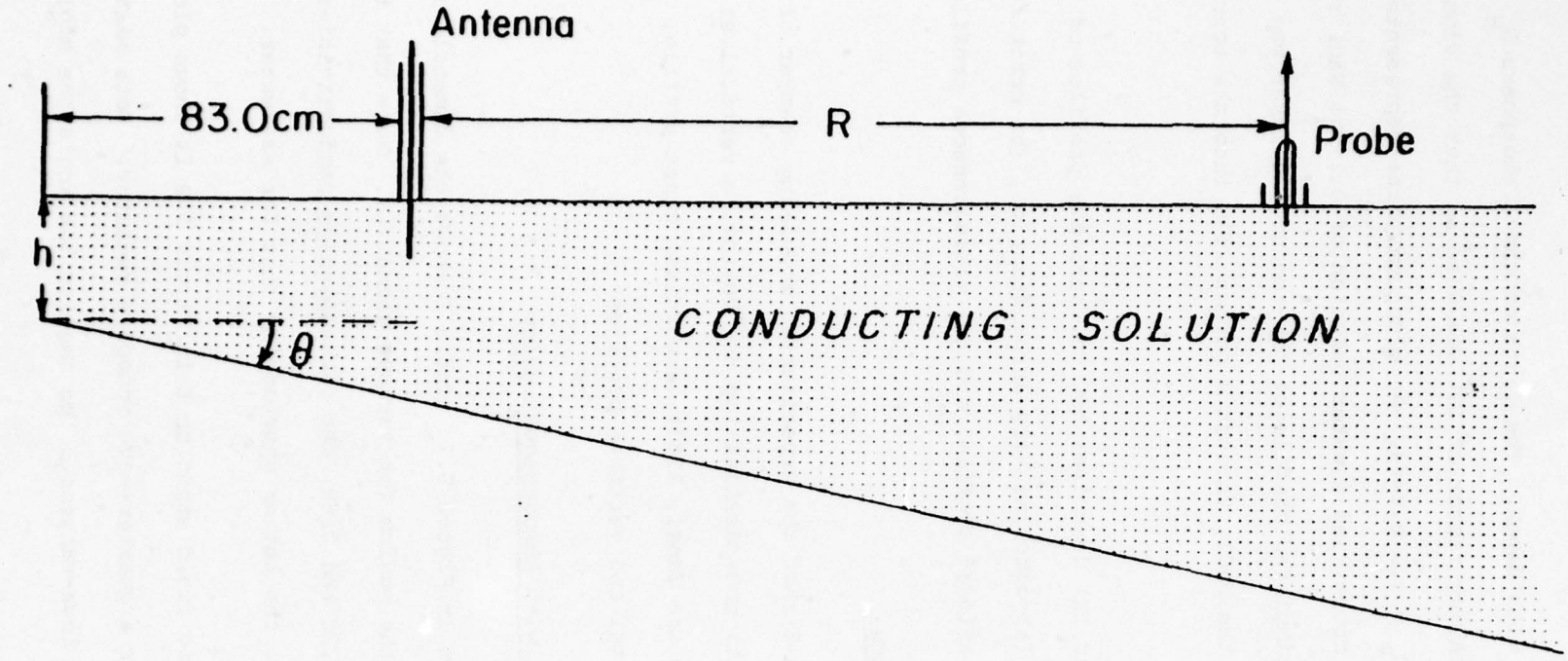

Fig. 5.7 Geometrical sketch of non-parallel plate region filled with lossy medium. (From Iizuka, 1969)

TABLE 5.1

Dimensions and electrical properties of the medium in a non-parallel plate region.

At 114 MHz

Coding	h (in cm)	Angle (in deg)	ε_r	tan δ
3a	8.3	$3^{\circ}53'$	78	0.036
3b	8.3	$3^{\circ}53'$	78	0.23
3c	8.3	$3^{\circ}53'$	78	0.88
$\bar{3}$a	29.0	$-3^{\circ}53'$	78	0.036
$\bar{3}$b	29.0	$-3^{\circ}53'$	78	0.23
$\bar{3}$c	29.0	$-3^{\circ}53'$	78	0.88
5b	7.7	5°	78	0.23
5c	7.7	5°	78	0.88
$\bar{6}$a	39.0	$5^{\circ}57'$	78	0.036
$\bar{6}$b	39.0	$5^{\circ}57'$	78	0.23
$\bar{6}$c	39.0	$5^{\circ}57'$	78	0.88

See Fig. 5.7 for geometry

(From Iizuka, 1969)

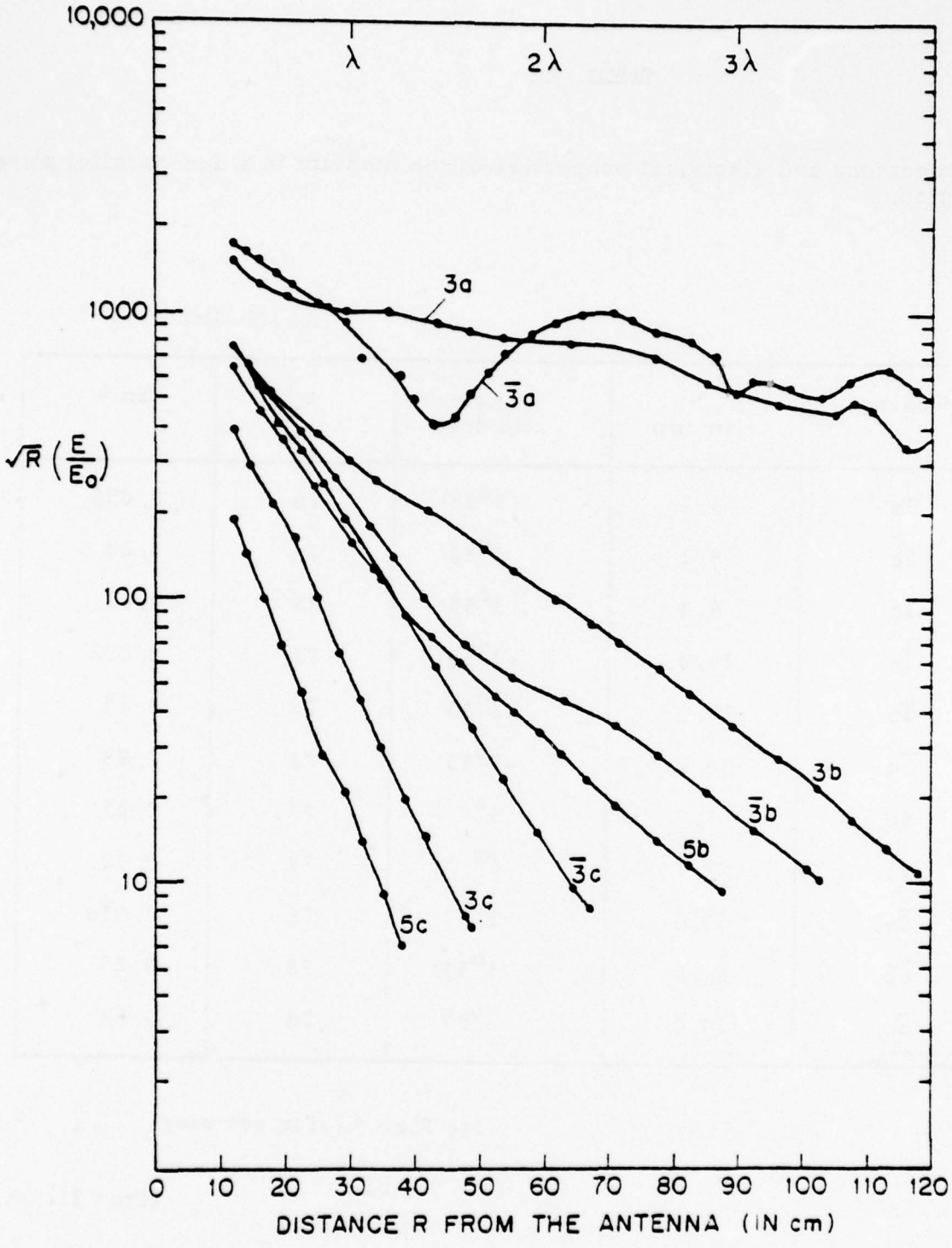

FIG. 5.8 PLOT OF $E\sqrt{R}$ vs. R IN UNPARALLEL PLATE REGION FILLED WITH A CONDUCTING MEDIUM AT 114 MHz. SEE THE PARAMETERS IN TABLE 5.1 (IZUKA, 1969)

the attenuation. As conductivity increases, the attenuation becomes less sensitive to angle changes. That is, at high conductivity the propagation depends more on the losses of the medium than by the geometry of the bottom. This is useful to know for operation at sloping shore lines.

5.3.2.1.2 Field strength measurements in an inhomogeneous medium

For the lithospheric guide model an agar-agar gel represented the lithosphere, covered with a metal plate top. A quarter-wave monopole extended through the plane into the medium. As such, the configuration was similar to a parallel waveguide with metallic walls except that the bottom was replaced by an inhomogeneously conducting wall. Figure 5.9 is a representative result. The depth profile of ε_r and loss-tangent is shown in Figure 5.9 (b), while the amplitude and phase of the magnetic field strength H_ϕ are shown in Figure 5.9 (a). Note the model was 0.383 λ thick, yet the field strength decreases monotonically with depth. The field was measured at R = 50 cm; a perfect guide, less than half a wavelength thick would have a field magnitude invariant with depth.

5.3.2.1.3 Comment - Images

Figure 5.9 represents measurements on a model lithosphere for which the upper wall was a metal plate above the inhomogeneous lithospheric model. In essence, this could be considered one-half of a lithosphere having a symmetrical inhomogeneous profile, the upper half being the image of the lower one shown. Since the excitation was by a vertical monopole, the result would be that of a center-driven dipole, giving maximum field strength at the center where the conductivity (loss tangent) is minimum.

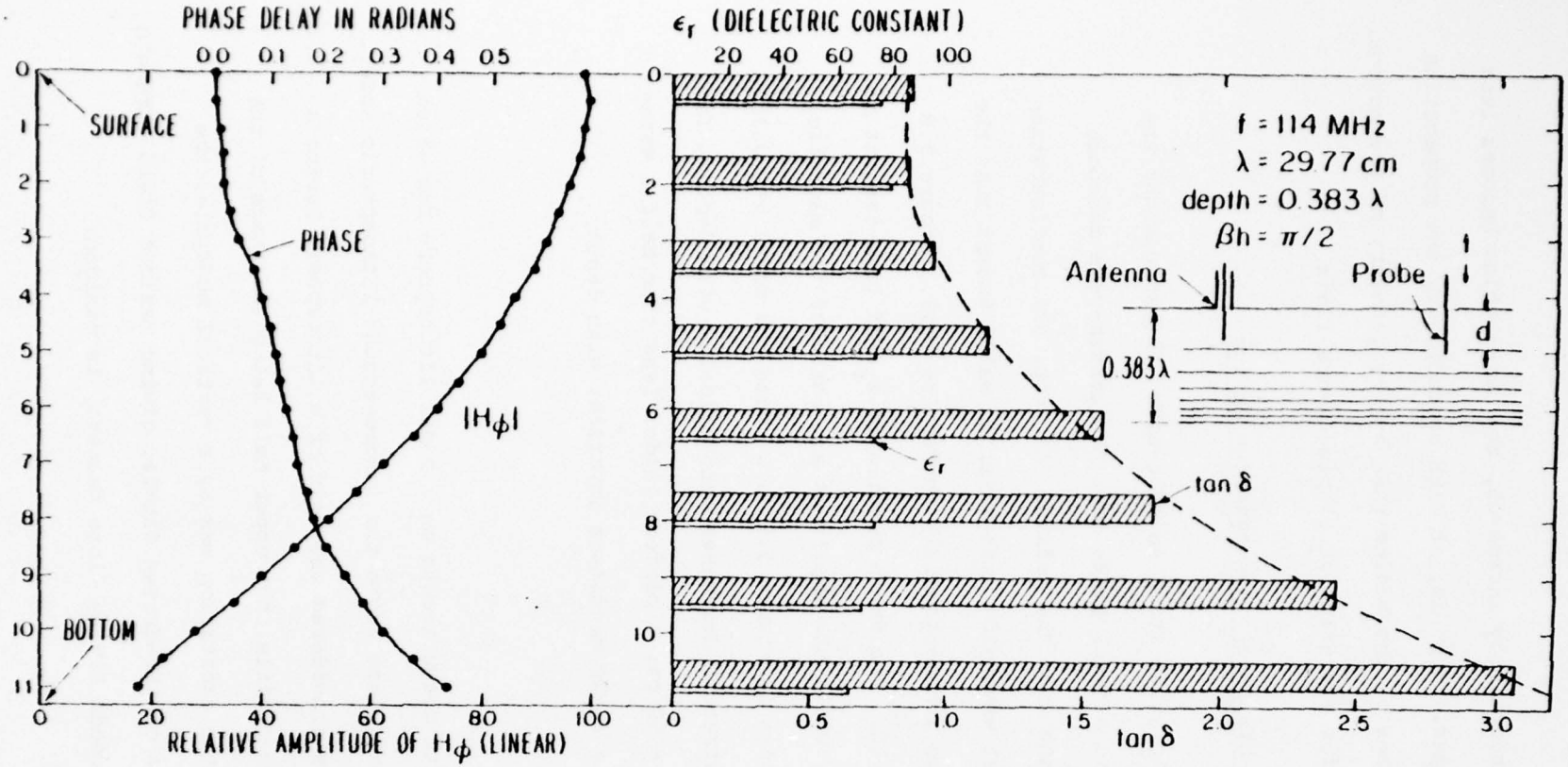

(a) FIELD DISTRIBUTION vs DEPTH (b) PROFILES OF PROPERTIES OF MEDIUM vs DEPTH

FIG. 5.9 DISTRIBUTION OF FIELD INTENSITY AS A FUNCTION OF DEPTH (IIZUKA, 1969)

Several of the more recently postulated profiles, such as those of Keller or of Housely discussed in Chapter 2, can be approximated by quasi-symmetrical profiles. Calculations of Field and Dore (1973) show maximum field strengths near that for minimum conductivity.

Advantage could be taken of this image effect along with the various inhomogeneous model profiles achieved by Iizuka using the agar-agar gel with sodium chloride and ethyl alcohol diffusion discussed in Section 5.3.2. The uniform profiles of Brown and Gangi (1963) with saline water could likewise be treated - the scaling parameters would have to be reconsidered. See Chapter 6.

The use of images for measuring wall losses is also discussed in Chapter 6. Here, however, the question of similitude scaling application is difficult to answer because the walls are necessarily water instead of metal, in order to make distance or depth dependent measurements in the "walls" be the fields excited by dipoles in the lithosphere or in the walls. Nevertheless, the principles will be demonstrated and the simpler measurements understood before proceeding step by step to more complex cases.

This leads to a discussion of modelling materials.

5.4 Modelling Materials

5.4.1 Typical High-conductivity Materials

Fritschkneckt (1971) gives a table of typical high conductivity materials which might be considered for modelling purposes, and is shown in Table 5.2. Listed are values for metals, other solids, and some

Material	Conductivity mho/m
Metals	
Aluminum	3.84×10^7
Aluminum, commercial alloys	$1.22 - 3.60 \times 10^7$
Brass	$1.2 - 1.5 \times 10^7$
Bronze, phosphor	$0.97 - 1.04 \times 10^7$
Bronze, "Everdur"	$3.8 - 5.3 \times 10^6$
Copper	5.81×10^7
Copper, tube (DHP copper)	5.01×10^7
Lead	4.55×10^6
Magnesium	2.17×10^7
Manganin	2.27×10^7
Mercury	1.04×10^6
Steel, nonmagnetic stainless	$1.35 - 2.34 \times 10^6$
Zinc	1.92×10^7
Other solids	
Carbon	$2.0 - 2.8 \times 10^4$
Graphite	$0.7 - 1.2 \times 10^5$
Epoxy, commercial silver loaded	5.0×10^5
Epoxy, commercial copper loaded	2.5×10^4
"Lay-up" resin, graphite loaded	$0 - 1.0 \times 10^4$
Wax, bronze loaded	$1 - 1.25 \times 10^4$
Silicone rubber, silver loaded	1.3×10^5
Liquids	
Ammonium chloride, 10% by weight in water at 18°C	17.8
Copper sulfate, as above	3.2
Hydrochloric acid, as above	62.9
Sodium chloride, as above	12.0
Sulfuric acid, as above	39.2
Sea water	3 - 5

TABLE 5.2 Higher conductivity modelling materials (from Frischkneckt,1971)

NAME OF SOLVENT	FORMULA	DIELECT CONST	CONDUCTIVITY	SOLUBILITY*	TOXICITY	FLAMMABILITY	PRICE/100g OR GAL.	BOILING PT	DRAWBACKS*
BENZENE	C_6H_6	2.296	$5.32 \cdot 10^{-17}$	H	CHRO	FLAM	58/GAL.	80.09	S
TOLUENE	$C_6H_5CH_3$	2.378	$1.4 \cdot 10^{-14}$	H	ACUTE	"	55/GAL.	110.8	S
OXYLENE	$C_6H_4(CH_3)_2$	2.567		H	"	FLAM., EXPL.	02/100 g	144.4	S
p-CYMENE	$CH_3C_6H_4CH(CH_3)_2$	2.249	$2 \cdot 10^{-8}$	H		FLAM	5.15/100 g	334.0	S
NAPHTHALENE	$C_{10}H_8$	3.22	$4 \cdot 10^{-10}$	H	CHRO	"	3.88/500g	217.9	S
TETRAHYDRONAPHTHALENE	$C_{10}H_{12}$	2.66		H	"	"	8.22/3 kg	207.2	S
PINENE	$C_{10}H_{16}$	2.70		H		"	7.24/1 kg	155.5	S
OIL OF TURPENTINE		2.25		H	ACUTE	"	1.50/GAL.	153.0	S
O-CRESOL	$CH_3C_6H_4OH$	5.65	$0.12 \cdot 10^{-8}$	F or H	"	"	1.25/500g	191.50	POISONOUS
m-CRESOL	$CH_3C_6H_4OH$	4.95	$1.397 \cdot 10^{-8}$	F or H	"	"	1.80/250g	202.8	POISONOUS
p-CRESOL	$CH_3C_6H_4OH$	5.48	$1.378 \cdot 10^{-8}$	F or H	"	"	1.89/kg	202.0	POISONOUS
DIETHYL ETHER	$C_2H_5OC_2H_5$	4.355	$3.7 \cdot 10^{-13}$	H	CHRO	FLAM., EXPL.	6.22/GAL.	34.6	
DI ISO AMYL ETHER	$[(CH_3)_2CH(CH_2)_2]_2O$	2.817		H			2.30/100g	172.5	C
BENZYL ETHYL ETHER	$C_6H_5CH_2OC_2H_5$	3.87		H			2.14/500g	184.7	C
ANISOYL CHLORIDE	$CH_3OC_6H_4COCl$	4.35	$1 \cdot 10^{-13}$	F	ACUTE			170.59	UNSTABLE
PHENETOLE	$C_6H_5-O-C_2H_5$	4.47	$17.0 \cdot 10^{-9}$	H	"	FLAM.	1.62/250g	182.0	C
o-CRESYL	$(CH_3C_6H_4)_2O$	3.57		H	"	"		198.8	C
m-CRESYL METHYL	$(CH_3C_6H_4)_2O$	4.08		H	"	"		202.8	C
p-CRESYL METHYL	$(CH_3C_6H_4)_2O$	4.03		H	"	"		202.0	C
DIOXANE	$OCH_2CH_2OCH_2CH_2$	2.235	$5 \cdot 10^{-15}$	G		FLAM., EXPL.	14/100 g	101.5	
METHYLAL	$CH_2(OCH_3)_2$	2.7		G	CHRO	FLAM		76.09	C
ACETAL	$CH_3CO CH_2OH$	3.79		F	ACUTE		5.40/100 g	118.17	C
ACETIC ACID	CH_3COOH	6.13	$11.2 \cdot 10^{-9}$	G	"	"	1.80/lb.	118.1	EATS METALS
n-BUTYL ACETATE	$CH_3COO(CH_2)_3CH_3$	5.00	$2.55 \cdot 10^{-8}$	F	CHRO	"	2.85/250g	126.5	C
ISO-BUTYL ACETATE	$CH_3COO C_4H_9$	5.32		F			1.50/500g	126.0	C
ISO-AMYL PROPIONATE	$CH_3CH_2COO(CH_2)_4CH_3$	4.25		F		"		144.2	C
ISO-AMYL n-BUTYRATE	$(CH_3)_2(CH_2)_4COO$	3.95		F				178.6	C
ISO-AMYL ISO-VALERIANATE	$(CH_3)_2(CH_2)_3CH_2COO$	3.62		F				190.3	C
METHYL BENZOATE	$C_6H_5COOCH_3$	6.58	$1.37 \cdot 10^{-9}$	H	CHRO	FLAM., EXPL.	3.25/500g	199.6	S
ISO-AMYL BENZOATE	$C_6H_5C_5H_{11}O_2$	5.03		H		FLAM.		365.0	S
BENZYL BENZOATE	$C_6H_5COOCH_2C_6H_5$	4.85	$1 \cdot 10^{-9}$	H				316.0	S
DIETHYL CARBONATE	$CO(OC_2H_5)_2$	3.15	$17 \cdot 10^{-9}$	F			66/100g	115.6	UNSTABLE
CHLOROFORM	$CHCl_3$	4.64	$1 \cdot 10^{-10}$	H	ACUTE		1.00/1 lb.	61.26	S
CARBONTETRACHLORIDE	CCl_4	2.22	$4 \cdot 10^{-8}$	H	CHRO		80/1 lb	153.84	S
PENTACHLORETHANE	$CHCl_2CCl_3$	3.60	N/M	H	"			162.0	S
CIS ACETYLENE DICHLORIDE	$CHCl CHCl$	3.67	$1 \cdot 10^{-9}$	H	"	FLAM., EXPL.		59.0	S
TRICHLORCETHYLENE	$CHCl CCl_2$	3.42	N/M	H	CHRO.		2.70/kg	87.0	S
TETRACHLORCETHYLENE	$O(CHCl_2)_2$	2.37		H	"		1.65/kg	145.0	S
BROMOFORM	$CHBr_3$	4.73	$2 \cdot 10^{-8}$	H	ACUTE		1.59/100g	149.5	S
ETHYL BROMIDE	CH_3CH_2Br	4.965	$2 \cdot 10^{-10}$	H	"	FLAM., EXPL.	4.30/100g	38.0	S
BROMBENZENE	C_6H_5Br	5.397	$1.2 \cdot 10^{-11}$	H		FLAM.		156.15	S
a-BROMNAPHTHALENE	$(C_6H_4)_2CBr$	5.17	$3.6 \cdot 10^{-11}$	H				281.8	S
CIS ACETYLENE DIBROMIDE	$HCBr_2CH$	7.08		H				112.5	S
TRANSACETYLENE DETROMIDE	$HCBr_2CH$	2.98		H				108.0	S
p-TOLUIDINE	$CH_3C_6H_4NH_2$	4.88	$62 \cdot 10^{-9}$	G	CHRO.	FLAM	1.70/200g	200.4	C
DIMETHYLANILINE	$C_6H_5N(CH_3)_2$	4.48		F	"	"		192.3	C
CARBON DISULPHIDE	CS_2	2.675	$3.7 \cdot 10^{-3}$	F	ACUTE	FLAM., EXPL.	1.14/lb.	76.1	POISONOUS
ISO AMYL SALICYLATE	$C_6H_4(OH)COOCH_2CH(CH_3)_2$	5.4		H				208.1	S
n-PENTANE	$CH_3(CH_2)_3CH_3$	1.845	$2.1 \cdot 10^{-10}$	H		FLAM.	1.25/100g	36.0	S
n-HEXANE	$CH_3(CH_2)_4CH_3$	1.901		H	CHRO	"	35/kg	68.7	S
n-HEPTANE	$CH_3(CH_2)_5CH_3$	1.973		H	ACUTE	FLAM., EXPL.		98.4	S
n-OCTANE	$CH_3(CH_2)_6CH_3$	1.962		H	CHRO.	" "	2.05/100g	125.9	S
n-NONANE	$CH_3(CH_2)_7CH_3$	1.972	N/M	H		FLAM		150.7	S
n-DECANE	$CH_3(CH_2)_8CH_3$	1.956		H		FLAM., EXPL.		137.9	S
CYCLOHEXANE	$(CH_2)_6$	2.012		H	ACUTE	FLAM	9.42/kg	80.8	S
METHYLCYCLOHEXANE	$(CH_2)_5CHCH_3$	2.071		H	"			100.8	S
DECAHYDRONAPHTHALENE	$(CH_2)_8(CH)_2$	2.11		H	CHRO.	FLAM.	3.65/500g	193.0	S

*H = HARD
G = GOOD
F = FAIR

*S = SOLUBILITY
C = COST

TABLE 5.3 Low dielectric constant solvents (from Iizuka, 1961)

liquids. When large scaling ratios are required for models, a difficulty appears. One would like to have a material with conductivity between that for saline water and carbon, for certain frequency ranges. For distance-dependent field measurements, liquids or gels (such as agar-agar gels of Iizuka) are indicated.

5.4.2 Low Dielectric Constant Solvents

While searching for materials of low dielectric constants, Iizuka (1961) tabulated the results of his survey, shown here as Table 5.3. Dioxane was indicated but was too toxic and dangerous, so other solvents were used. The materials were desired in obtaining the performance of antennas in stratified media. The solvents were separated by thin films such as nylon (having low dielectric constants and conductivities). The horizontal stratification effects are reported by Iizuka (1961) and Iizuka and King (1962b).

5.4.3 Higher Dielectric Constant Liquids

For scaled modelling purposes, higher dielectric constant liquids are desired. For this purpose, water is most often used, or ethyl alcohol or a mixture of the two, providing a range of 20 to 80 or so for relative dielectric constant. By adding salt, the conductivity can then be varied from 10^{-4} to about 10 Si/m.

While less desirable for showing smooth profiles than the agar-agar mixtures of Iizuka, inhomogeneous profiles can be simulated by horizontally stratified layers of solvents with differing electrical constants according to the profile desired. Such stratification might ultimately be considered in the schemes of Chapter 6 as one of the steps in building up from simpler models.

6. Theory and Experiment in Lithospheric Propagation: Models

6.1 Introduction

The possibility of wave-guide-like propagation of electromagnetic waves in the earth's lithosphere has been studied extensively by numerous investigators. The theoretical models are all quite similar and are based on idealizations of cross sections of the earth's crust such as that given by Levin [1966] and shown in Fig. 6.1. These idealizations in general include (a) a planar slab of a dielectric material with low conductivity to represent a lithosphere composed of granitic rock and basalt, (b) an upper layer of quite highly conducting material corresponding to the overburden on the continent and the ocean basin beyond this, and (c) a lower also highly conducting layer to represent the mantle. Refinements sometimes added include the air and the ionosphere above the overburden and ocean as shown in Fig. 6.2, but their presence usually has a negligible effect. The excitation of electromagnetic waves in the dielectric slab and their reception at distant points has taken several forms. The first and most commonly described source consists of a vertical antenna in a borehole extending into the lithosphere or, short of this, ending in the overburden at some distance from the lithosphere. Wait's analysis [1966] shows that if the vertical antenna is not in the lithosphere or very close to it, adequate excitation is not possible. He suggests [1966, p.923] that "every effort should be made to locate both the (vertical) source dipole and the observer within the waveguide. Otherwise, some other mechanism of excitation should be used such as a horizontal electric dipole." This suggestion is followed by Frieman and Kroll [1973] whose investigations include excitation not only by a vertical electric dipole but also by a horizontal electric dipole at the upper boundary of the lithosphere. They conclude that "the horizontal electric dipole case proves to be more interesting", that it "permits the utilization of much larger antennas and hence more efficient antenna design." They suggest that "a horizontal electric dipole is far superior to a vertical electric dipole."

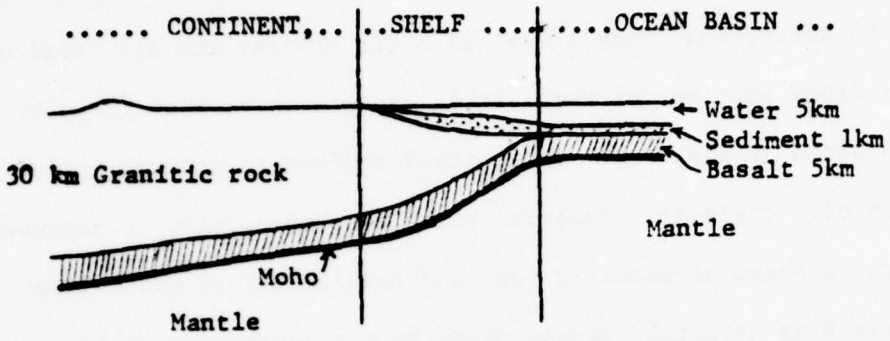

Fig.6.1 Profile of earth's crust according to S.B. Levin

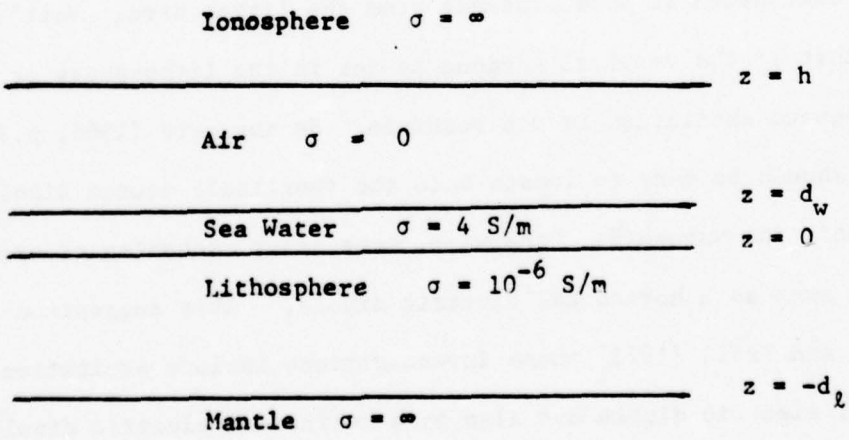

Fig.6.2 Model used by Frieman and Kroll

The method of analysis of Frieman and Kroll is similar to that of Wait and others in that the relevant waveguide modes are determined. Their study of the propagating characteristics of the several modes led them to the conclusion that for a horizontal antenna and receiver on the ocean floor the behavior of the field "should be very similar to that of horizontal-dipole excitation near the plane boundary of two semi-infinite conducting media." However, it is well known [Baños, 1966; King and Sandler, 1977] that transmission along such an interface is primarily by so-called lateral waves for which a complete theory is available. To date it has not been applied to an interface between two half-spaces with the properties of sea water and basalt or of the earth's overburden and granitic rock. It appears, therefore, that for the idealized theoretical model consisting of a dielectric slab between conducting regions, analytical and numerical solutions of Maxwell's equations are available and should suffice to determine the nature of propagation between a pair of vertical or horizontal dipoles in the slab or near its boundary in the upper conducting layer. In particular, it should be possible to calculate the electric field at the receiver as a function of distance, frequency, and the assumed electrical parameters of the media. Alternatives to such computations include,on the one hand, the very difficult and costly full-scale experiments and, on the other hand, suitably scaled and constructed experiments that satisfy all of the conditions of electromagnetic similitude. Model measurements have the advantage over theoretical computations that they permit a variety of realistic modifications of the over-idealized theoretical models.

In the absence of magnetic materials the conditions for modelling are:

$$f_m^2 \varepsilon_m r_m^2 = f_e^2 \varepsilon_e r_e^2 \quad ; \quad f_m \sigma_m r_m^2 = f_e \sigma_e r_e^2 \tag{6.1}$$

where f is the frequency, r is a characteristic length, $\varepsilon = \varepsilon_o \varepsilon_r$ is the permittivity and σ is the conductivity. The subscript m denotes the model, the subscript e the earth. Unfortunately such modelling is severely limited by the distances involved and by the materials and frequencies available for the

simulation and the experiments. A model of practical size requires a scale factor in the distances of the order of $r_e/r_m = 10^5$. With ε_{er} = 4 to 8 for the lithosphere and ε_{mr} = 80 for the water solutions most commonly used in the model, $\varepsilon_{mr}/\varepsilon_{er}$ = 20 to 10. It follows that $f_e/f_m = (\varepsilon_{mr}/\varepsilon_{er})^{1/2}(r_m/r_e) = 4 \times 10^{-5}$ to 3×10^{-5} . Since accurate electrical measurements are difficult unless $f_m \leq 1$ GHz, it follows that $f_e \leq$ (45 to 30) KHz. That is, completely scaled modeling of the lithosphere and its upper and lower bounding regions is limited to actual frequencies that satisfy $f \leq 45$ KHz. While this condition presents no practical limitation on VLF propagation in the lithosphere using vertical dipole excitation, it excludes all of the high frequencies which may be the most promising for lateral wave transmission using horizontal dipole excitation. The second condition for similitude requires that for $\varepsilon_{er} = 4$, $\sigma_e/\sigma_m = f_m r_m^2/f_e r_e^2 = 2 \times 10^{-6}$. If the lithosphere is modeled with water solutions as was done by Brown and Gangi and by Iizuka, $\sigma_m = 10^{-4}$ to 10 Si/m, so that $\sigma_e = 2 \times 10^{-10}$ to 2×10^{-5} Si/m. This includes the entire useful range. On the other hand for an overburden with $\sigma_e = 10^{-2}$ to 10^{-3} Si/m, σ_m = 3000 to 300 Si/m for which convenient materials are difficult to find. The same is true for the ocean with σ_e = 4 Si/m and $\sigma_m = 4 \times 10^5$ Si/m, with ε_{er} = 80.

Actual models constructed by Brown and Gangi [1963] were designed to simulate a frequency f_e = 2 to 4 KHz. The lithosphere was quite accurately scaled by salt water, the overburden or ocean and the mantle less accurately by metal or carbon plates. For waveguide propagation when the transmitting and receiving antennas are both vertical and embedded in the lithosphere, a less than exact scaling of the properties of the upper and lower conducting media may be adequate so long as the principal attenuation is due to losses in the lithosphere and not in the bounding walls. Note, however, that the use of solid plates for the overburden or ocean is neither convenient nor sufficiently accurate when the excitation is by a vertical or horizontal dipole located at some point above the surface of the lithosphere.

The interesting models developed by Iizuka [1971,1972] have similar general limiations as those of Brown and Gangi with respect to the frequency range and the properties of materials. They are also restricted to excitation by dipoles in the model lithosphere. However, they do provide the means for producing a specified non-uniform conductivity profile across the lithosphere and for providing boundaries that are not plane parallel. In a restricted range of frequencies and with excitation by a vertical antenna within the lithosphere Iizuka's models offer a powerful tool for obtaining information about wave propagation in the earth insofar as the assumed profiles are good approximations of reality. Unfortunaely they are not readily generalized to permit the use of vertical or horizontal dipoles in the model overburden or ocean and for determining the electromagnetic field in this.

6.2 Suggested Experimental Studies in Lithospheric Propagation

Measurements on models combined with the principle of similitude provide a powerful and practical alternative to full-sized experiments in the earth and to theoretical studies. Owing to the very large scale factors involved and the limitations of experimental techniques and available materials the method is for all practical purposes limited to low frequency applications in the actual earth. Even for these the accurate modelling of the lithosphere virtually precludes a corresponding accuracy in the modelling of the overburden or the ocean and so requires the exciting and receiving antennas to be in the model lithosphere. In the actual earth this is possible only in boreholes through the overburden or into the ocean bed with vertical dipoles. In view of the theoretically derived conclusion by Frieman and Kroll [1973] that horizontal dipoles are a very promising alternative, future experimental studies should be concerned with a comparative investigation of the characteristics of both horizontal and vertical electric dipoles when located in the ocean near its interface with the lithosphere and not only with vertical dipoles in the litho-

sphere. Suggested experiments might include:a) vertical transmitting and receiving dipoles in the model lithosphere and at increasing heights in the model overburden or ocean; b) a vertical transmitting antenna in the model lithosphere and a horizontal receiving dipole in the model overburden or ocean near the interface with the lithosphere; and c) horizontal transmitting and and receiving antennas in the model overburden or ocean. In each case the receiving dipole is to be moved to measure the magnitude and phase of the electric field as the distance from the transmitting antenna is increased. Further measurements are indicated to determine the effect of non-parallel boundaries of the model lithosphere, boundary surfaces between the lithosphere and the overburden or ocean that are not smooth but undulate or are otherwise irregular or discontinuous, a layer of properly modelled sediment on the ocean bottom including the effect of embedding both transmitting and receiving antennas at various depths.

Since communication between two horizontal dipoles in the overburden or ocean near its interface with the lithosphere is primarily by lateral waves [Banos, 1966; King and Sandler, 1977], experiments that involve such antennas must be designed to take maximum advantage of the somewhat unusual characteristics of this type of transmission. In particular, note must be taken of the fact that when the horizontal transmitting antenna is not far from the interface, the most useful component of the electric field is the radial one in a direction along the axis of the dipole. Furthermore, the optimum frequency for transmission is well above the low frequency range. Since accurate modelling according to the principle of similitude cannot be carried out above full scale frequencies of two to three kilohertz, it is not practical to study lateral wave transmission in a comprehensive manner by models that satisfy the equations of similitude as formulated for the lithosphere. While this means that a completely scaled set of experiments is unavailable, it does not mean that meaningful and illuminating information cannot be obtained from suitably designed model experi-

ments. These must, of course, be planned and interpretted in conjunction with the theory of lateral-wave transmission.

In carrying out the suggested experiments it may be convenient and expedient to separate the transmission losses in the model lithosphere from those in the model overburden, ocean, and mantle . This can be done initially by making use of a perfect dielectric (e.g. air or styrofoam) in the model lithosphere and sea water for the bounding regions. Subsequently a dielectric with losses and specified conductivity profiles comparable to those believed to obtain in the earth can be introduced in the simpler and more crucial experiments.

6.3 Some Possible Laboratory Models for Lithospheric Experiments

The simple model used by Brown and Gangi [1963] and the much more complicated one developed by Iizuka [1971,1972] stress the accurate modelling of the lithosphere but represent the overburden or ocean and the mantle by highly conducting metal or carbon plates. In order to study the significance of the bounding regions in their effect on the transmission and simultaneously to make possible the embedding and moving of antennas in them, it is possible to model them with a liquid like water or alcohol or a mixture of these to obtain relative permittivities between 20 and 80 and to add salt to vary the conductivity in the range from 10^{-4} to 10 Si/m. The model lithosphere can be composed initially of air or styrofoam with negligible losses and subsequently by wood or alcohol with higher conductivity. The bounding styrofoam can be smooth, undulating, or arbitrarily irregular. Above the air or styrofoam is a metal plate that can be parallel to the surface of the water or inclined at an arbitrary angle. It serves as an image plane for the entire structure below it. This effectively provides a model lithosphere that has twice the thickness between the metal plate and the surface of the water. It is bounded above and below by salt water to model both the overburden or ocean and the mantle.

A sketch of the suggested model is shown in Fig. 6.3. The vertical transmitting and receiving monopoles when combined with their images act as

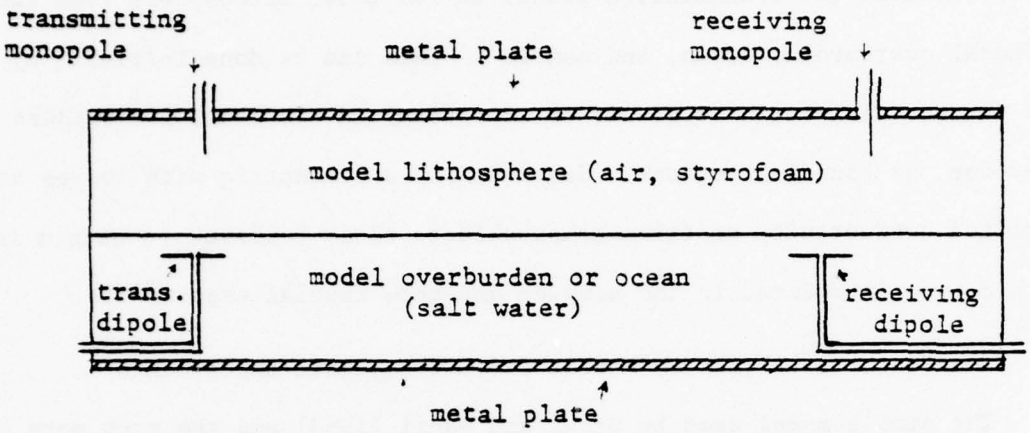

(a) Schematic diagram of apparatus

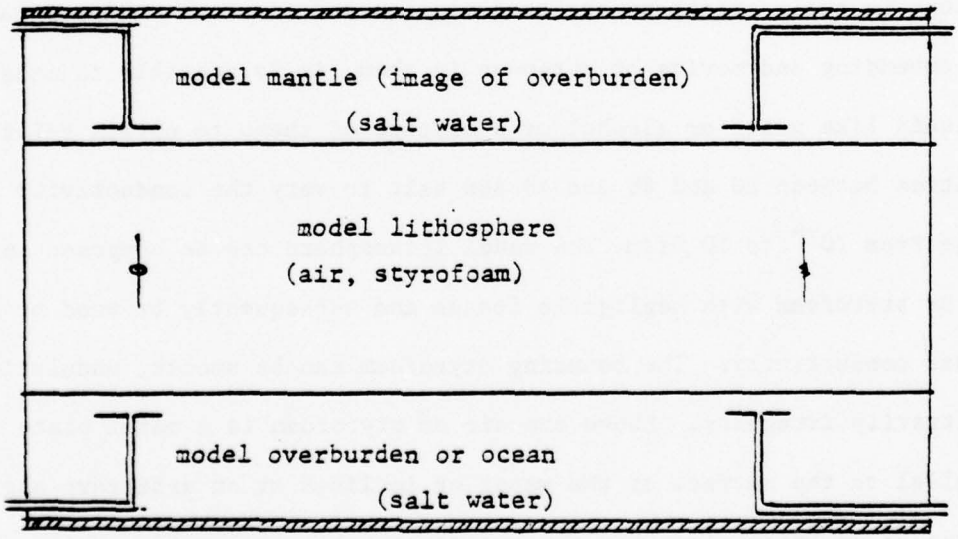

(b) Schematic diagram of apparatus with image

Fig. 6.3 Suggested apparatus for lithospheric and lateral-wave transmission.

dipoles in the center of the model lithosphere. The receiving monopole travels in a slot to measure the amplitude and phase of the vertical electric field from near the transmitter to distant points. The upper plate can be inclined and the water-styrofoam surface can be made undulating or otherwise irregular, Fig. 6.4.

Also shown in Fig. 6.3 are transmitting and receiving dipoles in the salt water. In the figure they are horizontal but in practice they can be oriented to be vertical or at any desired angle. The receiving element can be used to measure the amplitude and phase of the electric field in the model overburden or ocean. All components of the electric field can be determined. Since the dipoles have identical images which are symmetrically located in the model mantle, the field actually measured is due to both the source and the image. However, the contributions are readily separated theoretically, so that the field due to one source alone can be studied.

In order to carry out the suggested measurements in a tank approximately 3 x 2 meters, a frequency in the range from 0.3 to 1 GHz is required. This gives between three and ten wavelengths in air for studying the decay of the electric field in the model lithosphere when excited by a horizontal dipole in the overburden or ocean or by a vertical monopole in the model lithosphere. With the former the effect of varying the distance between the antenna and the bounding surface can also be investigated. The general arrangement shown in Fig. 6.3 provides the means for carrying out the suggested experiments and so obtaining direct information on the transmission of electromagnetic waves through the lithosphere and of lateral waves along its boundary under a variety of circumstances arranged to simulate possible conditions in the earth. Such a program of experimentation and its correlation with theory would seem to be a logical and necessary continuation and extension of the basic work by Brown and Gangi and especially by Iizuka.

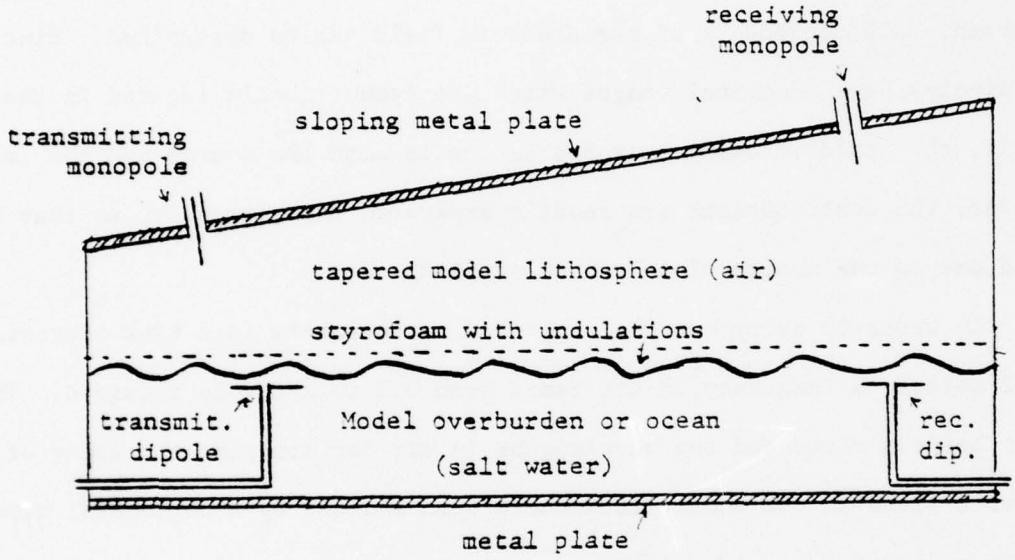

Fig. 6.4 Model with tapered lithosphere and undualating overburden or ocean.

7. Summary and Conclusions

Propagation in the earth's crustal waveguide has been studied by numerous investigators. The properties of available conceptual depth profiles of electric constants, mainly conductivity, are reviewed. The propagating region was assumed to be a planar slab, bounded on top by an ocean or overburden and on the bottom by the mantle or Moho, the bounding regions being of very large loss-tangent.

The waveguide theories extant are then summarized. Earlier analyses assumed a slab of uniform depth profile. Many of the investigators illustrate the modal properties for modes of low attenuation, others give samples of field calculations. Usually the exciting sources were vertical electric dipoles (VED) extending through bore-holes in the overburden (or ocean) into the lower loss-tangent crustal waveguide. Analyses for non-homogeneous profiles included the modal solutions of Wait for an exponential conductivity profile, and those of Schwering, Peterson, and Levin for an inverse-square depth profile of both dielectric constant and conductivity. Full wave modal solutions were employed by Field and Dore using recent conceptual "bell-shaped" profiles of Keller and of Housley which showed minima and very much smaller conductivities at depths of the order of 10 km.

Lacking VED excitation in the waveguide, Wait suggested HED excitation, a suggestion which was followed up by Frieman and Kroll who showed that for ocean emplaced antennas at the ocean-lithosphere interface, the HED was superior to the VED. Excitation should be like that for HED excitation near the plane boundary of two semi-infinite media. For dipoles in the ocean near the ocean-air boundary, King and Sandler extended the work of Banos.

Propagation is by means of lateral waves. This work was extended to the case where the air was replaced by the lithosphere. Calculations were made for a wide range of parameters for the radial component of electric field from the HED, which component is the useful one especially for intermediate and large ranges. The mechanism may be described as "down-under-and-up" in consonance with the popular notation of "up-over-and-down" for HED sources in the sea near the sea-air boundary. The advantages and disadvantages of the lateral wave transmission were discussed for the ocean-lithosphere case.

The relations for the scaling of models according to electrodynamic similitude are presented. Examples are given from the work of Brown and Gangi for homogeneous depth profiles where the modelled crustal slab (saline) water is bounded on top by metal plates. For non-homogeneous profiles, examples are given from the work of Iizuka who used an agar-agar gel with diffusion of sodium chloride to vary the loss-tangent with depth. The top boundary was a metal plate, the bottom being the higher conductivity sodium chloride diffuser. Measurements were made with planar and sloping boundaries.

To study the effects of bounding regions on transmission including losses and simultaneously make measurements of the effects of embedding and moving antennas in them, the laboratory models should have "walls" composed of a liquid like water or alcohol or a mixture of them which can vary the relative dielectric constant from 20 to 80 and to add salt to vary the conductivity from 10^{-4} to 10 Si/m. Above such a wall would be the lithosphere, initially air or styrofoam, and subsequently a substance like wood or alcohol to increase the complex dielectric constant. Above the "lithosphere" is a metal plate which can be parallel or inclined. The styrofoam boundary can be

undulating or irregular. The metal plate, which has movable probes, acts as an image plate.

It is recommended that an orderly build-up of modelling experiments be initiated with a laboratory model just described, and continuing with more complicated depth profiles. Although available materials may limit accurate modelling according to the principles of similitude, meaningful and illuminating information can be obtained for a better understanding of lithospheric transmission including lateral waves and losses.

The more complicated crustal depth profiles require a much more elaborate set-up possibly patterned after that of Iizuka. For measurements and their interpretation then, there will be a need for scientists of considerable experience including support personnel. The program should be long range in anticipation of the development of more accurate depth profiles from full scale geophysical experiments and analyses.

8. References

Acker, M., and L. J. Mueller, (1966), "Some measured electrical characteristics of the earth's crust", NATO 12th Symposium of the Avionics Panel of AGARD, "Sub-surface Communications", Paris, Conference Proceedings No. 20, pp. 211-238, (April).

Ames, L. A., J. W. Frazier, and A. S. Orange, (1963), "Geological and geophysical considerations in radio propagation through the earth's crust", IEEE Trans. on Antennas and Propagation, vol. AP-11, pp. 369-371, (May).

Bannister, P. R., (1978), "Electromagnetic propagation", paper presented at ONR Lithospheric Workshop, Wash., D.C., (March).

Banos, A., (1966), "Dipole Radiation in the Presence of a Conducting Half-Space", Pergamon Press, Inc., New York, N.Y.

Brown, G. L., and A. F. Gangi, (1962), "Lithospheric communications", Space General Corp. paper presented at IRE 8th National Communications Symposium, Utica, N.Y.

Brown, G. L., and A. F. Gangi, (1963), "Electromagnetic modelling studies of lithospheric propagation", IEEE Transactions of Geoscience Electronics, vol. GE-1, No. 1, pp. 17-23.

Bubenik, D. M., and A. C. Fraser-Smith, (1978), "ULF/ELF electromagnetic fields generated in a sea of finite depth by a submerged vertically-directed harmonic magnetic dipole", Radio Science, vol. 13, No. 6, pp. 1011-1020, (Nov.-Dec.).

Cantwell, T., and T. R. Madden, (1960), "Preliminary report on crustal magneto-telluric measurements", J. Geophys. Res., vol. 65, pp. 4202-4205, (Dec.).

Carolan, J., Jr., and J. T. deBettencourt, (1963), "Radio waves in rock near overburden-rock interface", IEEE Trans. Ant. and Prop., v. AP-11, No. 3, pp. 336-338, (May).

Cox, C. S., (1971), "The electrical conductivity of the oceanic lithosphere", in "The Structure and Physical Properties of the Earth's Crust", pp. 227-234, American Geophysical Union, Geophysical Monograph No. 14, Wash., D.C., J. G. Heacock, Editor.

Cox, C. S., (1978), "The electrical conductivity of the oceanic crust and upper mantle", paper presented at ONR Lithospheric Workshop, Wash., D.C., (March).

deBettencourt, J. T., (1962), "Sub-surface modes of propagation", Chapter I, Section B, "Very Deep Strata, Low-loss, Waveguide Mode", Final Report Raytheon Co., CADPO, Norwood, Mass., Contract AF19(604)-8359, pp. I-13 to I-21.

deBettencourt, J. T., (1966), "Review of radio propagation below the earth's surface", Survey paper presented at the XVth General Assembly of URSI, Munich.

deBettencourt, J. T. and J. W. Frazier, (1963), "Rock electrical characteristics deduced from depth attenuation rates (in drill holes)", IEEE Trans. Ant. and Prop., vol. AP-11, pp. 358-363, (May).

deBettencourt, J. T., and R. A. Sutcliffe, (1962), "Studies in deep strata communication", Final Report Raytheon Co., CADPO, Norwood, Mass., Contract AF19(604)-8359.

Field, E., and M. Dore, (1973), "Electromagnetic communication in the earth's crust", Pacific Sierra Corp. Report PSR 306, ARPA Order No. 2270, (June).

Frieman, E. A., and N. M. Kroll, (1973), "Lithospheric Propagation for undersea Communication", Tech. Rept. (JASON) JSR-73-5, Stanford Research Inst., Menlo Park, Calif. (Nov.).

Frischknecht, F. C., (1971), "Electromagnetic scale modelling", Chapter 8, in "Electromagnetic Probing in Geophysics", ed. J. R. Wait, The Golem Press, See Section 2 of Chapter 8.

Gabillard, R., (1966), "Communications a travers le sol", Conf. Proc. No. 20, 12th NATO/AGARD Symposium on "Subsurface Communication", Paris, pp. 355-386, (April).

Gabillard, R., P. Degauque, and J. R. Wait, (1971), "Subsurface Electromagnetic telecommunications - a review", IEEE Trans. Comm. Tech., Vol. COM-19, pp. 1217-1228, No. 6, (Dec.).

Gallawa, R. L., and L. A. Haidle, (1972), "An engineering study feasibility of communications via a subterranean waveguide, ITS, OT/TRER 39. (Nov.).

Gangi, A. F., (1966), "Model results in underground communications", paper presented at NATO 12th Symposium of the Avionics Panel of AGARD, "Sub-surface Communications", Paris, Conference Proceedings No. 20, pp. 387-408.

Garland, G. D., and T. F. Webster, (1960), "Studies of natural electric and magnetic fields", J. Res. NBS, Vol. 64D, pp. 405-408, (July).

Heacock, J. G., ed., (1971), "The Structure and Physical Properties of the Earth's Crust", AGU Geophysical Monograph Series, No. 14.

Housley, R. M., (1973), private communication, in Field and Dore (1973).

Hughes, H., (1953), "The electrical conductivity of the earth's interior", Ph.D. dissertation, Univ. of Cambridge, Cambridge, England.

Iizuka, K., (1961), "The dipole antenna immersed in a conducting medium", Ph.D. Thesis, Div. of Eng. and Applied Phys., Harvard Univ., Cambridge, Mass. (May).

Iizuka, K., (1967), "Technique of fabricating inhomogeneous mediums and the behavior of a dipole in such a medium", Proc. IEE (London), Vol. 114, No. 5, pp. 595-603.

Iizuka, K., (1968), "An agar-agar chamber for the study of electromagnetic waves in an inhomogeneous medium", Technical Report 565, Div. Appl. Sciences, Harvard Univ., ONR Contract N00014-67-A-0298-0005 NR 372-012. See Ch. IV, "Similitude".

Iizuka, K., (1969), "An agar-agar chamber for the study of electromagnetic waves in an inhomogeneous medium-Part II", Technical Report 586, DEAP, Harvard Univ., ONR Contract N00014-67-A-0298-0005 NR 371-016.

Iizuka, K., (1971), "An agar-agar chamber for the study of electromagnetic waves in an inhomogeneous medium", IEEE Trans. Ant. and Prop., Vol. AP-19, pp. 365-377.

Iizuka, K., (1972), "Application of an agar-agar chamber for the study of electromagnetic waves in an inhomogeneous medium", IEEE Transactions of Antennas and Propagation, Vol. AP-20, No. 5, 602-612.

Iizuka, K., and R. W. P. King, (1962a), "The dipole antenna immersed in a homogeneous medium", IRE Transactions of Antennas and Propagation, Vol. AP-10, No. 4, pp. 384-392.

Iizuka, K., and R. W. P. King, (1962b), "An experimental study of the half-wave dipole antenna immersed in a stratified conducting medium", IRE Transactions of Antennas and Propagation, Vol. AP-10, No. 4, pp. 393-399.

Keller, G. V., (1963), "Electrical properties in the deep crust", IEEE Transactions of Antennas and Propagation, Vol. AP-11, No. 3, pp. 334-357, (May).

Keller, G. V., (1971), "Electrical studies of the crust and upper mantle", in "The Structure and Physical Properties of the Earth's Crust", ed. J. G. Heacock, AGU Geophysical Monograph Series, No. 14, pp. 107-125.

Keller, G. V., (1972), private communication to R. L. Gallawa, in Gallawa and Haidle (1972).

Keller, G. V., (1978a), "Status of electrical methods for studying a crustal wave guide", paper presented at ONR Lithospheric Workshop, Wash., D.C., (March).

Keller, G. V., (1978b), private communication with J. T. deBettencourt (Nov.).

Keller, G. V., and F. C. Frischknecht, (1966), "Electrical Methods in Geophysical Prospecting", Pergamon Press, See Chapter VI, "Induction methods", Section 37, "Model studies", pp. 295-299.

King, R. J., and S. W. Maley, (1966), "Model experiments on propagation of ground waves across an abrupt boundary at oblique incidence", Radio Science, Vol. 1, No. 1, pp. 111-115.

King, R. J., S. W. Maley, and J. R. Wait, (1967), "Experimental and theoretical studies of propagation of ground waves across mixed paths", Proc. Electromagnetic Wave Theory Symposium, Delft, Netherlands, Part I, 1965, Pergamon Press, ed. J. Brown, N.Y.

King, R. W. P., and B. Sandler, (1977), "Subsurface Communication between dipoles in general media", IEEE Trans. Ant. and Prop., Vol. AP-25, No. 6, pp. 770-775, (Nov.). See correction, IEEE Trans. Ant. and Prop., Vol. AP-26, No. 3, pp. 511, (1978).

Kraichman, M. G., (1970), "Handbook of Electromagnetic Propagation in Conducting Media", Headquarters Naval Material Command, sale by U.S. Gov't Printing Off.

Lahiri, B. N., and A. T. Price, (1939), "Electromagnetic induction in non-uniform conductors and the determination of the conductivity of the earth from terrestrial magnetic variations", Phil. Trans. Roy. Soc. (London), A, Vol. 237, pp. 509-540, (Jan.).

Levin, S. B., (1966), "Lithospheric propagation - a review", NATO 12th Symposium of the Avionics Panel of AGARD, "Sub-surface Communications", Paris, Conference Proceedings No. 20, pp. 147-178.

Levin, S. B., (1971), "Radio propagation through the crust-retrospect and prospect", in "The Structure and Physical Properties of the Earth's Crust", ed. J. G. Heacock, AGU Geophysical Monograph Series, No. 14, pp. 333-336.

MacDonald, G. J. F., (1954), "Calculations on the thermal history of the earth", J. Geophys. Res., Vol. 64, pp. 1967-2000, (Nov.).

Millington, G., (1949a), "Ground-wave propagation over a land-sea boundary", Nature, Vol. 164, p. 114.

Millington, G., (1949b), "Ground-wave propagation over an inhomogeneous smooth earth", Part I, Proc. IEE (London), Vol. 9B, p. 53. See also (1948) Nature (London, Vol. 163, p. 128, and (1949) Nature (London), Vol. 164, p. 114.

Mott, H., and A. W. Biggs, (1963), "Very-low-frequency propagation below the bottom of the sea", in IEEE Trans. Ant. and Prop., Vol. AP-11, No. 3, pp. 232-239, (May).

Pressey, B. G., G. E. Ashwell, and C. S. Fowler, (1956), "Change in phase of a low-frequency groundwave propagated across a coast line", Proc. IEE (London), Vol. 103B, p. 527.

Raytheon Co., (M. D. Grossi, Project Director, (1973), "Design of a propagation experiment at sub-Hertz frequencies", Chaps. 2-7, (Unclassified), Final Report ER-73-4469, under Contract N00014-73-C-0035, Sudbury, Mass., (Oct.).

Rjazanev, A. K., and A. V. Shabel'nikov, (1966), "Propagation of radio waves in the earth's crust (a review)", French translation 1494 du CNET, presented by J. Odoux, Conf. Proc. No. 20, NATO/AGARD Symposium on "Subsurface Communications", Paris, pp. 179-210, (April).

Schwering, F. K., D. W. Peterson, and S. B. Levin, (1969), "A model for electromagnetic propagation in the lithosphere", Proc. IEEE, Vol. 56, No. 5, pp. 799-804, (May).

Simmons, G., (1978), "Electrical resistivity of the upper crust: new laboratory data", paper presented at ONR Lithospheric Workshop, Wash., D.C., (March).

Sinclair, G., (1948), "Theory of models of Electromagnetic systems", Proc. IRE, Vol. 36, No. 11, pp. 1364-1370.

Spies, K. P., and J. R. Wait, (1971), "On calculations of the modal parameters of an idealized earth-crust waveguide", ONR Technical Report 1, AD 721 371, Cont. NR 081-270.

Staiman, D., and T. Tamir, (1966), "Nature and optimisation of the ground (lateral) wave excited by submerged antennas", Proc. IEE (London), Vol. 113, No. 8, pp. 1299-1310, (Aug.).

Stratton, J. A., "Electromagnetic Theory", (1941), 1st ed., McGraw-Hill Book Co., N.Y., pp. 488-490, Section 9.3, "Electrodynamic Similitude".

Viggh, M. E., (1963), "Modes in lossy stratified media with application to underground propagation of radio waves", IEEE Trans. Ant. and Prop., Vol. AP-11, pp. 318-323, (May).

vonHippel, A. R., (1954), "Dielectric Materials and Applications", Technology Press of MIT, Cambridge, Mass., and John Wylie and Sons, Inc., New York, N.Y., p. 323.

Wait, J. R., (1957), "The mode theory of VLF ionospheric propagation for finite ground conductivity", Proc. IRE, Vol. 45, No. 6, pp. 760-767, (June).

Wait, J. R., (1962), "Electromagnetic Waves in Stratified Media", Pergamon Press, Inc., New York, N.Y.

Wait, J. R., (1963), "The possibility of guided electromagnetic waves in the earth's crust", IEEE Trans. Ant. and Prop., Vol. AP-11, No. 3, pp. 330-335.

Wait, J. R., (1966), "Electromagnetic propagation in idealized earth crust waveguide", Radio Science, Vol. 1, pp. 913-924, (Aug.).

Wait, J. R., (1966a), "Electromagnetic propagation in an idealized earth crust waveguide", NATO 12th Symposium of the Avionics Panel of AGARD, "Sub-surface Communications", Paris, Conference Proceedings No. 20, pp. 115-132, (Apr.).

Wait, J. R., (1966b), "Influence of subterranean insulating layer on electromagnetic ground-wave propagation", NATO 12th Symposium of the Avionics Panel of AGARD, "Sub-surface Communications", Paris, Conference Proceedings No. 20, pp. 133-146, (April).

Wait, J. R., (1966c), "Some factors concerning electromagnetic wave propagation in the earth's crust", Proc. IEEE, Vol. 54, pp. 1020-1025, (Aug.).

Wait, J. R., (1971), "Analytical investigation of electromagnetic wave propagation in the earth's crust", in "The Structure and Physical Properties of the Earth's Crust", ed. J. G. Heacock, AGU Geophysical Monograph Series, No. 14.

Wait, J. R., and K. P. Spies, (1971), "Note on calculations of propagation parameters for an idealized earth-crust wave-guide", in "The Structure and Physical Properties of the Earth's Crust", ed. J. G. Heacock, AGU Geophysical Monograph Series, No. 14, pp. 325-336.

Wait, J. R., and K. P. Spies, (1972), "Attenuations of electromagnetic waves in the earth-crust waveguide from ELF to VLF", Radio Science, Vol. 7, No. 6, pp. 689-690, (June).

Watt, A. D., G. F. Leydorf, and A. N. Smith, (1966), "Notes regarding possible field strength versus distance in earth crust waveguides", NATO 12th Symposium of the Avionics Panel of AGARD, "Sub-surface Communications", Paris, Conference Proceedings No. 20, pp. 491-520.

Watt, A. D., F. S. Mathews, and E. L. Maxwell, (1963), "Some electrical characteristics of the earth's crust", Proc. IEEE, Vol. 51, pp. 897-910, (June).

Wheeler, H. A., (1961), "Radio-wave propagation in the earth's crust", J. RES. NBS (D), Vol. 65D, No. 2, pp. 189-191.

Supplemental References

Bannister, P. R., and R. L. Dube, (1977), "Numerical results for modified image theory quasi-static range subsurface-to-subsurface and subsurface-to-air propagation equations", NUSC Tech. Rept. 5775, Naval Underwater Systems Center, New London, CT. (7 December)

Bannister, P. R., (1978a), "Extension of quasi-static range finitely conducting earth image theory techniques to other ranges", IEEE Trans Ant. and Prop., Vol. AP-26, No. 3, pp. 507-508.

Bannister, P. R., (1978b), "Quasi-static range propagation equations for the approximate fields within a conducting slab", NUSC Tech. Rept. 5807, Naval Underwater Systems Center, New London, CT. (2 October)

Bannister, P. R., L. C. Shen, and R. W. P. King, (1978), "Further comments on 'Measured field of a directional antenna submerged in a lake'", IEEE Trans. Ant. and Prop., Vol. AP-26, No. 6, pp. 872-873, (Nov.).

Bostick, F. X., C. S. Cox, and E. C. Field, Jr., (1978), "Land-to-seafloor electromagnetic transmissions in the 0.1 to 15 Hz band", Radio Science, Vol. 13, No. 4, pp. 701-708, (July-August).

Burrows, C. R., (1963), "Radio propagation within the earth's crust", IEEE Trans. Ant. and Prop., Vol. AP-11, No. 3, pp. 311-317, (May).

Feves, M., G. Simmons, and R. W. Siegfried, (1976), "Microcracks in crustal igneous rocks: physical properties", Report of Department of Earth and Planetary Sciences, Mass. Inst. of Tech., Cambridge, Mass., (1 Aug.).

Haidle, L. L., and R. L. Gallawa, (1972), "An engineering study of communications in a subterranean waveguide", Telecommunications Tech. Memo OT-TM-88, U.S. Dep't Comm, Office of Telecommunications, Inst. for Telecomm. Sci., Boulder, Colo. (April).

Maxwell, E. L., (1967), "Atmospheric noise from 20 Hz to 30 kHz", Radio Science, Vol. 2, No. 6, pp. 637-644, (June).

Sarbacher, R. I., and W. A. Edson, (1943), "Hyper and Ultrahigh Frequency Engineering", John Wiley and Sons, Inc., New York, N.Y. See Chap. 5, "Parallel plane wave guides", especially Sect. 5.23, "The Attenuation Constants".

Shen, L. C., R. W. P. King, and R. M. Sorbello, (1976), "Measured field of a directional antenna submerged in a lake", IEEE Trans. Ant. and Prop., Vol. AP-24, pp. 891-894.

Soderberg, E. F., (1969), "ELF noise in the sea at depths from 30 to 300 meters", J. Geo. Res. (Space Physics), Vol. 74, No. 9, pp. 2376-2387.

Spence, J. E., E. J. Sullivan, and J. L. Bevilie, (1966), "Electromagnetic fields in the ocean near a shoreline", NATO 12th Symposium of the Avionics Panel of AGARD, "Sub-surface Communications", Paris, Conference Proceedings No. 20, pp. 87-113.

Spies, K. S., and J. R. Wait, (1972), "Propagation of electromagnetic waves in the earth crust waveguide from ELF to VLF", Tech. Rept. No. 3, under ONR order No. NA-ONR-15-71, Proj. No. NR 081-270, (1 May).

Tamir, T., (1970), "Experimental verification of a lateral wave above a lossy interface", Electronics Letters, Vol. 6, No. 12, pp. 357-358, (11 June).

Tsao, C. K. H., and J. T. deBettencourt, (1966), "Sub-surface radio propagation measurements", NATO 12th Symposium of the Avionics Panel of AGARD, "Sub-surface Communication", Paris, Conference Proceedings No. 20, pp. 471-490.

Wait, J. R., Editor, (1971), "Electromagnetic Probing in Geophysics", Golem Press, Boulder, Colorado.

Wait, Jr. R., L. C. Shen, and R. W. P. King, (1978), "Comments on 'Measured field of a directional antenna submerged in a lake'", IEEE Trans. Ant. and Prop., Vol. AP-26, No. 2, p. 366, (March).

Wait, J. R., and K. P. Spies, (1972), "On mode conversion in the earth-crust waveguide", ONR Technical Report No. 4, AD 756693, Cont. NR 081-270.

Watt, A. D., (1967), "VLF Radio Engineering", Pergamon Press, Inc., New York, New York.

9. Acknowledgments

We wish to acknowledge the guidance and encouragement of Dr. Robert S. Andrews and Mr. John G. Heacock of the Earth Physics Program, Office of Naval Research. For helpful discussions we wish to thank Dr. Peter R. Bannister of NUSC, Messrs. Douglas Crombie, Robert L. Gallawa, and David Hill of NTIA, Prof. George V. Keller of the Colorado School of Mines, Prof. Liang C. Shen, Department of Electrical Engineering of the University of Houston, Prof. Gene Simmons, Division of Earth and Planetary Sciences of the Massachusetts Institute of Technology, and Prof. Tai T. Wu of Harvard University. We are grateful for the effective and timely assistance of Mr. Thomas J. Dolan, Jr. and Mrs. Mary E. Rockett of the ONRRR Office at Harvard University. Mrs. Barbara H. Sandler programmed the calculations.

Office of Naval Research (*)
Director, Earth Physics Program
Code 463
800 North Quincy Street
Arlington, Virginia 22217

Commanding Officer
Office of Naval Research
Boston Branch Office
Building 114, Section D
666 Summer Street
Boston, Massachusetts 02210

Naval Research Laboratory (*)
Code 2627
Washington, D.C. 20375

Defense Documentation Center (**)
Building 5, Cameron Station
Alexandria, Virginia 22314

Defense Contract Administration Services
Management Area, Boston
666 Summer Street
Boston, Massachusetts 02210

Mr. Morris Acker
U.S. Army Electronic Command
Headquarter
Ft. Monmouth, New Jersey

Dr. Ken R. Allen
Naval Coastal Systems Center
Panama City, Florida 32407

Mr. William Andahazy
Naval Ships Research and
Development Center
Annapolis, Maryland 21402

Dr. Peter Bannister
Naval Underwater Systems Center
Code 341
New London, Connecticut 96320

Ms. Joan Bertram
Naval Electronics Systems Command
NAVELEX 320
Department of the Navy
Washington, D.C. 20360

Mr. William J. Best
AFOSR/NP, Building 410
Bolling Air Force Base
Washington, D.C. 20332

Dr. Roger Booth
ACDA MA-AT
Room 5499
State Department
Washington, D.C. 20451

Professor Francis Bostick
University of Texas at Austin
Austin, Texas 78712

Dr. Bill Brace
Department of Earth and
Planetary Sciences
MIT
Cambridge, Massachusetts 02139

Dr. Nikolas I. Christensen
University of Washington
Department of Geological Sciences
Seattle, Washington 98195

Dr. John Clarke
University of California, Berkeley
Berkeley, California 94720

Dr. C. S. Clay
University of Wisconsin
Lewis G. Weeks Hall
Department of Geology and Geophysics
1215 West Dayton Street
Madison, Wisconsin 53706

Dr. Charles S. Cox
Scripps Institution of Oceanography
University of California
La Jolla, California 92037

Dr. Richard L. Crawford
WWMCCS Systems Engineering
Organization
Attention: SD&A
Washington, D.C. 20305

*Requires 5 copies
**Requires 2 copies

Mr. Edward M. Davin
Program Manager, Seabed Asses. Program
IDOE/Div. of Ocean Sci/OCE
National Science Foundation
1800 G Street, NW.
Washington, D.C. 20550

Dr. John R. Davis
Naval Research Laboratory
Code 5450
CSD Building 54, Room 112
4555 Overlook Avenue, SW.
Washington, D.C. 20375

Mr. Ferdinand P. Diemer
Office of Naval Research
Code 102B
800 North Quincy Street
Arlington, Virginia 22217

Mr. Thomas J. Dolan, Jr.
ONR Resident Representative
Harvard University
Room 113 - Gordon McKay Laboratory
Cambridge, Massachusetts 02138

Mr. Ed Edelsack
Office of Naval Research
Code 427
800 North Quincy Street
Arlington, Virginia 22217

Dr. Edward C. Field, Jr.
Pacific Sierra Research Corp
1456 Cloverfield Boulevard
Santa Monica, California 90404

Dr. Jean Filloux
Scripps Institution of Oceanography
University of California
La Jolla, California 92093

Dr. Anthony Fraser-Smith
Radioscience Laboratory
Stanford University
Stanford, California 94505

Dr. Frank C. Frischknech
Room 1244
U.S. Geological Survey
Denver Federal Center
Denver, Colorado 80225

Dr. Bob Helliwell
Stanford Electronics Laboratory
Stanford University
Stanford, California 94305

Mr. Robert H. Higgs
Code 3500
U.S. Naval Oceanographic Office
Hydrographic Department
NSTL Station, Mississippi 39522

Dr. Robert M. Housley
Science Center Rockwell International
Planetary Physics
P. O. Box 1085
1049 Camino Dos Rios
Thousand Oaks, California 91360

Mr. R. Gracen Joiner
Office of Naval Research
Code 465
800 North Quincy Street
Arlington, Virginia 22217

Dr. George Keller
Chairman
Department of Geophysics
Colorado School of Mines
Golden, Colorado 80401

Professor R.W.P. King
Gordon McKay Laboratory
Harvard University
Cambridge, Massachusetts 02138

Dr. George A. Kolstad
Eng., Math/Geosciences
Div. of Basic Energy Science
Department of Energy
Washington, D.C. 02545

Dr. Bodo Kruger
Naval Electronics Systems Command
Code PME 117-21, Room 6S008
Washington, D.C. 20360

Dr. Mark Landisman
Geosciences Division
University of Texas at Dallas
Richardson, Texas 75080

Dr. Bob Meyer
University of Wisconsin
Dept. of Geology/Geophysics
Madison, Wisconsin 53706

Dr. Steve Mock
Army Research Office
P.O. Box CM
Duke Station
Durham, North Carolina 27706

Dr. Frank Moore
Defense Communication Agency
DCA/CCTC, Code C672
8th and South Courthouse Road
Arlington, Virginia 222204

Professor Frank Morrison
Department of Geoscience
Engineering
University of California/Berkeley
Berkeley, California 94720

Dr. Henry W. Mullaney
Office of Naval Research
Code 427
800 North Quincy Street
Arlington, Virginia 22217

Dr. Martin Nisenoff
Naval Research Laboratory
Code 6435
MSD Building 60, Room 109
4555 Overlook Avenue, SW.
Washington, D.C. 20375

Dr. Mark Odegard
Office of Naval Research
Code 483
800 North Quincy Street
Arlington, Virginia 22217

Dr. Tom Pyle
Office of Naval Research
Code 480
800 North Quincy Street
Arlington, Virginia 22217

Dr. Tom P. Quinn
Office of Secretary of Navy
(Res. Eng/Science)
The Pentagon, Room 4D745
Washington, D.C. 20350

Dr. Robert D. Reagon
Phoenix Corporation
1600 Anderson Road
McLean, Virginia 22102

Dr. Sidney G. Reed, Jr.
Office of Naval Research
Code 100B1
800 North Quincy Street
Arlington, Virginia 22217

Dr. Gene Simmons
Department of Earth/Planetary
Sciences
MIT
Building 54-314
Cambridge, Massachusetts 02139

Dr. Emil Sodeberg
Naval Underwater Systems Center
New London, Connecticut 96320

Dr. Ker Thompson
Chief, Wave Propagation Branch
Air Force Cambridge Research Lab
Hanscom Field
Bedford, Massachusetts 01730

Dr. R. P. Von Herzen
Woods Hole Oceanographic Institute
Dept. of Geology/Geophysics
Woods Hole, Massachusetts 02543

Dr. James Wait, Senior Scientist
U.S. Department of Commerce
NOAA, Environ. Research Lab
Room 242, RB #1
Boulder, Colorado 80302

Dr. Howard Wilcox
Naval Ocean Systems Center
San Diego, California 92152